

University of Windsor

## Scholarship at UWindor

---

Electronic Theses and Dissertations

Theses, Dissertations, and Major Papers

---

Spring 2021

# Comparative Investigations from Tribological and Corrosion Properties of Alumina and Nickel-Alumina Coatings on Cast Iron

Jiayi Sun

*University of Windsor*

Follow this and additional works at: <https://scholar.uwindsor.ca/etd>



Part of the [Mechanical Engineering Commons](#)

---

### Recommended Citation

Sun, Jiayi, "Comparative Investigations from Tribological and Corrosion Properties of Alumina and Nickel-Alumina Coatings on Cast Iron" (2021). *Electronic Theses and Dissertations*. 8895.

<https://scholar.uwindsor.ca/etd/8895>

This online database contains the full-text of PhD dissertations and Masters' theses of University of Windsor students from 1954 forward. These documents are made available for personal study and research purposes only, in accordance with the Canadian Copyright Act and the Creative Commons license—CC BY-NC-ND (Attribution, Non-Commercial, No Derivative Works). Under this license, works must always be attributed to the copyright holder (original author), cannot be used for any commercial purposes, and may not be altered. Any other use would require the permission of the copyright holder. Students may inquire about withdrawing their dissertation and/or thesis from this database. For additional inquiries, please contact the repository administrator via email ([scholarship@uwindsor.ca](mailto:scholarship@uwindsor.ca)) or by telephone at 519-253-3000ext. 3208.

**Comparative Investigations from Tribological and Corrosion Properties of Alumina  
and Nickel-Alumina Coatings on Cast Iron**

By

**Jiayi Sun**

A Thesis  
Submitted to the Faculty of Graduate Studies  
through the Department of Mechanical, Automotive & Materials Engineering  
in Partial Fulfillment of the Requirements for  
the Degree of Master of Applied Science  
at the University of Windsor

Windsor, Ontario, Canada

2021

© 2021 Jiayi Sun

**Comparative Investigations from Tribological and Corrosion Properties of Alumina  
and Nickel-Alumina Coatings on Cast Iron**

by

**Jiayi Sun**

APPROVED BY:

---

V. Roussinova  
Department of Mechanical, Automotive & Materials Engineering

---

H. Hu  
Department of Mechanical, Automotive & Materials Engineering

---

X. Nie, Advisor  
Department of Mechanical, Automotive & Materials Engineering

May 04, 2021

## DECLARATION OF ORIGINALITY

I hereby certify that I am the sole author of this thesis and that no part of this thesis has been published or submitted for publication.

I certify that, to the best of my knowledge, my thesis does not infringe upon anyone's copyright nor violate any proprietary rights and that any ideas, techniques, quotations, or any other material from the work of other people included in my thesis, published or otherwise, are fully acknowledged in accordance with the standard referencing practices. Furthermore, to the extent that I have included copyrighted material that surpasses the bounds of fair dealing within the meaning of the Canada Copyright Act, I certify that I have obtained a written permission from the copyright owner(s) to include such material(s) in my thesis and have included copies of such copyright clearances to my appendix.

I declare that this is a true copy of my thesis, including any final revisions, as approved by my thesis committee and the Graduate Studies office, and that this thesis has not been submitted for a higher degree to any other University or Institution.

## ABSTRACT

Plasma Electrolytic Aluminating (PEA) Alumina coating on cast iron has a high wear/ corrosion resistance, but porous structure could cause pitting corrosion. Nickel is a widely used anti-corrosion material, but the wear resistance of nickel could still be developed. To explore advantages and disadvantages of combination of these two materials, electroless Nickel plating was applied on PEA Alumina coating. Electroless plated Ni grew from the interface of the alumina coating and cast iron and then sealed the micropores of the alumina coating in a nickel acetate bath, which could protect cast iron substrate from the pitting corrosion. In addition, some PEA Alumina coated samples were 500 °C heat treated to observe differences between unheated and heated samples in chemical composition and wear behaviours. The microstructure, chemical composition and phase structure of the coatings were investigated with scanning electron microscope (SEM), Energy-Dispersive X-Ray Spectroscopy (EDX) and X-ray diffraction (XRD). The tribology test data was from Pin-on-Disk (POD) dry sliding tests, and the corrosion resistance was evaluated by Open Circuit Potential (EOC), Potential Resistance ( $R_p$ ), and electrochemical impedance spectroscopy (EIS) tests. Comparing with as-coated PEA Alumina coating, 500 °C heated sample had a higher oxygen content and worse wear behaviours. The Alumina coated sample had a lower coefficient of friction (COF) and longer durability. Ni-Alumina coating had a better corrosion resistance but slightly lower wear resistance. Thus, Ni-Alumina coating can benefit in wet corrosion environment, and the Alumina only coating can have a lower friction at the dry sliding condition.

## DEDICATION

To my beloved family

## ACKNOWLEDGEMENTS

Firstly, appreciate to my advisor, Dr. Xueyuan Nie, for his endless help on this project and my future career. Appreciate to my committee members, Dr. Henry Hu and Dr. Vesselina Roussinova, for their patience and advices.

I would also like to thank my colleagues, Dr. Chen Zhao, Miss Ran Cai and Mr. Guang Wang for their assistance and support on experiments.

Finally, appreciate to the faculty, staff and department of Mechanical, Automotive and Materials Engineering of University of Windsor for their supports.

## TABLE OF CONTENTS

DECLARATION OF ORIGINALITY .....	iii
ABSTRACT.....	iv
ACKNOWLEDGEMENTS.....	vi
LIST OF TABLES .....	x
LIST OF FIGURES .....	xi
LIST OF ABBREVIATIONS/SYMBOLS.....	xvii
CHAPTER 1 Introduction.....	1
1.1 Motivation.....	1
1.2 Objectives.....	3
1.3 Organization of This Thesis .....	3
CHAPTER 2 Literature Review .....	4
2.1 Methods of Generating Thin Film Coatings .....	4
2.1.1 Electroplating .....	4
2.1.2 Electroless Plating .....	7
2.1.3 Thermal Spray Coating .....	9
2.1.4 Physical Vapour Deposition Coating .....	11
2.1.5 Plasma Electrolytic Oxidation Coating .....	12
2.1.6 Plasma Electrolytic Aluminating Coating .....	14
2.2 Wear Behaviours of Materials .....	16
2.2.1 Wear Behaviours of Alloys.....	16
2.2.2 Wear Behaviours of Plasma Electrolytic Oxidation Coating .....	18
2.3 Anti-Corrosion Behaviours of Materials .....	21
2.3.1 Anti-corrosion Behaviours of Alloys.....	21
2.3.2 Anti-corrosion Behaviours of Plasma Electrolytic Oxidation Coating .....	24
2.4 Summary .....	25



CHAPTER 3 Experimental Details .....	27
3.1 Sample Preparation .....	27
3.1.1 PEA Alumina Coating .....	27
3.1.2 Electroless Nickel Plating .....	28
3.1.3 Other Treatments Before Further Tests .....	29
3.2 Hardness Tests .....	32
3.3 Pin-on-Disk Tribology Tests .....	33
3.4 Morphology Observation .....	34
3.5 Element and Structure Analysis .....	35
3.6 Electrochemical Tests .....	37
CHAPTER 4 PEA Alumina and Ni-Alumina Coatings Generation.....	38
4.1 PEA Alumina Coatings on Gray Cast Iron .....	38
4.1.1 Surface Morphology .....	39
4.1.2 Chemical Compounds .....	39
4.2 Ni-Alumina Coatings on Gray Cast Iron .....	41
4.2.1 Surface Morphology .....	41
4.2.2 Chemical Compounds .....	42
4.2.3 Generating Mechanism .....	44
4.3 500 °C heated PEA Alumina Coatings .....	45
4.3.1 Surface Morphology .....	45
4.3.2 Chemical Compounds .....	46
4.4 Microhardness of Coatings .....	48
4.5 Summary .....	50
CHAPTER 5 Wear Behaviours of Coatings against Steel and WC Balls .....	52
5.1 Wear Behaviours of PEA Alumina Coatings on Gray Cast Iron .....	52
5.1.1 Wear Track Morphology .....	53
5.1.2 Chemical Composition .....	54
5.2 Wear Behaviours of Ni-Alumina Coatings on Gray Cast Iron .....	56
5.2.1 Wear Track Morphology .....	57
5.2.2 Chemical Composition .....	58
5.3 Wear Behaviours of 500°C heated PEA Alumina Coatings.....	60

5.3.1 <i>Wear Track Morphology</i> .....	61
5.3.2 <i>Chemical Compounds</i> .....	62
5.4 <i>Wear Mechanisms Analysis</i> .....	64
5.5 <i>Summary</i> .....	66
CHAPTER 6 <i>Electrochemical Corrosion Behaviours</i> .....	68
6.1 <i>Open Circuit Potential Tests</i> .....	68
6.2 <i>Polarization Resistance Tests</i> .....	69
6.3 <i>Electrochemical Impedance Spectroscopy Tests</i> .....	71
6.4 <i>Summary</i> .....	74
CHAPTER 7 <i>Conclusions and Future Works</i> .....	76
7.1 <i>Conclusions</i> .....	76
7.2 <i>Future Works</i> .....	79
REFERENCES/BIBLIOGRAPHY.....	80
VITA AUCTORIS.....	92

## LIST OF TABLES

Table 4.1: EDX elements analysis of PEA Alumina coating.....	40
Table 4.2: EDX elements analysis of as-coated and 500 °C heated PEA Alumina coatings.....	47
Table 5.1: EDX elements analysis of PEA Alumina coatings wear tracks.....	55
Table 5.2: EDX elements analysis of Ni-Alumina coatings wear tracks.....	59
Table 5.3: EDX elements analysis of 500 °C heated PEA Alumina coatings wear tracks.....	63
Table 6.1 Kinetic parameters from the polarization resistance tests.....	70
Table 6.2: Parameters of EIS curves.....	73

## LIST OF FIGURES

Figure 2.1 Illustration of electroplating chromium process [27].....	5
Figure 2.2: SEM micrographs of surface morphology of nickel coatings deposited from: (a) a saccharin-free bath at $i=100 \text{ mA/cm}^2$ , (b) a bath containing 5 g/L saccharin at $i=100 \text{ mA/cm}^2$ , (c) a bath containing 5 g/L saccharin at $i=300 \text{ mA/cm}^2$ [29].....	6
Figure 2.3: Types of electroless coatings [32].....	7
Figure 2.4: Influence of bath temperature on coating growth (pH = 6.5, 60 min) [39].....	8
Figure 2.5: General schematic diagram of thermal spray coating process [40].....	9
Figure 2.6: Schematics of the coating layer formation following deposition by a thermal spray process [43].....	10
Figure 2.7: Schematic drawing of two conventional PVD processes: (a) sputtering and (b) evaporating using ionized Argon ( $\text{Ar}^+$ ) gas. [46] .....	11
Figure 2.8: Backscattered scanning electron micrographs of the cross sections of PEO coating on 6082-T6 Al alloy [58].....	12
Figure 2.9: Surface morphology of $\text{Al}_2\text{O}_3$ and $\text{Al}_2\text{O}_3/\text{TiO}_2$ composite coatings produced using unipolar and bipolar waveforms: a) S1W1, b) S1W2, c) S1W3, d) S2W1, e) S2W2 and f) S2W3 [59].....	13

Figure 2.10: SEM cross-section images of Al<sub>2</sub>O<sub>3</sub> and Al<sub>2</sub>O<sub>3</sub>/TiO<sub>2</sub> composite coatings produced using unipolar and bipolar waveforms: a) S1W1, b) S1W2, c) S1W3, d) S2W1, e) S2W2 and f) S2W3 [59].....14

Figure 2.11: Schematic illustration of the PEA of cast iron. (a) System before applying current, (b) dissolution of iron into the electrolyte and migration of Al(OH)<sub>4</sub><sup>-</sup> anions toward the anode after applying current, (c) formation of hercynite film on the iron surface and the initiation of plasma discharge sparks, and (d) growth of the hercynite-alumina composite ceramic coating via strong plasma discharge. [11]..... 15

Figure 2.12: Typical friction curves at 500 N load for the investigated tool steels. The point X, shown for the tools, was used as indication of galling [64].....16

Figure 2.13: Typical wear mechanisms in the different stages. The pictures show the D2 tool material and corresponding worn sheet at 500 N. Arrows indicates disc sliding direction. [64].....17

Figure 2.14: Evolution of friction coefficients during LRWT of PEO coatings with different residual thickness (180, 135, 90, and 45 μm). Normal loads are (a) 5 N and (b) 10 N. The counter-face material is WC-4% [73].....18

Figure 2.15: Friction coefficients of PEO 6082-T6 alloy [58].....19

Figure 2.16: (a, b, c, d) Plan views and (e, f) cross-sections of the wear tracks of PEO coating without added particles. (a, c, e) 2 N 1000 m and (b, d, f) 10 N 1000 m [58].....20

Figure 2.17: Effect of temperature on the corrosion rates of steel in  $\text{Cl}^-/\text{S}_2\text{O}_3^{3-}/\text{sat. CO}_2$  system; (1) 1 M NaCl, (2) 1 M NaCl +  $\text{CO}_2$  (sat.), (3) 1 M NaCl + 0.01 M  $\text{Na}_2\text{S}_2\text{O}_3$ , (4) 1 M NaCl + 0.1 M  $\text{Na}_2\text{S}_2\text{O}_3$ , (5) 1 M NaCl + 1.0 M  $\text{Na}_2\text{S}_2\text{O}_3$ , (6) 1 M NaCl + 0.01 M  $\text{Na}_2\text{S}_2\text{O}_3$  +  $\text{CO}_2$  (sat.), (7) 1 M NaCl + 0.1 M  $\text{Na}_2\text{S}_2\text{O}_3$  +  $\text{CO}_2$  (sat.) and (8) 1 M NaCl + 1.0 M  $\text{Na}_2\text{S}_2\text{O}_3$  +  $\text{CO}_2$  (sat.). [79].....21

Figure 2.18: Surface appearance of the corroded irons after the polarization tests: (a) DI, (b) 4%Ni–DI, (c) ADI, and (d) 4%Ni–ADI. [85].....22

Figure 2.19: Mass loss of LY12 Al alloy vs test time in different solutions: 1-0.02 mol/L  $\text{NaHSO}_3$ +0.006 mol/L NaCl; 2-0.02 mol/L  $\text{NaHSO}_3$ ;3-0.006 mol/L NaCl; (a) With cladding; (b) Without cladding [88].....23

Figure 2.20: Potentiodynamic polarization plots for the coated specimens and 7075 aluminum alloy substrates as the reference. The tests are performed in 3.5% NaCl solution at pH 4 after 1 h immersion at 1 mV S<sup>-1</sup> [59].....24

Figure 3.1: Schematic draft of PEA Alumina coating process.....28

Figure 3.2: Illustration of BUEHLER SimpliMet™ XPS1 Mounting System.....30

Figure 3.3: Illustration of BUEHLER MATASERV Grinder-Polisher.....31

Figure 3.4: Illustration of SYBRON Thermolyne™ FURNATROL II furnace.....31

Figure 3.5: Illustration of BUEHLER MICROMET II microhardness tester.....33

Figure 3.6: Illustration of SCILAND PIN/DISK TRIBOMETER & SURFCORDER.....34

Figure 3.7: Illustration of HITACHI TM3030Plus Tabletop Microscope.....	35
Figure 3.8: Illustration of BRUKER QUANTAX 70 Energy-Dispersive X-Ray Spectroscopy.....	36
Figure 3.9: Illustration of AXRD X-Ray Diffraction Spectroscopy.....	36
Figure 3.10: Illustration of Bio-logic electrochemical workstation.....	37
Figure 4.1: Surface morphology of PEA Alumina coating.....	39
Figure 4.2: SEM image of cross-section of PEA Alumina coating.....	40
Figure 4.3: SEM images of (a) PEA Alumina coating and (b) Ni-Alumina coating.....	41
Figure 4.4: XRD results of (a) Ni-Alumina coating and (b) PEA Alumina coating.....	42
Figure 4.5: (a)(c) SEM images of Ni-Alumina coating with 10 min and 30 min electroless nickel plating, respectively; (b)(d) EDX analysis of coating in (a) and (c).....	43
Figure 4.6: SEM images of Ni-Alumina coating with electroless nickel plating duration of (a) 10 min and (b) 30 min.....	44
Figure 4.7: SEM images of PEA Alumina coatings (a) 500 °C heated and (b) as-coated.....	46

Figure 4.8: Selected points for EDX point analysis on (a) 500 °C heated and (b) as-coated.....	46
Figure 4.9: Vickers Microhardness results of as-coated PEA Alumina coating, 500 °C heated PEA Alumina coating and Ni-Alumina coating .....	48
Figure 5.1: COF data of PEA Alumina coatings against (a) steel ball and (b) WC ball.....	52
Figure 5.2: SEM images of wear tracks of PEA Alumina coating against (a) steel ball and (b) WC ball.....	53
Figure 5.3: Selected points for EDX point analysis of PEA Alumina coatings wear tracks against (a) steel ball and (b) WC ball.....	54
Figure 5.4: Comparison in COF data of PEA Alumina coatings and Ni-Alumina coating against (a) steel ball and (b) WC ball.....	56
Figure 5.5: SEM Images of Ni-Alumina wear tracks against (a) steel ball and (b) WC ball.....	57
Figure 5.6: Selected points for EDX point analysis of Ni-Alumina coatings wear tracks against (a) steel ball and (b) WC ball.....	58
Figure 5.7: Comparison in COF data of as-coated and 500 °C heated PEA Alumina coatings against (a) steel ball and (b) WC ball.....	60
Figure 5.8: SEM Images of PEA Alumina coatings wear tracks (a) as-coated and (b) 500 °C heated against steel ball.....	61



Figure 5.9: SEM Images of 500 °C heated PEA Alumina coatings wear tracks against (a) steel ball and (b) WC ball.....62

Figure 5.10: Selected points for EDX point analysis of 500 °C heated PEA Alumina coatings wear tracks against (a) steel ball and (b) WC ball.....63

Figure 6.1: EOC results of PEA Alumina coating and Ni-Alumina coating .....68

Figure 6.2: Rp results of PEA Alumina coating and Ni-Alumina coating .....70

Figure 6.3: (a), (b) Nyquist plots of PEA Alumina and Ni-Alumina coated cast iron; (c), (d) Bode plots corresponding to EIS spectra in (a) and (b), respectively; (e), (f) equivalent circuits of PEA Alumina and Ni-Alumina coated cast iron, respectively.....72

## LIST OF ABBREVIATIONS/SYMBOLS

PVD	Physical Vapour Deposition
CVD	Chemical Vapour Deposition
TS	Thermal Spray
PEO	Plasma Electrolytic Oxidation
PEA	Plasma Electrolytic Aluminating
SEM	Scanning Electron Microscopy
EDX	Energy-Dispersive X-Ray Spectroscopy
XRD	X-Ray Diffraction
XPS	X-Ray Photoelectron Spectroscopy
POD	Pin-on-Disk
COF	Coefficient of Friction
R <sub>p</sub>	Polarization Resistance
EOC	Open Circuit Potential
EIS	Electrochemical Impedance Spectroscopy
CPE	Constant Phase Element

## CHAPTER 1

### Introduction

#### ***1.1 Motivation***

Corrosion is a process which occurs on most of metals contacting with air and water and is a serious problem. [1][2] Corroded and uncorroded parts have large differences in mechanical properties such as, wear resistance, electrical conductivity, life length, corrosion resistance, etc. [3] . If corrosion happens on buildings or bridges without a careful maintenance, there could be a failure leading to engineering disasters. [7] Once a material has become corroded, it is not easy to fix. Some methods to get remove rust on a surface involve, grinding, chemical reaction and cathodic treatment. [4-6] Time and money is spent on maintaining corroded metals as it is not only a financial problem but also a severe safety problem. Therefore, applying corrosion resistant materials is the perfect method to prevent this problem.

Aluminum Oxide ( $\text{Al}_2\text{O}_3$ , also called Alumina) is naturally formed on aluminum in an oxidizing process, which produces a compact thin film that prevents corrosion. However, the naturally-generating alumina film is too thin and can easily be destroyed by long-term sliding wear and is susceptible to a corrosion in acidic or alkaline environments. The corrosive resistive properties of an alumina film are the inspiration for creating thicker alumina ceramic coating on target metals. [8-10] From previous work, anodic Plasma Electrolytic Aluminating (PEA, also named as Plasma Electrolytic Deposition) could be applied on cast iron and steel to grow the Alumina coating. [11] However, the porous structure of PEA alumina coating causes sample facing pitting corrosion and crevice corrosion.

Nickel as a metallic material has good anti-corrosion property because there is a compact anti-corrosion oxidation layer like aluminum, but it still will be slowly corroded. [12] Electrical plating is harmful to both humans and the environment, so electroless nickel plating, which could be safely disposed, is a better choice. [13-14] Electroless nickel has a more compact structure than electroplated nickel, because the deposition rate is slow (25  $\mu\text{m}$  per hour on average). However, electroless nickel plating has poor wear resistance. [15-16] To avoid these disadvantages and to maximize these advantages of alumina and nickel, producing the composite coating is a desired method. Applying nickel plating can fill up the micropores and crevices of alumina, preventing the corrosive liquid and dirt from contacting the metal substrate. [17] Additionally, nickel only occupy the micropores, so same amount of nickel will grow thicker on alumina coated sample than bare sample. Because the rate of nickel-plating corroding is depending on the thickness, Ni-Alumina coated sample could have better life length. [16] [18-19] Therefore, Ni-Alumina coating is valuable to be discussed. The mechanism of electroless nickel plating on alumina-coated cast iron is also valuable to understand the feasibility and increase the efficiency. If nickel only cover the top surface of alumina but not occupying the pits, the structure will still be corroded after the nickel layer get worn off or corroded.

The anti-wear and anti-corrosion behaviours of PEA Alumina coating and Ni-Alumina coating on cast iron were not comparatively investigated. In addition, the wear mechanisms of two coatings are likely different. The Coefficient of Friction of PEA Alumina coating on cast iron is much lower than the COF of Plasma Electrolytic Oxidization (PEO) Alumina coating on aluminum, and this phenomenon may come from the ferrous oxide co-existed in the PEA Alumina coating. [11] [20] This work also included

500°C heat treatment on the coated cast iron; at such a temperature, the ferrous oxide could be fully oxidized to become ferric oxide, which might affect the wear behaviours. [20] Therefore, it could be reversely proved the contribution from the ferrous oxide which may reduce friction and thus a better wear behaviour than ferric oxide.

### ***1.2 Objectives***

- 1) To generate PEA Alumina coatings and Ni-Alumina coatings on gray cast iron and study the deposition process
- 2) To investigate wear behaviours of PEA Alumina coatings and Ni-Alumina coatings using Pin-on-Disk tribology tests, SEM and EDX analysis
- 3) To comparatively study the wear behaviours of PEA Alumina coatings at 500°C post-heated vs non heat treatment conditions
- 4) To analyze anti-corrosion behaviours of coatings by electrochemical tests

### ***1.3 Organization of This Thesis***

This thesis is divided in seven chapters. In Chapter 1, the introduction of the research project is presented, which includes the motivation, research objectives and the organization of the thesis. Chapter 2 shows the literature review including generating thin film coating, anti-wear and anti-corrosion behaviours. The experimental methodologies are introduced in Chapter 3. In Chapter 4, the coating generating mechanisms, morphology and chemical composition of PEA Alumina coating and Ni-Alumina coating on gray cast iron is described. The wear behaviours including COF and wear track analysis as well as the wear mechanisms of coatings is discussed in Chapter 5. Chapter 6 introduces the corrosion behaviours by EOC, Rp and EIS analysis. The present works and future works are concluded in Chapter 7.

## CHAPTER 2

### Literature Review

#### ***2.1 Methods of Generating Thin Film Coatings***

##### ***2.1.1 Electroplating***

Ferrous alloys (iron and steel) are commonly used engineering materials, but unfortunately, they are often susceptible to rusting. To address this issue, electroplated metallic coatings (such as Zinc, Chromium and nickel) and conversion treatments such as chromating or phosphating are widely used, but the process of them are usually toxic to some degree. [7] [20-23] Cyanide from the electroplating baths,  $\text{Cr}^{6+}$  from Chromium plating, and high concentration of  $\text{PO}_4^{3-}$  in bath residue are harmful to human body and to the environment. [24-26] The electroplating chromium process was illustrated in Figure 2.1 with plating bath solution of  $\text{HCrO}_3$  and  $\text{H}_2\text{SO}_4$ . The anode is connected to the bath, and the cathode is connected to the part to be plated. Cr starts depositing when ions separate from the chemical bath due to the current flow to the part. The current flow and the duration process will vary depends on the size of specimen. [27-28] The general current density to apply electroplating chromium is  $0.3\text{-}0.4 \text{ A/cm}^2$ , and the deposition rate is  $25\text{-}30 \text{ }\mu\text{m}$  per hour. [27]

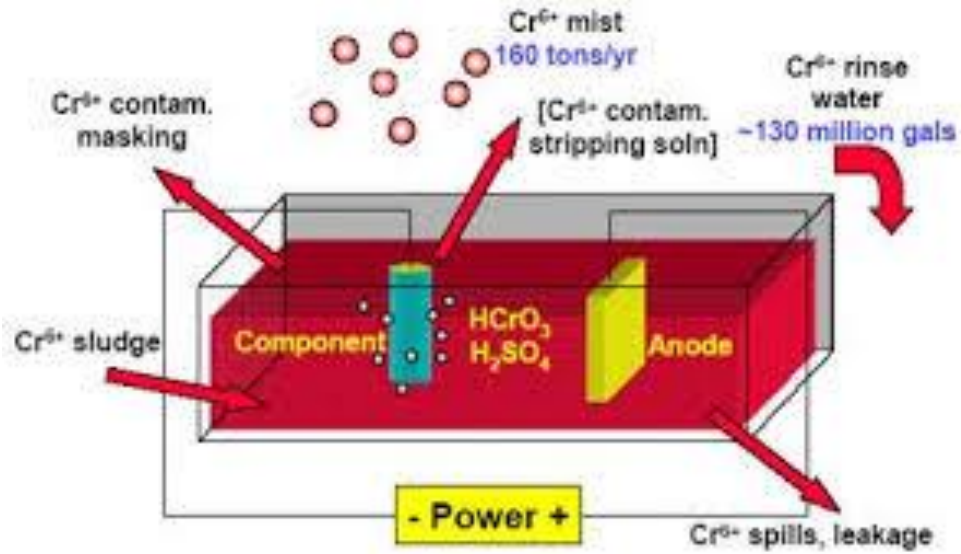


Figure 2.1 Illustration of electroplating chromium process [27]

Figure 2.2 is illustrating the Scanning Electron Microscopy (SEM) images of surface morphology of electroplated nickel on copper. [29] The plating bath containing 300 g/L nickel sulfate ( $\text{Ni}_2\text{SO}_4 \cdot 6\text{H}_2\text{O}$ ), 30 g/L nickel chloride ( $\text{NiCl}_2 \cdot 6\text{H}_2\text{O}$ ), and 30 g/L boric acid ( $\text{H}_3\text{BO}_3$ ). Saccharin is added in the solution to explore the effects on grain size. In Figure 2.2 (a), the grain size of nickel plating without saccharin is small but the surface is not uniform. Figure 2.2 (b) illustrates the morphology of nickel plating with saccharin, and the surface is bubble-like appearance with small grain size. As shown in Figure 2.2 (c), the grain size of high current density plating is much larger than in low current density. [29-30]

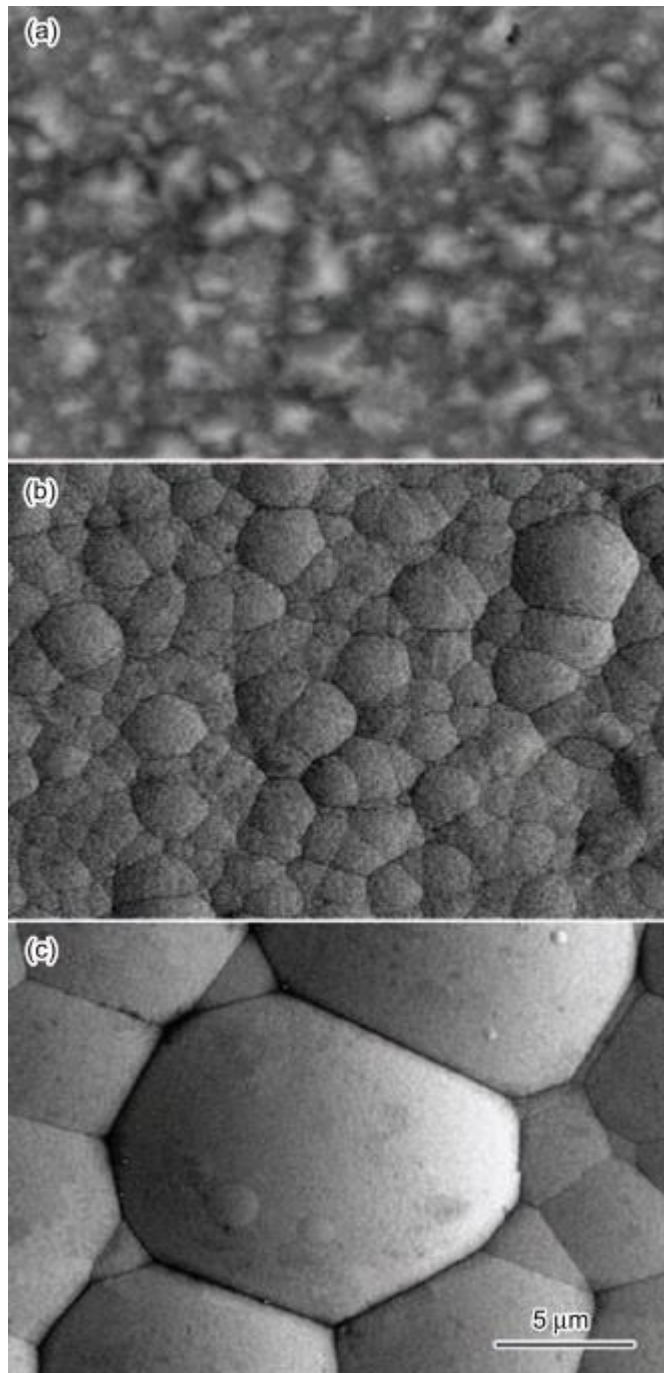


Figure 2.2: SEM micrographs of surface morphology of nickel coatings deposited from:  
(a) a saccharin-free bath at  $i=100 \text{ mA/cm}^2$ , (b) a bath containing 5 g/L saccharin at  $i=100 \text{ mA/cm}^2$ , (c) a bath containing 5 g/L saccharin at  $i=300 \text{ mA/cm}^2$  [29]



### 2.1.2 Electroless Plating

There are 3 main categories in electroless plating: alloy coatings, composite coatings and pure metallic coatings. [31] The formation process is dependent on the reductant and addition of metallic contents into binary electroless plating bath which could form tertiary or quaternary coating layers. [31] In addition, the electroless alloy coating is used on industrial applications because it has short coating duration and a satisfactory cost. The electroless composite coatings are generated by adding particles into the plating bath such as alumina, Teflon and so on. Different additions could provide different characteristics in impact, wear and corrosion resistances. [32-35] Electroless metallic coating is always referring to electroless pure nickel plating. This coating could provide high hardness, good anti-wear and anti-corrosion performances. [31] [35] The applicable plating materials in three categories are summarized in Figure 2.3.

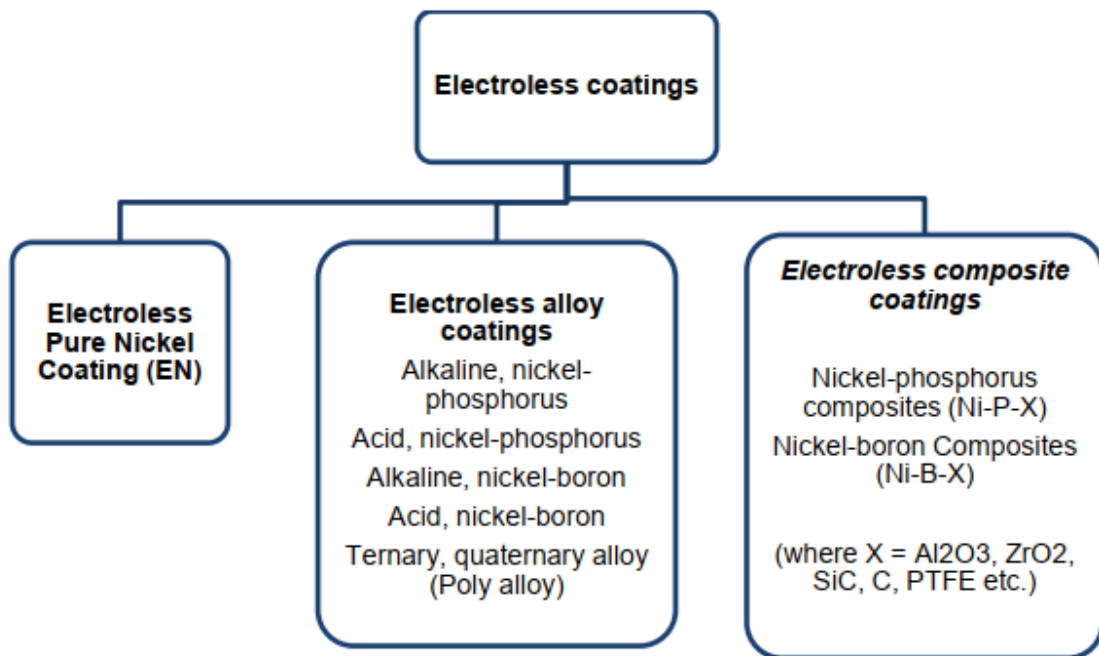


Figure 2.3: Types of electroless coatings [32]

Nickel plating can only generate on ferrous or nickelic metals directly, and a catalyst is required while plating on other materials. [36-37] The surface of sample needs to be degreased by 10 g/L  $\text{Na}_3\text{PO}_4$  and 50 g/L NaOH bath above 60 °C before electroless plating. [38-39] The acidic plating bath mainly consists of 10 g/L basic nickel carbonate ( $\text{NiCO}_3$ ), 5 g/L citric acid ( $\text{C}_6\text{H}_8\text{O}_7$ ), 20 g/L sodium hypophosphite ( $\text{NaH}_2\text{PO}_2$ ), 10 g/L ammonium bifluoride ( $\text{NH}_4\text{HF}_2$ ), and the generating temperature is 80 °C. [38] In addition, higher bath temperature results in a higher plating speed, which is illustrated in Figure 2.4. [39]

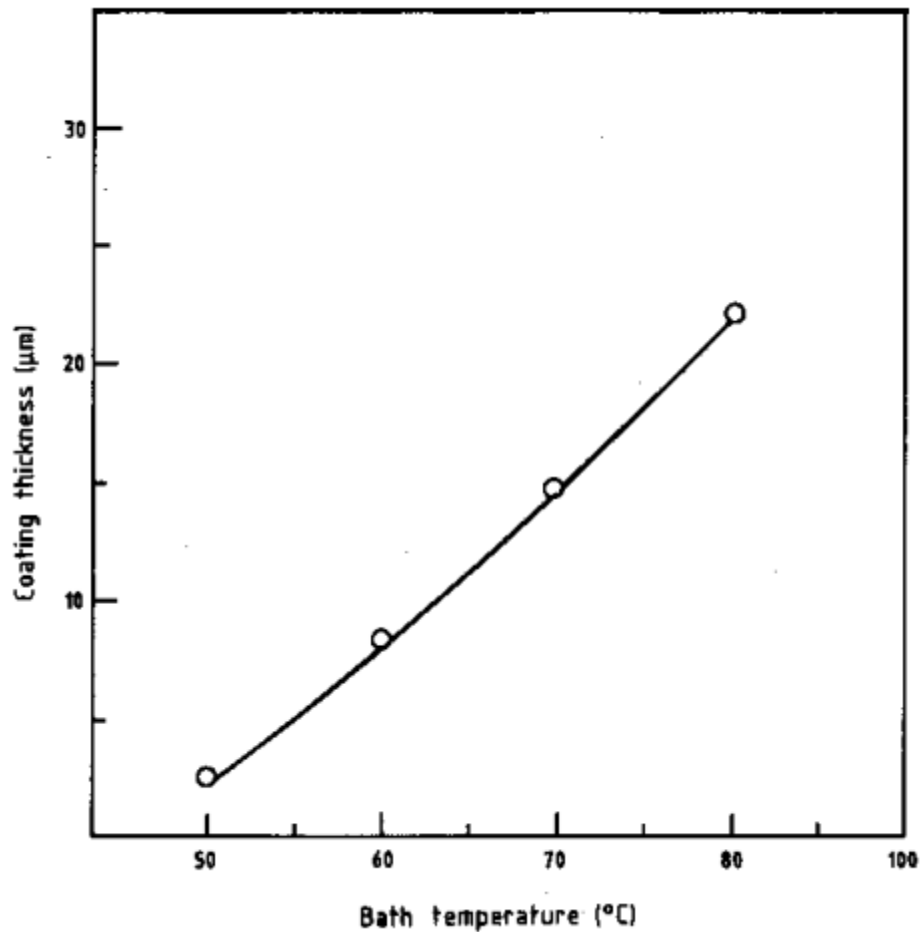


Figure 2.4: Influence of bath temperature on coating growth (pH = 6.5, 60 min) [39]

### 2.1.3 Thermal Spray Coating

Figure 2.5 is illustrating the thermal spray process. Metallic, ceramic or some polymer materials in forms of powder or rod are heated to their melting points. The melted materials are accelerated in a gas stream and sprayed on the surface to be coated. [40] Thermal spray coating can form a thick coating. [41] Additionally, thermal spray coating can be applied on many kinds of materials, including damaged parts that could be recoated without complicated treatments. A wide variety of materials could be melted and sprayed as coating materials. [42-43] Therefore, it is a commonly used coating method applied to many industrial applications. However, required line-of-sight from the spray gun head means the process cannot be done on complicated surfaces, which is the main disadvantage of thermal spraying process. [41]

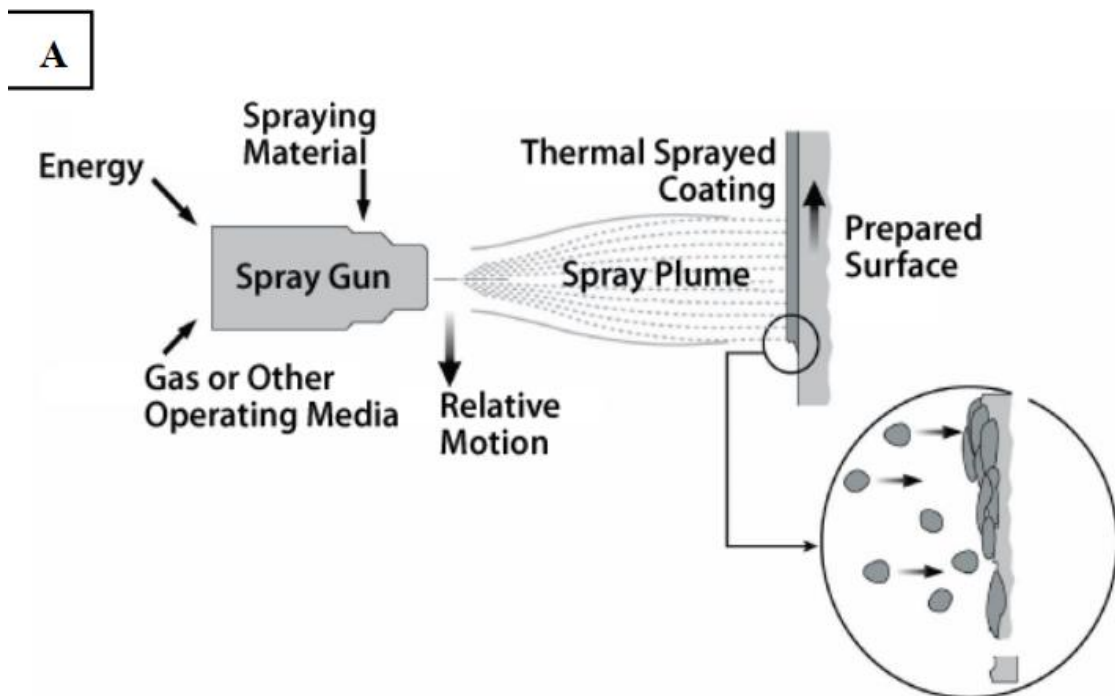


Figure 2.5: General schematic diagram of thermal spray coating process [40]

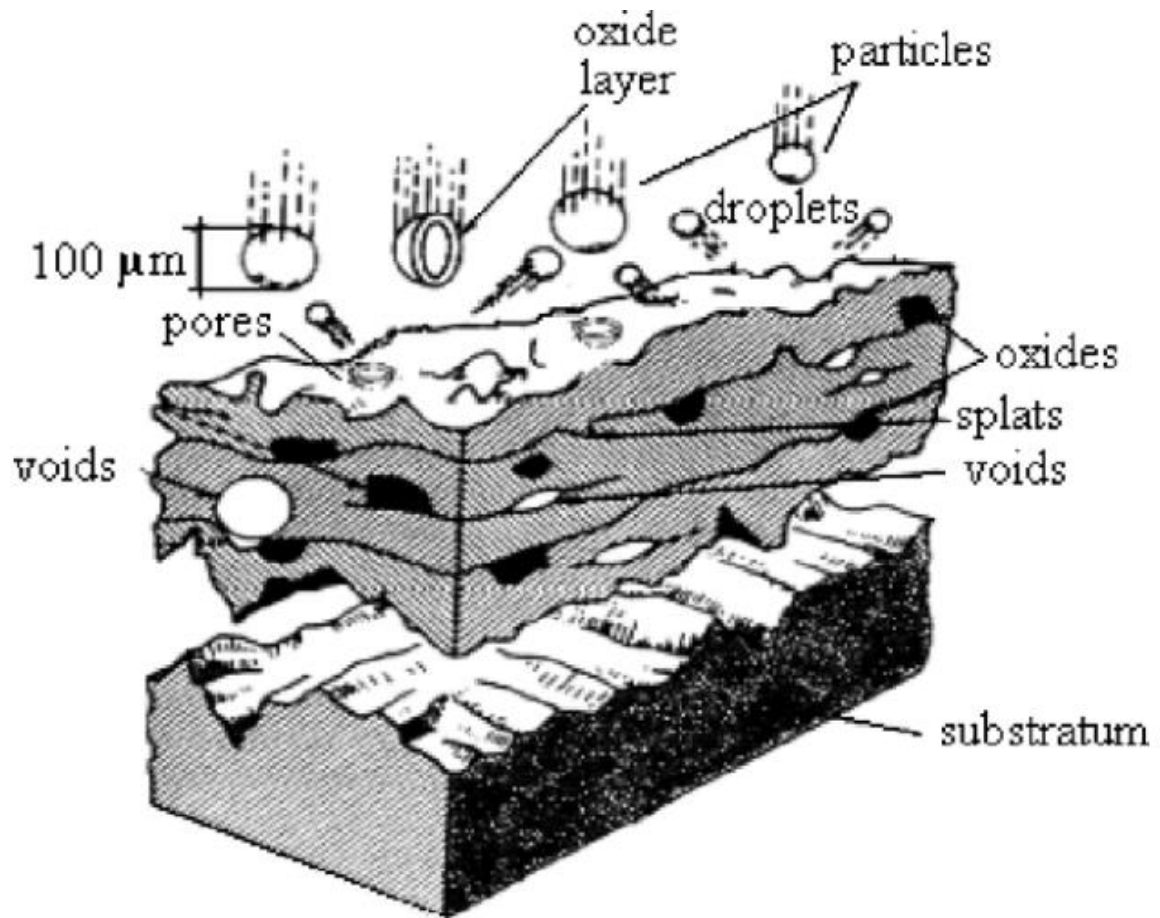


Figure 2.6: Schematics of the coating layer formation following deposition by a thermal spray process [43]

Figure 2.6 is a schematic draft of coating layer in thermal spraying process. There are voids, splats and oxides inside the coating and pores on the surface explored. [43] The thermal sprayed coating usually has a porous structure and crack due to the ununiformed heating on the surface. [44-45] The particle size of molten could affect the morphology of thermal sprayed coating. Smaller particles could make a coating with less pores and roughness than larger particles. [45]

### 2.1.4 Physical Vapour Deposition Coating

Physical vapour deposition (PVD) is a widely used thin film coating process. This process can provide an improved wear behaviour, optical enhancement and many other fields. [46-47] In some special cases, to increase the durability, to decrease friction, and to improve thermal properties, chemical vapour deposition (CVD) method is with PVD. [46] However, the CVD process is applied only in essentials because it results in high temperature and high stress to the coatings and substrate. [48-52] In addition, PVD coating process also has a line-of-sight problem, which cannot deposit coatings on complicated surfaces. [41] In order to improve these problems, the PVD process is optimized by increasing plasma ionization and deposition rate, improving the target metals, and decreasing area without depositions. [46]

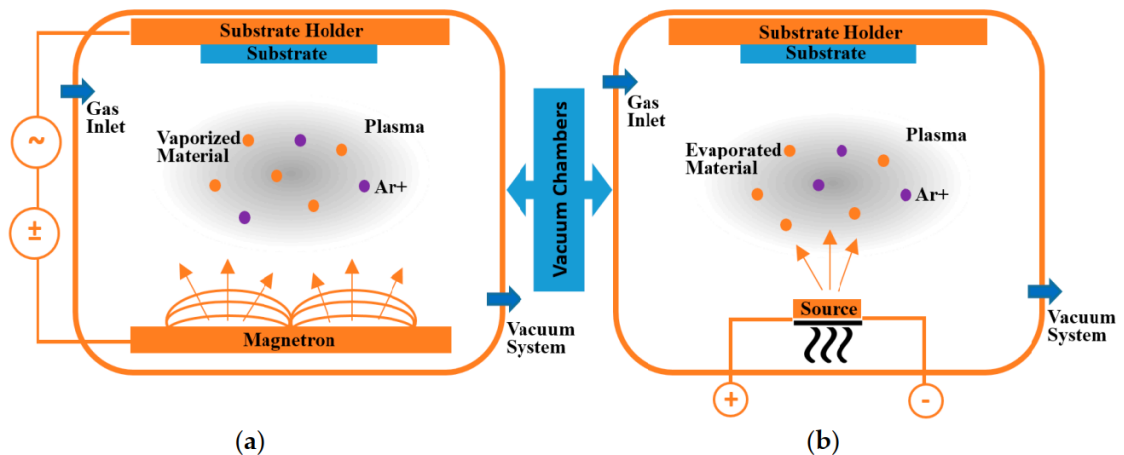


Figure 2.7: Schematic drawing of two conventional PVD processes: (a) sputtering and (b) evaporating using ionized Argon ( $Ar^+$ ) gas. [46]

Figure 2.7 is illustrating the Physical Vapour Deposition (PVD) processes of (a) sputtering and (b) evaporating. Sputtering process do not need a high vacuum environment,

but the deposition speed is low. Evaporating process needs to generate in high vacuum, and the deposition rate is high. [53-54] The PVD coatings generated by sputter process have higher adhesion and absorption than coatings by evaporating process. [55-56]

### ***2.1.5 Plasma Electrolytic Oxidation Coating***

PEO alumina coating is environment-friendly process usually used on aluminum and magnesium alloys, which is nontoxic and chemical stable on both acid and basic liquid. However, PEO coatings can only generate on valve metals such as aluminum and magnesium. [57]

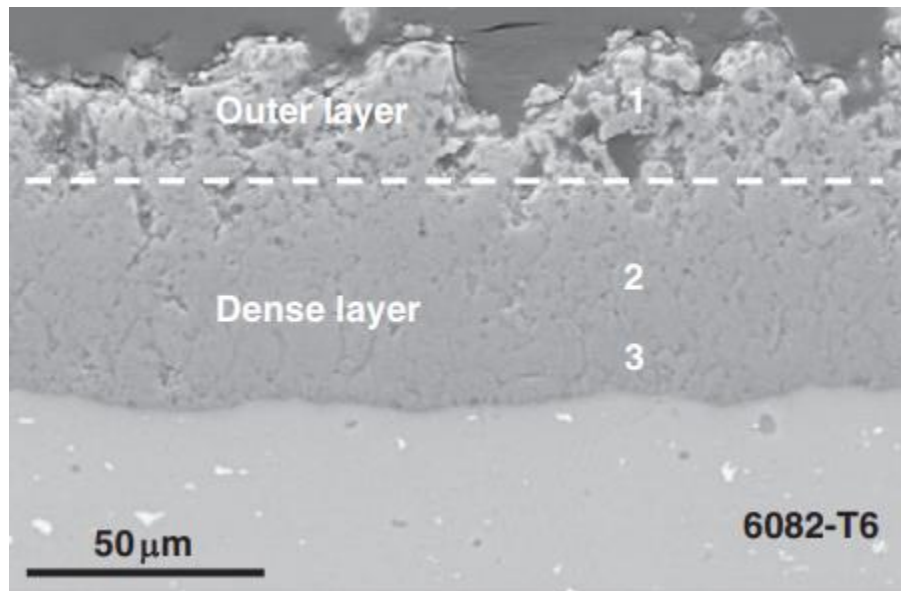


Figure 2.8: Backscattered scanning electron micrographs of the cross sections of PEO coating on 6082-T6 Al alloy [58]

As is shown in Figure 2.8, the PEO coating is generated on 6082-T6 Aluminum alloy. The coating is made from two parts which are inner layer and outer layer. Plenty of micropores and voids are found on the outer layer. The inner layer has a dense structure with less voids and crevices.

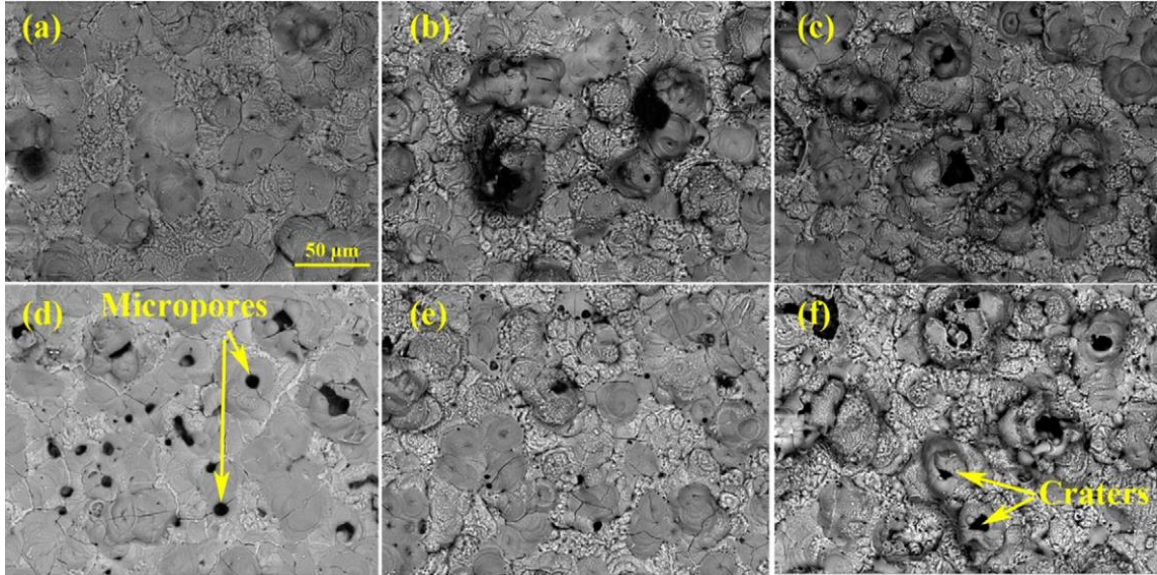


Figure 2.9: Surface morphology of  $\text{Al}_2\text{O}_3$  and  $\text{Al}_2\text{O}_3/\text{TiO}_2$  composite coatings produced using unipolar and bipolar waveforms: a) S1W1, b) S1W2, c) S1W3, d) S2W1, e) S2W2 and f) S2W3 [59]

Figure 2.9 is illustrating the surface morphologies of (a-c)  $\text{Al}_2\text{O}_3$  coatings and (d-f)  $\text{Al}_2\text{O}_3/\text{TiO}_2$  composite coatings. W1, W2 and W3 are representing 0, 0.2 and 0.4 cathodic duty ratios under frequency of 2 kHz and 0.2 anodic ratio, respectively. S1 and S2 are referring to  $\text{Al}_2\text{O}_3$  coatings and  $\text{Al}_2\text{O}_3/\text{TiO}_2$  composite coatings, respectively. Figure 2.10 is illustrating the cross-section views of coatings corresponding Figure 2.9. The coatings within same materials have similar thicknesses but different roughness. Higher cathodic ratio has a rougher surface, but less voids and pores are found. Therefore, applying a 0.4 of cathodic duty ratio could make the coating denser. [57] [60-61] Adding  $\text{TiO}_2$  nanoparticles could make the coatings have smoother surface. [62-63]

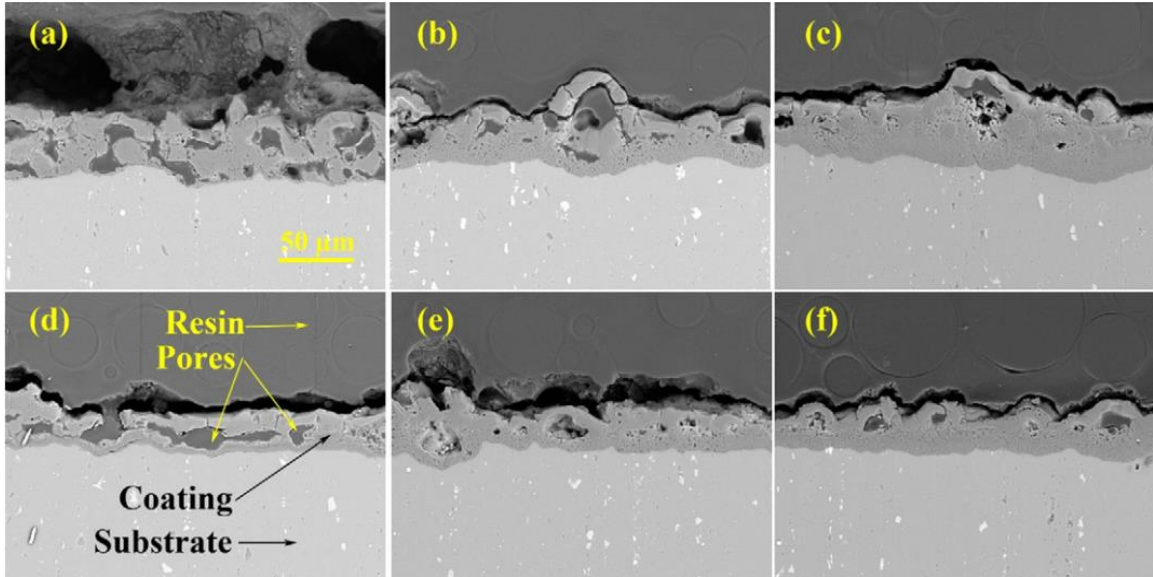


Figure 2.10: SEM cross-section images of Al<sub>2</sub>O<sub>3</sub> and Al<sub>2</sub>O<sub>3</sub>/TiO<sub>2</sub> composite coatings produced using unipolar and bipolar waveforms: a) S1W1, b) S1W2, c) S1W3, d) S2W1, e) S2W2 and f) S2W3 [59]

### ***2.1.6 Plasma Electrolytic Aluminating Coating***

An alumina coating cannot be formed on cast iron by a regular PEO process since the isolating passive film cannot be created. Therefore, Plasma Electrolytic Aluminating (PEA) method was applied to generate alumina coating on some ferrous alloys. [11] In Figure 2.11 (a), there are Al(OH)<sub>4</sub><sup>-</sup> ions surrounding the cast iron sample. Then the Fe<sup>2+</sup> ions were dissolved into the electrolyte while applying anodic current, as shown in Figure 2.11 (b). In (c), the Fe<sup>2+</sup> ions combine with the Al(OH)<sub>4</sub><sup>-</sup> ions and form a hercynite (FeAlO<sub>2</sub>) thin film on the surface of the cast iron substrate. Residual Al(OH)<sub>4</sub><sup>-</sup> ions transferred into Al<sub>2</sub>O<sub>3</sub> sintering with FeAlO<sub>2</sub> after the hercynite layer fully covered the cast iron substrate, as shown in (d).



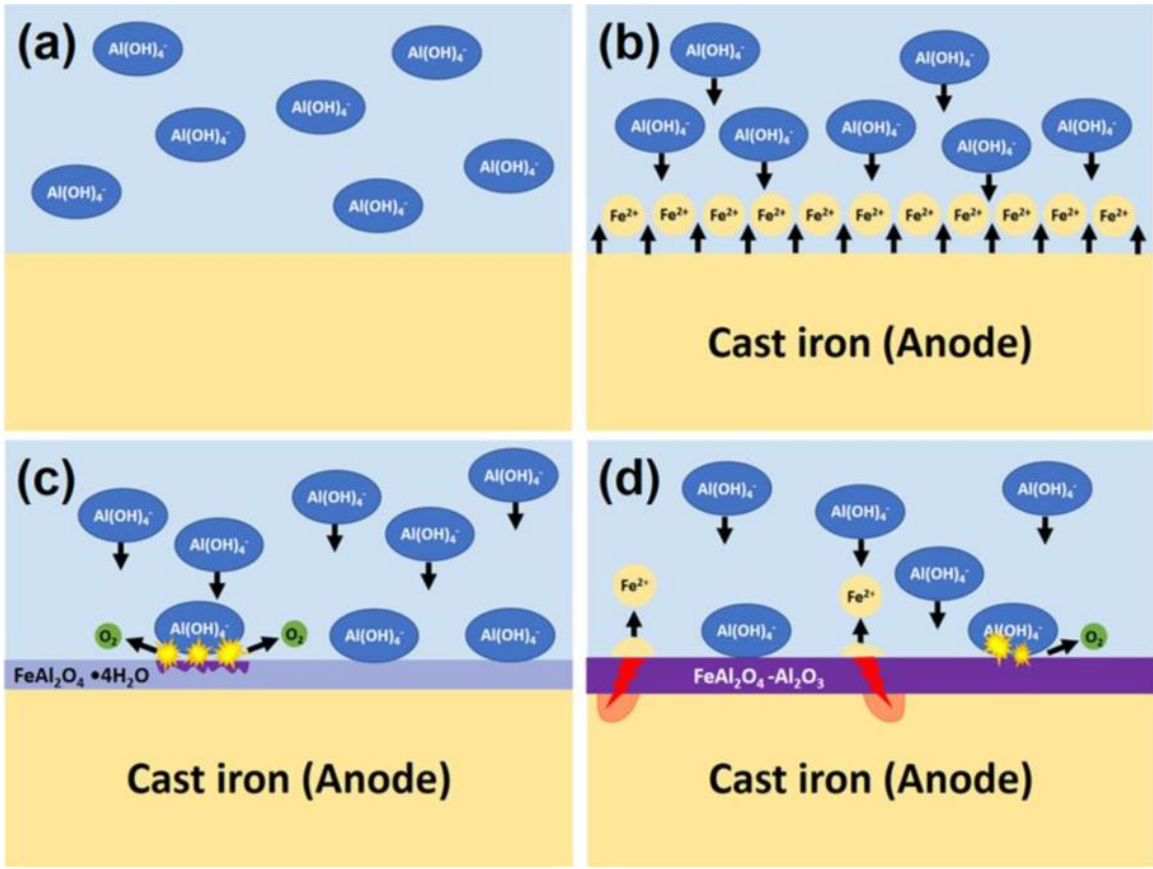


Figure 2.11: Schematic illustration of the PEA of cast iron. (a) System before applying current, (b) dissolution of iron into the electrolyte and migration of  $\text{Al(OH)}_4^-$  anions toward the anode after applying current, (c) formation of hercynite film on the iron surface and the initiation of plasma discharge sparks, and (d) growth of the hercynite-alumina composite ceramic coating via strong plasma discharge. [11]

## 2.2 Wear Behaviours of Materials

### 2.2.1 Wear Behaviours of Alloys

Figure 2.12 is illustrating the Coefficient of Friction (COF) results of lubricated AISI-D2 and P2-I cold-work tooling steels under 500 N normal load.

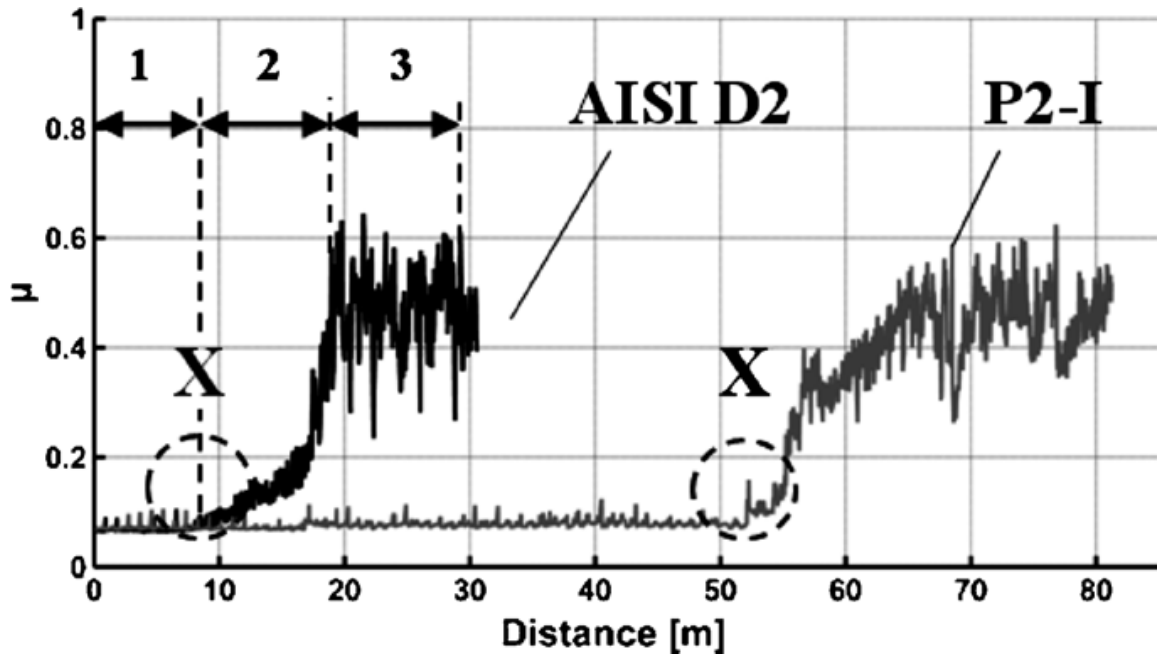


Figure 2.12: Typical friction curves at 500 N load for the investigated tool steels. The point X, shown for the tools, was used as indication of galling [64]

The results are showing that there are 3 stages in the wear tests. The COF remains low at 0.06 in stage 1, and suddenly increase starting at a point X in stage 2. Then the COF is tending to be stable around 0.5 in stage 3. The point X is considered as the galling problem occurring. Because P2-I steel has higher hardness than AISI-D2 steel, the galling behaviour starts later. [65-67] In addition, applying higher normal load could make the galling start earlier. [68-70]

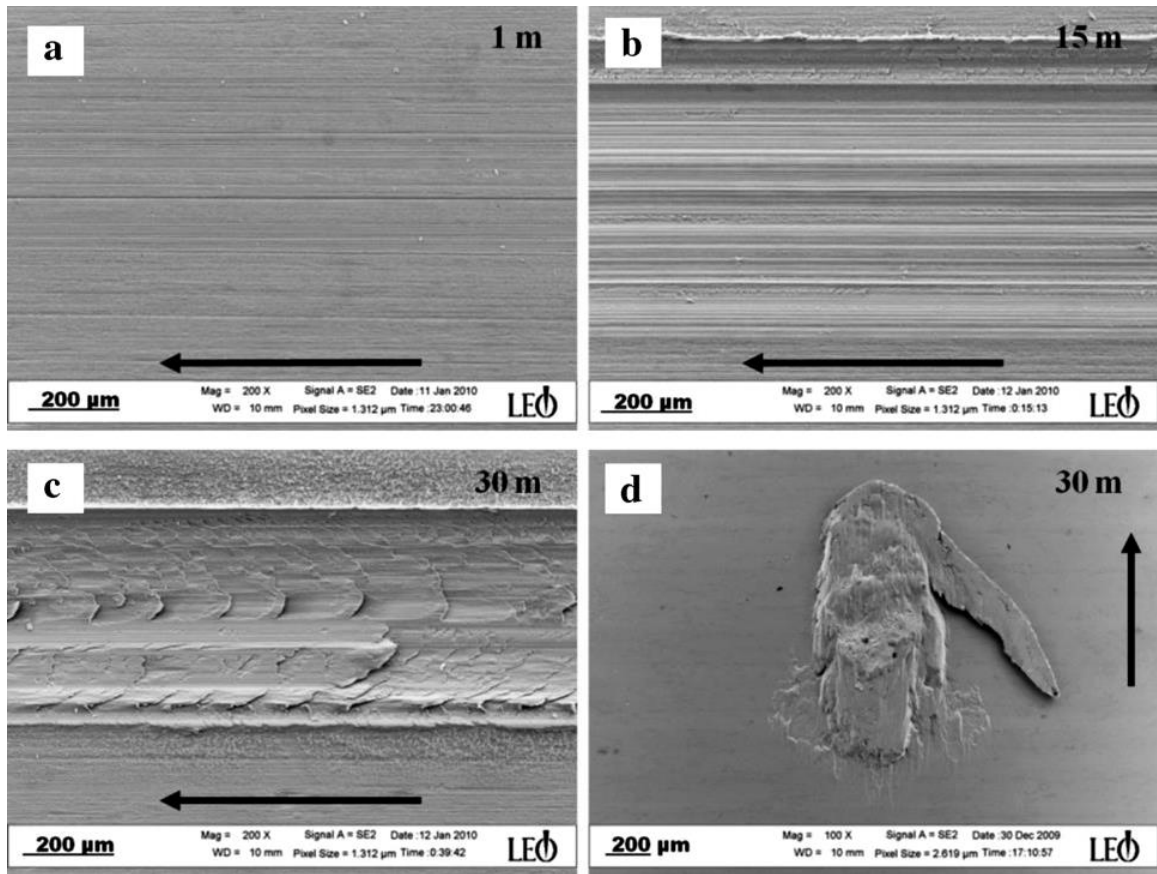


Figure 2.13: Typical wear mechanisms in the different stages. The pictures show the D2 tool material and corresponding worn sheet at 500 N. Arrows indicates disc sliding direction. [64]

Figure 2.13 is illustrating the wear track morphology of (a) in stage 1, (b) in stage 2 and (c) in stage 3. Figure 2.13 (d) shows the tool surface. In stage 1, surface flattening and micro-scratching of the sheet surface were observed, even though friction remained relatively constant and low. In stage 2, coarse scratching of the sheet was observed. In the stage 3, severe adhesive wear of the sheet was the main wear mechanism. [71-72] In the final stage 3, the tool surface was covered by adhered sheet material.

### 2.2.2 Wear Behaviours of Plasma Electrolytic Oxidation Coating

Figure 2.14 is illustrating the Coefficient of Friction (COF) of PEO coatings with different thickness under different normal loads.

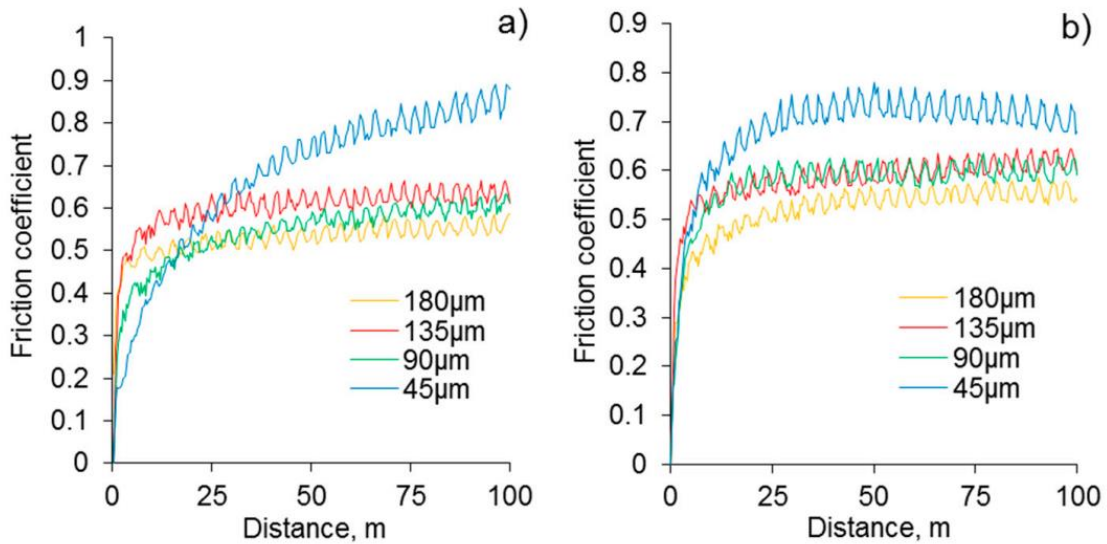


Figure 2.14: Evolution of friction coefficients during LRWT of PEO coatings with different residual thickness (180, 135, 90, and 45  $\mu\text{m}$ ). Normal loads are (a) 5 N and (b) 10 N. The counter-face material is WC-4% [73]

As, shown in Figure 2.14, the COF results at coating thicknesses of 90  $\mu\text{m}$  and 135  $\mu\text{m}$  are similar and they have a range of 0.55-0.6. The 180  $\mu\text{m}$  thick coating has the lowest COF which is 0.45-0.55, and 45  $\mu\text{m}$  thick coating has the highest COF varying from 0.75 to 0.85. Coating thicknesses of 135  $\mu\text{m}$  and 180  $\mu\text{m}$  are locating on the outer layer of PEO coatings, and coating with 45  $\mu\text{m}$  in thickness contains only the inner layer. The thickness of 90  $\mu\text{m}$  is located on the intermediate region between inner and outer layers. Therefore, the outer layer of PEO coating has lower COF than the inner layer. [73-75]

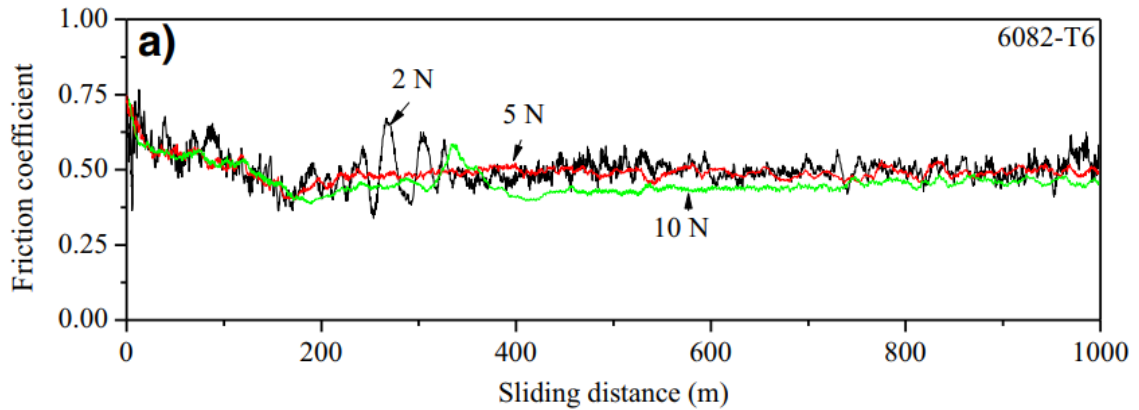


Figure 2.15: Friction coefficients of PEO 6082-T6 alloy [58]

In Figure 2.15, an applied 2 N and 5 N normal force have not made a significant difference in COF, but the sample against 10 N has a slightly lower COF. The average COFs of PEO coatings on 6082-T6 Al alloy under 2 N, 5 N and 10 N are about 0.5, 0.5 and 0.4, respectively.

In Figure 2.16 (a) and (b), a 10 N force makes a wider and uniform wear track, causing more damage to the coating. In (c) and (d), the wear tracks are covered by the material transfer layer, some transfer layer particles are chipped off in a 10 N test. Figure 2.16 (e) and (f) illustrate the cross-section of PEO 6082-T2 Al alloy with (e) 2N and (f) 10 N in normal load. Applying 2 N, the material transfer layer is adhering on the coating surface, and the coating is keeping intact. However, the outer coating surface is damaged by the 10 N force, so the tool ball is sliding with the inner surface of coating. That could explain why 10 N load on PEO coating has a lower COF than 2 N. [73] [76-77]

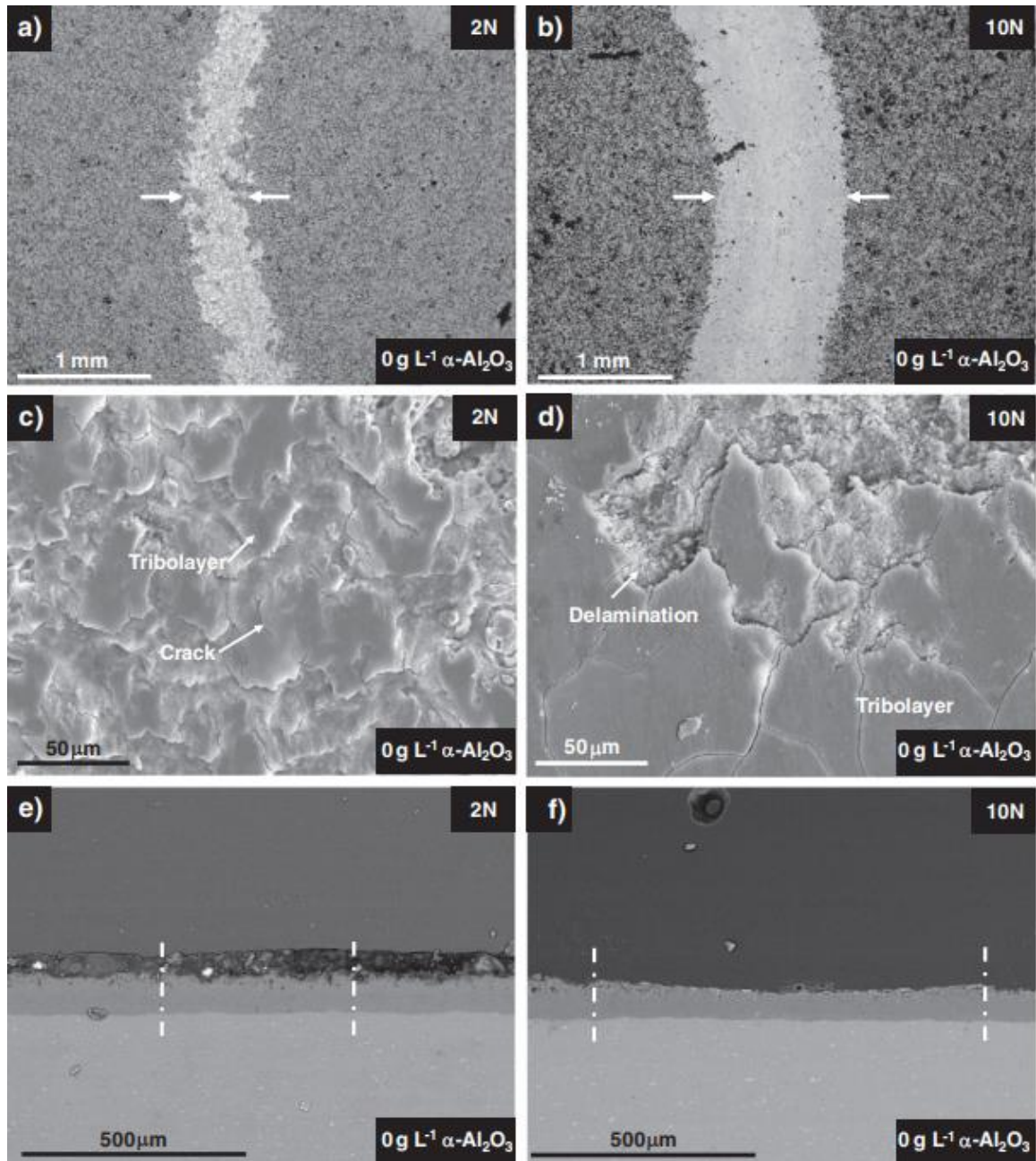


Figure 2.16: (a, b, c, d) Plan views and (e, f) cross-sections of the wear tracks of PEO coating without added particles. (a, c, e) 2 N 1000 m and (b, d, f) 10 N 1000 m [58]

### 2.3 Anti-Corrosion Behaviours of Materials

Pitting corrosion is extremely destructive and undiscoverable, which causes materials to fail because of perforation of whole structure with a slight weight loss. It is often difficult to be detected because the size of pits is small, and are often covered by corrosion products. In addition, pits could grow deeper and wider, so that increases difficulty to measure the extent of pitting. [78]

#### 2.3.1 Anti-corrosion Behaviours of Alloys

Figure 2.17 is illustrating the corrosion rates of steel immersing into different corrosive solutions at 22 °C and 50 °C.

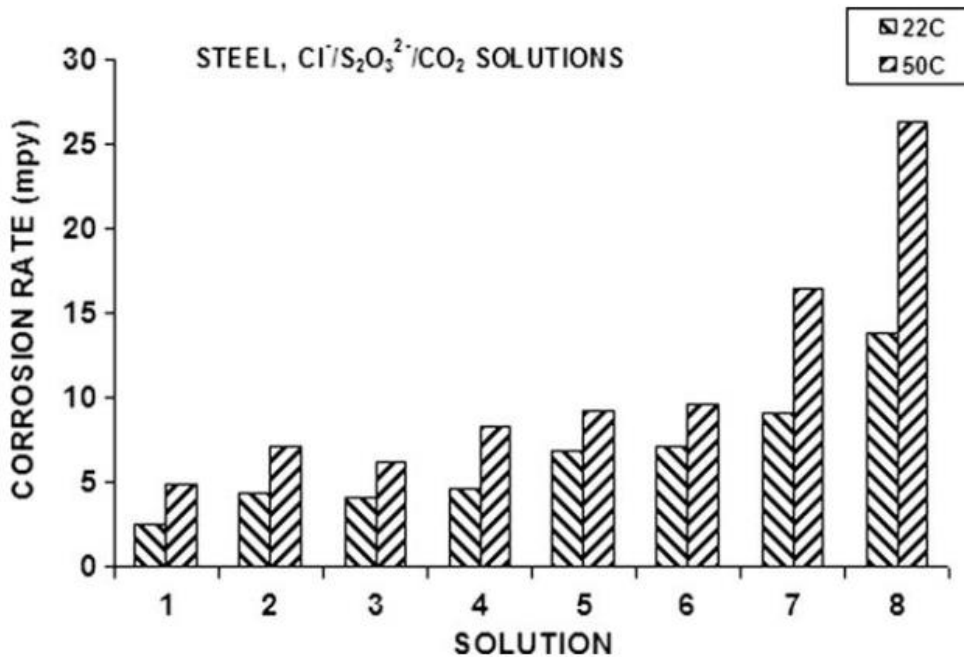


Figure 2.17: Effect of temperature on the corrosion rates of steel in  $\text{Cl}^-/\text{S}_2\text{O}_3^{3+}/\text{sat. CO}_2$  system; (1) 1 M NaCl, (2) 1 M NaCl +  $\text{CO}_2$  (sat.), (3) 1 M NaCl + 0.01 M  $\text{Na}_2\text{S}_2\text{O}_3$ , (4) 1 M NaCl + 0.1 M  $\text{Na}_2\text{S}_2\text{O}_3$ , (5) 1 M NaCl + 1.0 M  $\text{Na}_2\text{S}_2\text{O}_3$ , (6) 1 M NaCl + 0.01 M  $\text{Na}_2\text{S}_2\text{O}_3$  +  $\text{CO}_2$  (sat.), (7) 1 M NaCl + 0.1 M  $\text{Na}_2\text{S}_2\text{O}_3$  +  $\text{CO}_2$  (sat.) and (8) 1 M NaCl + 1.0 M  $\text{Na}_2\text{S}_2\text{O}_3$  +  $\text{CO}_2$  (sat.). [79]

From Figure 2.17, higher temperatures could increase the corrosion rate. Adding more saturated carbon dioxide (CO<sub>2</sub>) in a corrosive solution could increase the corrosion rate. [80-84] The amount of Na<sub>2</sub>S<sub>2</sub>O<sub>3</sub> in solution is also of a factor, and more Na<sub>2</sub>S<sub>2</sub>O<sub>3</sub> added causes higher corrosion rate. [82]

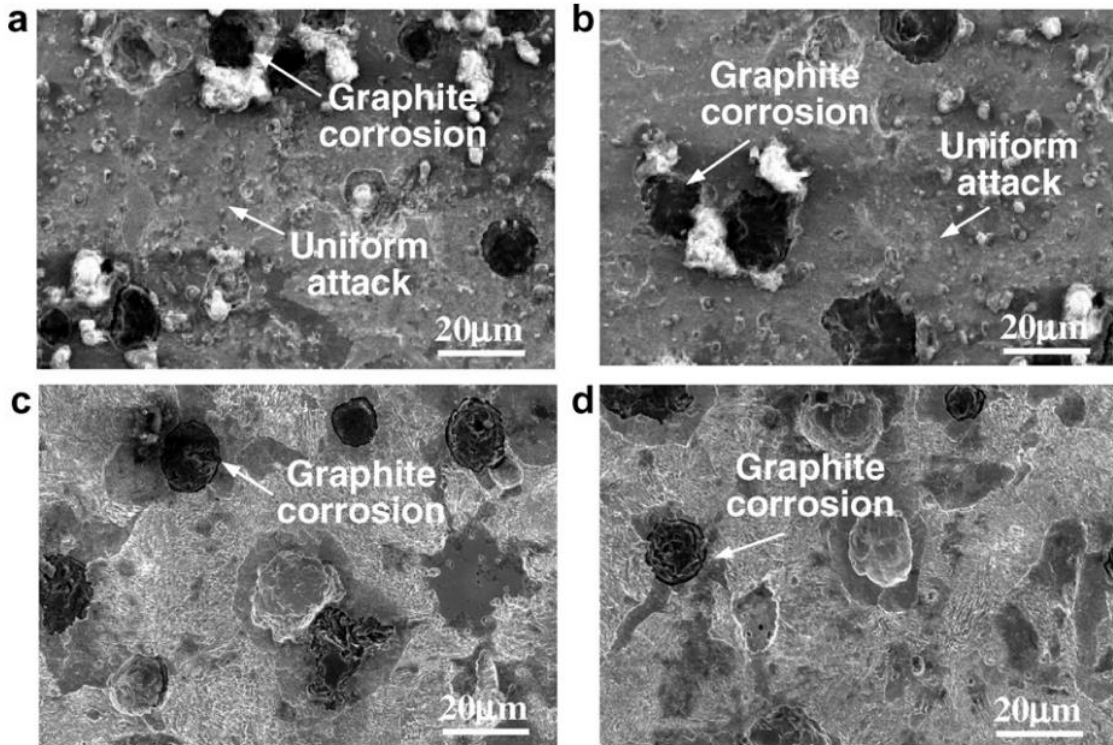


Figure 2.18: Surface appearance of the corroded irons after the polarization tests: (a) DI, (b) 4%Ni-DI, (c) ADI, and (d) 4%Ni-ADI. [85]

Figure 2.18 shows the SEM images of the four irons after a polarization test. DI, ADI, 4%Ni-DI and 4%Ni-ADI are referring to unalloyed ductile iron, austempered ductile iron, 4% Nickel alloyed ductile iron and 4% Ni alloyed austempered ductile iron. As shown in Figure 2.18 (a) and (b) of the as-cast samples, the matrix (anode) around the graphite (cathode) is severely corroded to form white FeCl<sub>2</sub> ( $\text{Fe}^{2+} + 2\text{Cl}^- = \text{FeCl}_2$ ) and graphite



particles are peeled off. There was a mixed type of graphitic corrosion and uniform attack. As shown in Figure 2.18 (c) and (d), there was much less corrosion around the graphite, and a uniform attack was not obvious due to the occurrence of retained austenite in the matrix. [86-87]

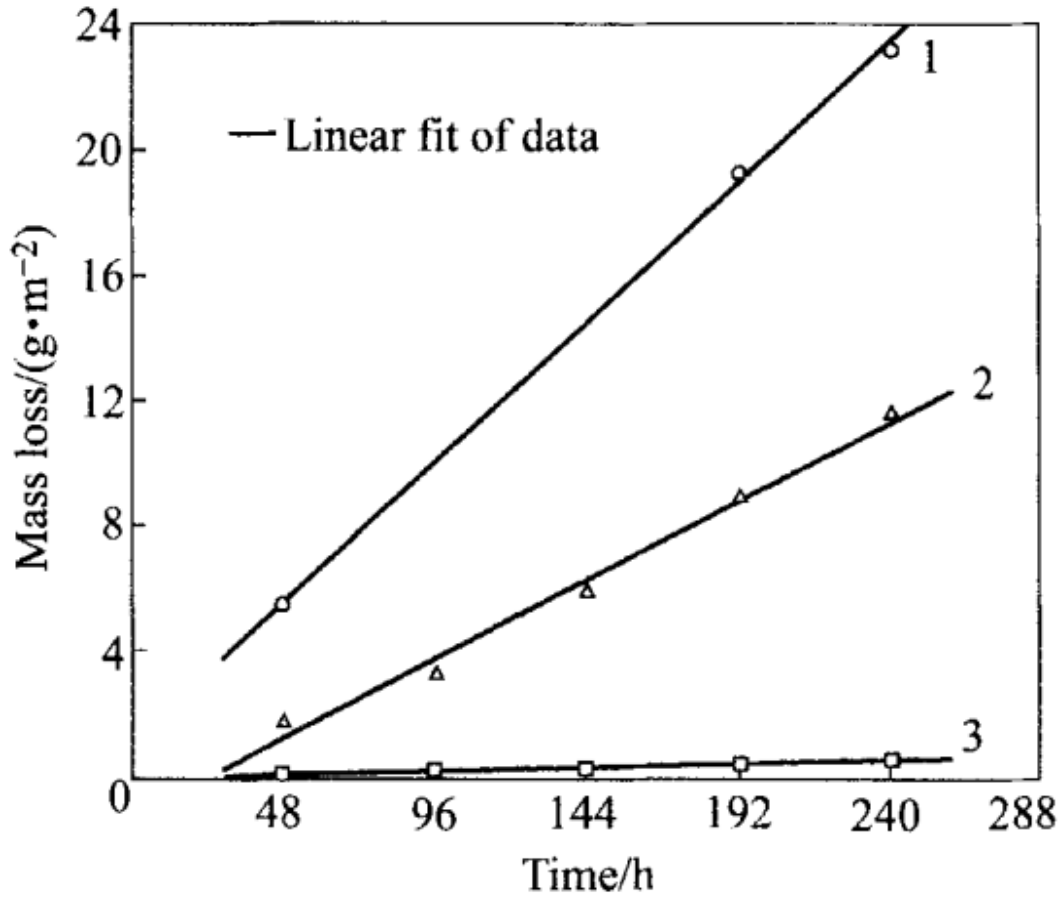


Figure 2.19: Mass loss of LY12 Al alloy vs test time in different solutions: 1-0.02 mol/L NaHSO<sub>3</sub>+0.006 mol/L NaCl; 2-0.02 mol/L NaHSO<sub>3</sub>;3-0.006 mol/L NaCl; (a) With cladding; (b) Without cladding [88]

As is shown in Figure 2.19, both NaHSO<sub>3</sub> and NaCl are the factors causing weight loss, and NaHSO<sub>3</sub> could react more in weight loss. There is a linear relationship between

immersing time and mass loss, in which the sample will be corroded more severely with the test duration. [79-81]

### 2.3.2 Anti-corrosion Behaviours of Plasma Electrolytic Oxidation Coating

Figure 2.20 is illustrating the Polarization Resistance ( $R_p$ ) of PEO coatings with different coating conditions corresponding to Figure 2.10.

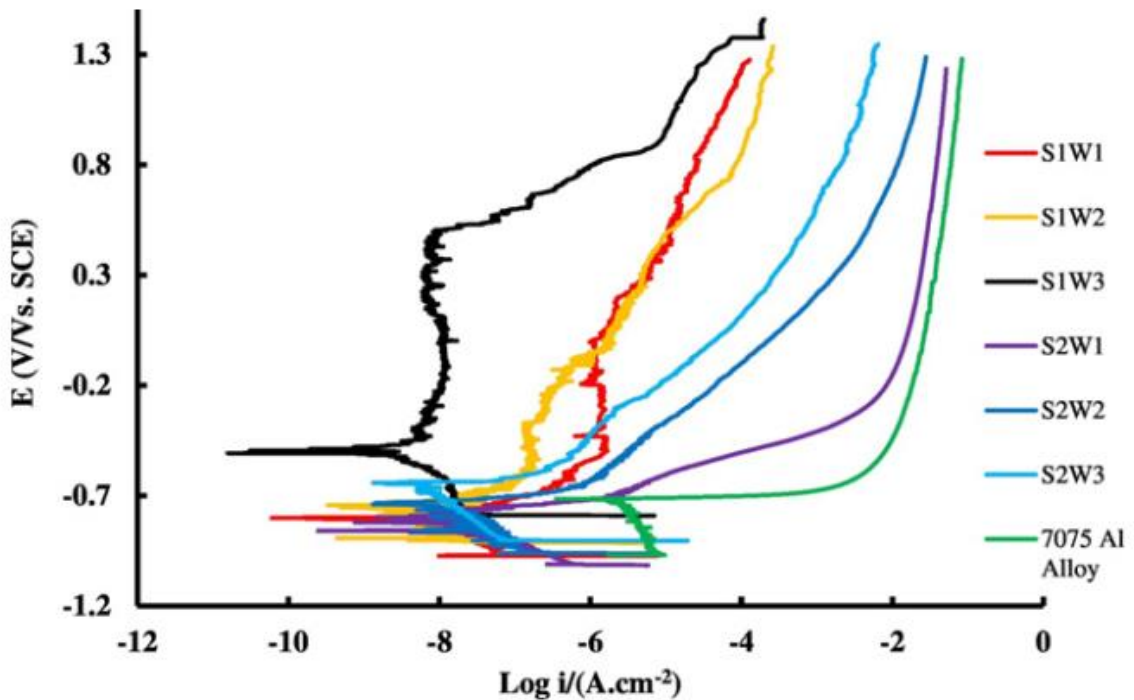


Figure 2.20: Potentiodynamic polarization plots for the coated specimens and 7075 aluminum alloy substrates as the reference. The tests are performed in 3.5% NaCl solution at pH 4 after 1 h immersion at 1 mV S<sup>-1</sup> [59]

From the results shown in Figure 2.20, samples without TiO<sub>2</sub> particles could form perfect passive layers. Higher cathodic ratio has higher corrosion potential, which refers to a low thermodynamic tendency of corrosion. Reviewing from Figure 2.10, the coating with

a higher cathodic ratio has less micropores and cracks on the surface. Therefore, the 0.4 cathodic ratio PEO coating has protected the sample from pitting corrosion. [89-90] In addition, bi-polar PEO coated sample has better corrosion resistance than unipolar coated one. [91]

## ***2.4 Summary***

There are several methods of forming thin film coatings to protect the substrate materials from wear and corrosion. The advantages and disadvantages of electroplating, electroless nickel plating, Thermal Spraying (TS), Physical Vapour Deposition (PVD), Plasma Electrolytic Oxidation (PEO) and Plasma Electrolytic Aluminating (PEA) are discussed. Electroplating is a low-cost method, but it could produce biohazard to human bodies and the environment. Electroless nickel plating could make a low-roughness coating, but the coating growth rate is slow. Thermal spray coating could be applied on a wide range of component materials to be coated, but the line-of-sight issue causes that it could only be applied on components with certain size and shape. PVD method could form ceramic coatings with low roughness, but the cost is very high. PEO coating can only be applied on valve metals such as aluminum and magnesium, but it could not generate on steel or cast iron. PEA Alumina coating is a technique to form aluminum oxide coating on cast iron or steel.

Galling behaviour often happens in the sliding wear tests. The Coefficient of Friction could stay on a low value before galling happens. After galling occurs, the COF significantly increase and stay on a high value, and the specimen is severely damaged. The hardness of contacting materials and the load applied are two factors could influence the wear behaviours. Applying lower load or softer material, the material transfer layer is

adhering on the coating surface, and the coating is keeping intact. Applying higher load or harder counter material, the specimen could be damaged, and weight of material is losing.

Pitting corrosion through pinholes in a coating could make a damage on substrate materials, but it could hardly be discovered before the coating spallation. The corrosion rate is depending on the composition of corrosive solution, temperature and test duration. Increasing the concentration of the solution, temperature and test duration time could obviously increase the corrosion rate. Applying sealing on the coatings could decrease the corrosion rate and adding some additives in the coating could also improve the corrosion resistance.

## CHAPTER 3

### Experimental Details

In this chapter, the experimental procedures including samples preparation and further tests are discussed. Chapter 3.1 is introducing the preparation of bare cast iron and methodologies of creating Plasma Electrolytic Aluminating (PEA) Alumina coatings and Ni-Alumina coatings. The Vickers microhardness tests and Pin-on-Disk (POD) wear tests details are mentioned in Chapter 3.2 and Chapter 3.3. The morphology and chemical compositions observation methods are introduced in Chapter 3.4 and Chapter 3.5. Chapter 3.6 is the electrochemical tests to figure out the anti-corrosion behaviours of PEA Alumina coating and Ni-Alumina coating.

#### ***3.1 Sample Preparation***

Gray cast iron (C: 2.60-3.75%; Mn: 0.60-0.95%; P: 0.12% max; Si: 1.80-3.00%; S: 0.07% max) samples were cut into 15 mm\*15 mm\*4 mm small pieces. They were grinded and polished by abrasive silicone paper (up to grit 1200). The samples after polishing were cleaned by an ultrasonic cleaning machine with acetone to remove redundant particles and grease.

##### ***3.1.1 PEA Alumina Coating***

Polished and cleaned samples were immersed in a stainless-steel tank containing PEA Alumina coating electrolyte. The electrolyte was made from 15-20 g/L  $\text{NaAlO}_2$  and 1-5 g/L  $\text{Na}_3\text{PO}_4$  with a pH value of 12. [11] The samples were connected to the plasma power supply as the anode, and the stainless-steel tank was connected as the cathode (shown in Figure 3.1). To avoid the electrolyte overheating problem, cooling water was necessary to set up in the tank. A pulsed DC current with a frequency of 1kHz, duty cycle of 0.2 at

constant voltage of 510 V was applied on the samples. The coating generating time in each run was 15 min for obtaining a 30  $\mu\text{m}$ -thick coating.

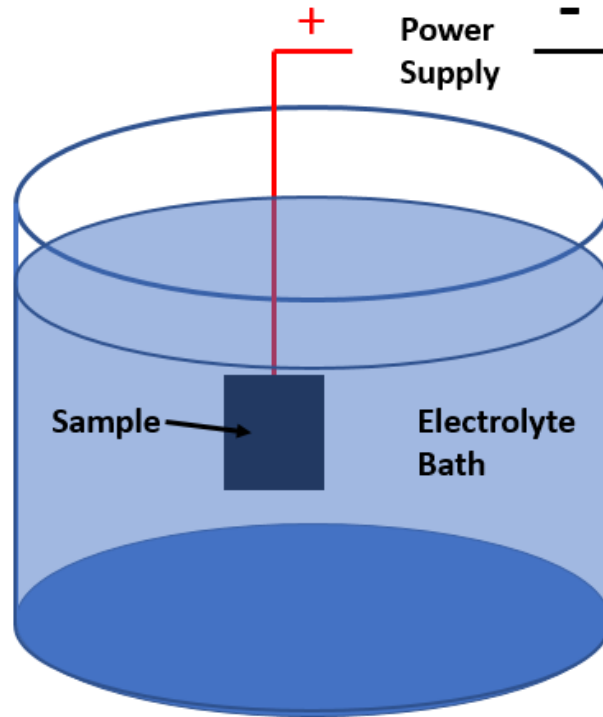


Figure 3.1: Schematic draft of PEA Alumina coating process

### ***3.1.2 Electroless Nickel Plating***

PEA Alumina coated samples were needed to be immersed into a degreaser bath at 75 °C for 5 minutes, and deionized water was used to rinse the samples before plating Nickel. After cleaning, the samples were boiled in an acidic nickelic electroless plating bath at 90 °C for 30 minutes. The plating bath was mainly consisted of nickelic salt (sulfate or chloride) and reducing agent (sodium hypophosphite). [38-39]

### ***3.1.3 Other Treatments Before Further Tests***

After the samples were coated, they were polished again by abrasive silicone paper (up to grit 1200) and diamond polishing paste (up to 0.5  $\mu\text{m}$ ). Polished samples were cleaned again by the ultrasonic cleaning machine in acetone. The thickness of samples was around 20  $\mu\text{m}$  after polishing, and some loose particles and sharp objects on coating surfaces were removed.

Some samples were hot mounted by BUEHLER SimpliMet™ XPS1 Mounting System (shown in Figure 3.2) and polished by BUEHLER MATASERV Grinder-Polisher (shown in Figure 3.3) to observe the cross-section morphology and analysis. Some samples were heated to 500°C and they were holden for 30 minutes by SYBRON Thermolyne™ FURNATROL II furnace which is shown in Figure 3.4.



Figure 3.2: Illustration of BUEHLER SimpliMet™ XPS1 Mounting System





Figure 3.3: Illustration of BUEHLER MATASERV Grinder-Polisher



Figure 3.4: Illustration of SYBRON Thermolyne™ FURNATROL II furnace

### ***3.2 Hardness Tests***

The hardness of coatings was tested by BUEHLER MICROMET II microhardness tester which was shown in Figure 3.5. The samples were placed in the sample holder, and diamond-shaped marks were made on the samples by an indenter. Then, the diagonal length of those marks were measured from an optical microscope, and the Vickers Hardness results were calculated by the equation below:

$$HV = 1854.4 \times \frac{F}{d^2} \text{ (Eq. 1)}$$

Where HV is standing for Vickers Hardness; F is representing load used on the indenter in grams; and d is the diagonal length in  $\mu\text{m}$ . A 25-gram load was used on every microhardness tests in this study.



Figure 3.5: Illustration of BUEHLER MICROMET II microhardness tester

### ***3.3 Pin-on-Disk Tribology Tests***

The polished samples were placed and tested by SCILAND PIN/DISK TRIBOMETER & SURFCORDER which is shown in Figure 3.6. Those samples were dry sliding tested with a 5N load against Hard Wear Resistance 52100 Alloy steel balls and Tungsten Carbide (WC) balls for 150 metres. The coefficient of friction (COF) results were collected after 150m tests.

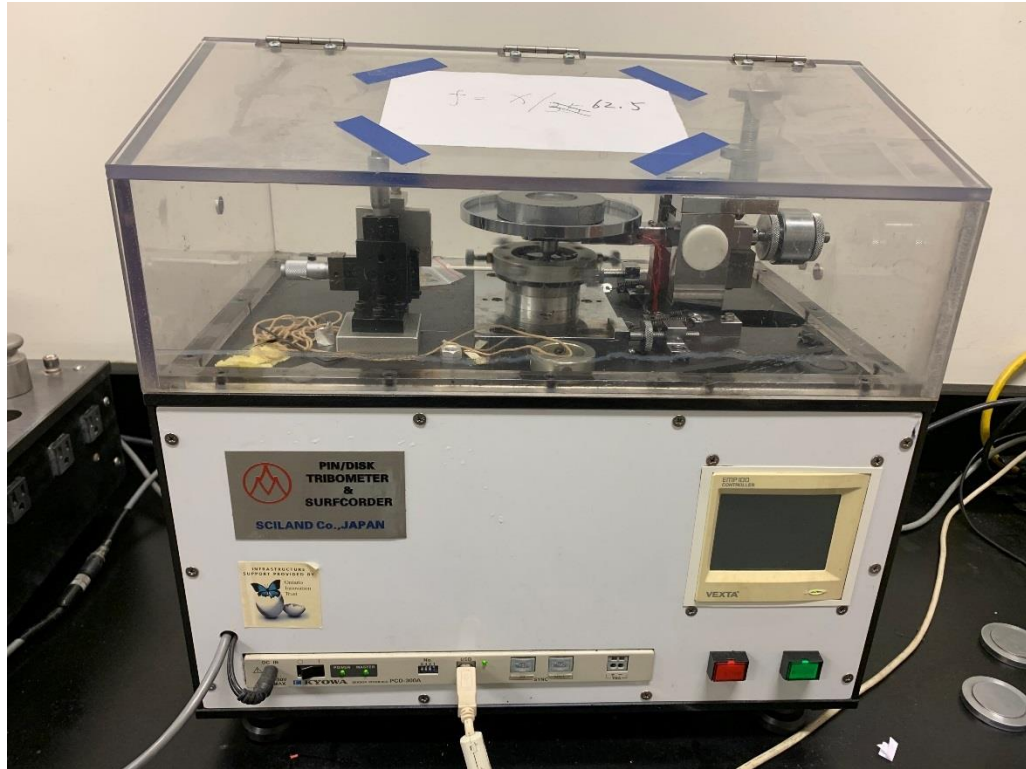


Figure 3.6: Illustration of SCILAND PIN/DISK TRIBOMETER & SURFCORDER

### ***3.4 Morphology Observation***

The surface and cross-section morphology of samples was observed by HITACHI TM3030Plus Tabletop Microscope (shown in Figure 3.7) which is a scanning electron microscopy (SEM). The coated samples were gold sputter coated before doing SEM observation to figure out some characteristics on coating surface and wear track easily.

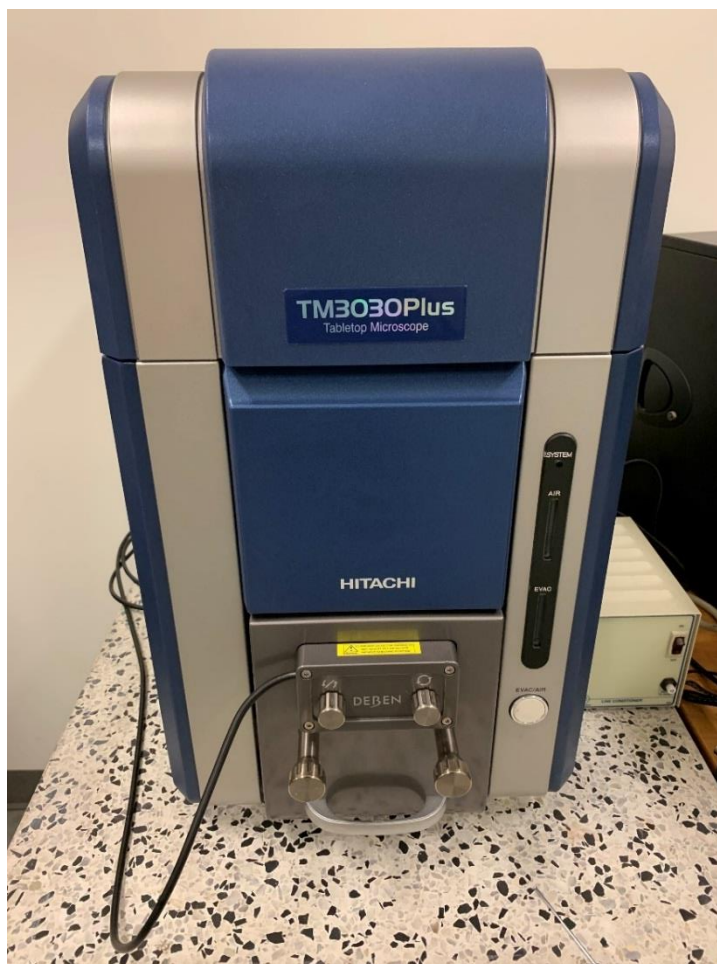


Figure 3.7: Illustration of HITACHI TM3030Plus Tabletop Microscope

### ***3.5 Element and Structure Analysis***

The chemical composition was observed by BRUKER QUANTAX 70 Energy-Dispersive X-Ray Spectroscopy (EDX) shown in Figure 3.8. The EDX analysis was done with the SEM observation. The chemical structure was observed by AXRD X-Ray Diffraction Spectroscopy (XRD) shown in Figure 3.9 with a Cu X-Ray source, and a Mythen 1K silicone strip detector. The XRD spectroscopy was operated at 30kV and 20mA. Scans were performed using  $\text{CuK}\alpha$  radiation from 20 to 100  $2\theta$  degrees with a 2 mm divergence slit.



Figure 3.8: Illustration of BRUKER QUANTAX 70 Energy-Dispersive X-Ray Spectroscopy



Figure 3.9: Illustration of AXRD X-Ray Diffraction Spectroscopy

### 3.6 Electrochemical Tests

The electrochemical anti-corrosion behaviours were observed by Bio-logic electrochemical workstation (shown in Figure 3.10). Open Circuit Potential (EOC), Polarization Resistance ( $R_p$ ) and Electrochemical Impedance Spectroscopy (EIS) were included in the corrosion tests.

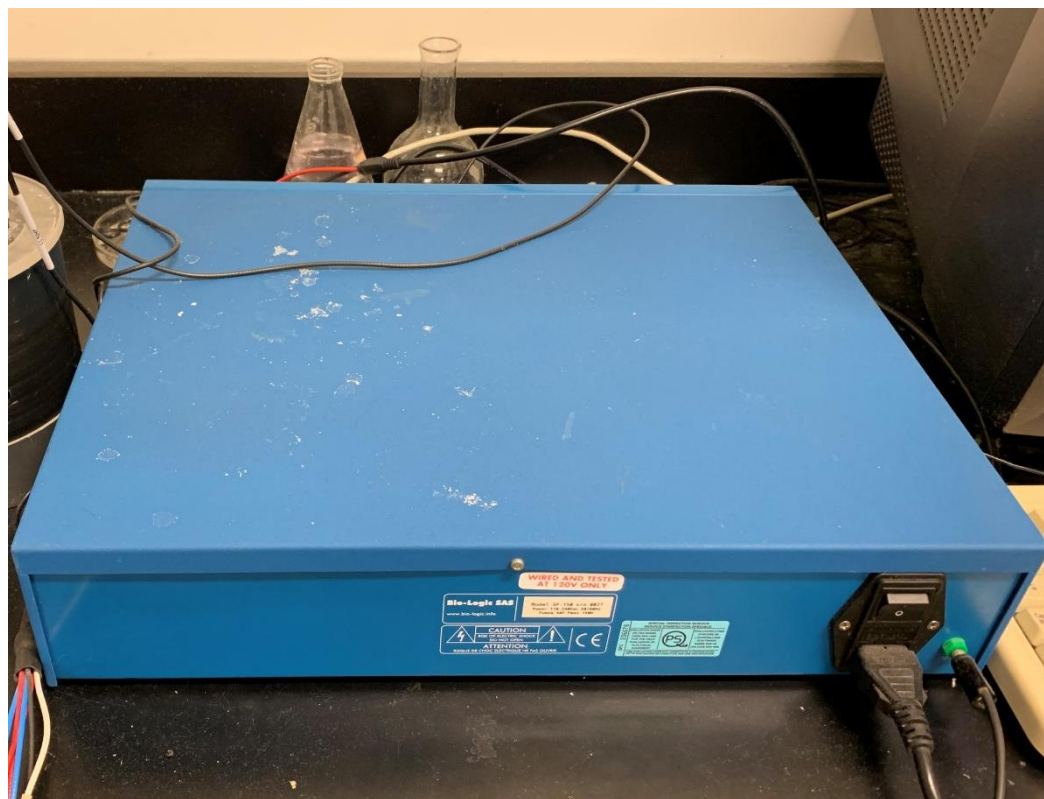


Figure 3.10: Illustration of Bio-logic electrochemical workstation

## CHAPTER 4

### PEA Alumina and Ni-Alumina Coatings Generation

In this chapter, PEA Alumina coating and Ni-Alumina coating were generated on gray cast iron substrate. Surface morphology observation was finished by Scanning electron microscopy (SEM). The element analysis was analyzed by Energy-Dispersive X-Ray Spectroscopy (EDX) and X-Ray Diffraction Spectroscopy (XRD). The surface morphology and elements were compared between PEA Alumina coating and Ni-Alumina coating. The wear behaviours including coefficient of friction and wear track morphology were also compared in these two coatings. Some PEA Alumina coated samples were heated up to 500 °C to figure out differences from as-coated PEA Alumina coating. Microhardness of coatings were measured by Vickers hardness tester, and differences in hardness within coatings were also discussed.

#### ***4.1 PEA Alumina Coatings on Gray Cast Iron***

Plasma electrolytic Aluminating (PEA) Alumina coatings were deposited on gray cast iron samples. Gray cast iron is a kind of non-valve metal, so a passive layer needed to be deposited before alumina generating. To create the passive layer, a high current density of 0.5 - 0.6 A/cm<sup>2</sup> was mandatory to apply, meaning that a 4 A current was used to achieve this. [11] After the passive layer formed, the current started dropping until it became zero. Higher current density had a faster coating generation rate, so the alumina deposited slower and slower with time. The coating duration for each sample was 15 min to obtain 30 µm in thickness.

The coating surface was presenting high roughness because of the porous structure. This characteristic could have both advantages and disadvantages on some applications.



The dimple surface of the coating had a reduced contact area while in tribology tests, so it would have a lower coefficient of friction and longer durability. [58] [77] However, a few of corrosive fluid could flow to the cast iron substrate through the micropores. Therefore, the PEA Alumina coating was still facing a pitting corrosion problem. [78]

#### ***4.1.1 Surface Morphology***

Scanning electron microscopy (SEM) image shown in Figure 4.1 was polished PEA Alumina coating. It could be easily observed in that the coating surface was poor in flatness and poor in roughness. There were some cracks and a plenty of micropores appearing on the surface. After polishing off some loose materials of the coating, the pores were still spreading all over the surface.

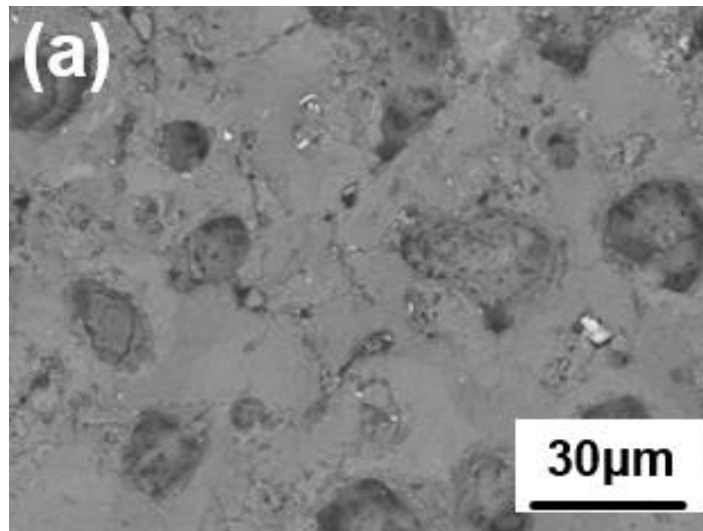


Figure 4.1: Surface morphology of PEA Alumina coating

#### ***4.1.2 Chemical Compounds***

The Point A in Figure 4.2 was a part of PEA Alumina coating. According to the Energy-Dispersive X-Ray Spectroscopy (EDX) element analysis results shown in Table

4.1, carbon (C), oxygen (O), aluminum (Al) and iron (Fe) were found. A few carbon was scattering from hot mounting material, which could be considered as error. Oxygen, aluminum, and iron particles were segments of alumina ( $\text{Al}_2\text{O}_3$ ) and hercynite ( $\text{FeAlO}_2$ ), where hercynite could be considered as a combination of  $\text{Al}_2\text{O}_3$  and ferrous oxide ( $\text{FeO}$ ).

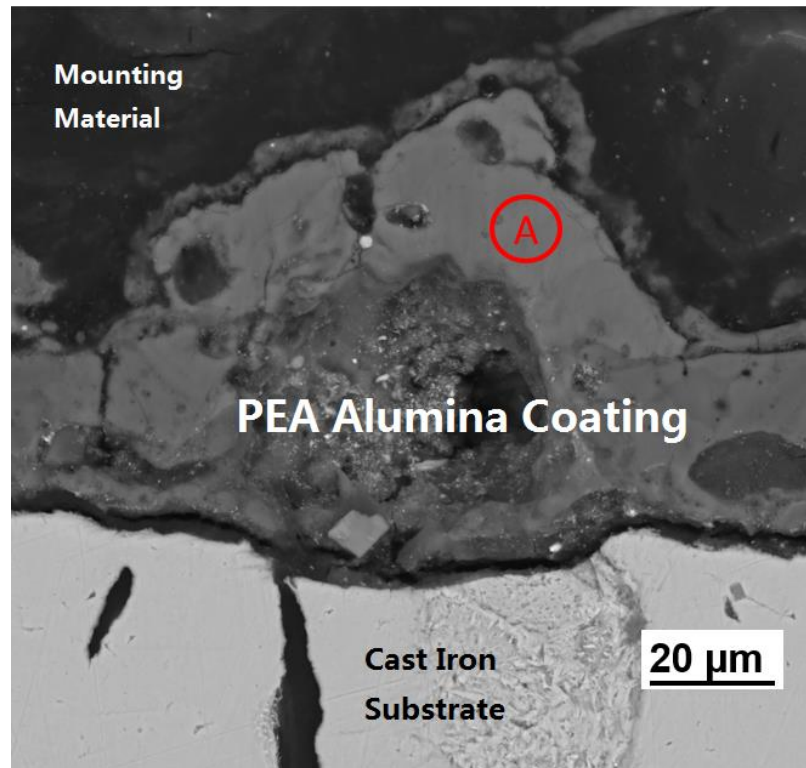


Figure 4.2: SEM image of cross-section of PEA Alumina coating

Table 4.1: EDX elements analysis of PEA Alumina coating

Element	Atomic %
C	1.57
O	58.18
Al	28.49
Fe	11.76

## ***4.2 Ni-Alumina Coatings on Gray Cast Iron***

Electroless nickel plating was deposited on PEA Alumina coatings to create Ni-Alumina coatings. Nickel could seal the micropores and cracks to prevent from pitting corrosion. In addition, nickel as a sticky metal could help the coating to have a better binding force with cast iron substrate. In the other hand, depositing nickel had changed the surface morphology of PEA Alumina coating, so the wear behaviours and wear mechanisms of PEA Alumina coating and Ni-Alumina coating would be different. Moreover, the nickel-plating time of 10 min and 30 min was applied to form Ni-Alumina coatings. The mechanisms of electroless nickel plating process could be figure out by comparing differences in these two coatings.

### ***4.2.1 Surface Morphology***

From Figure 4.3, the spots in white should be nickel and the gray area should be PEA Alumina coating. Therefore, nickel had deposited on the PEA Alumina coating surface and filled up the micropores.

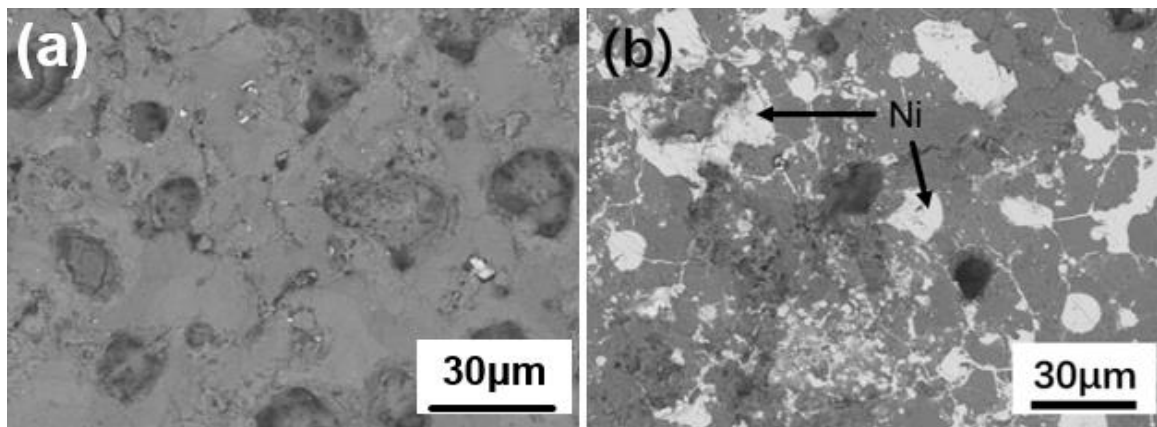


Figure 4.3: SEM images of (a) PEA Alumina coating and (b) Ni-Alumina coating

### 4.2.2 Chemical Compounds

From the X-Ray Diffraction Spectroscopy (XRD) results shown in Figure 4.4, some elements were figured out. The PEA Alumina coating consisted of iron, aluminum oxide and hercynite, which could prove the discussion of PEA Alumina coating contents. In addition, nickel was found in the Ni-Alumina coating as well, so this could be evidence that nickel has deposited on the PEA Alumina coating. As is discussed above, hercynite ( $\text{FeAlO}_2$ ) has the same pattern with ferrous oxide ( $\text{FeO}$ ), so this is a clue that  $\text{FeAlO}_2$  could be considered as a combination of alumina and ferrous oxide.

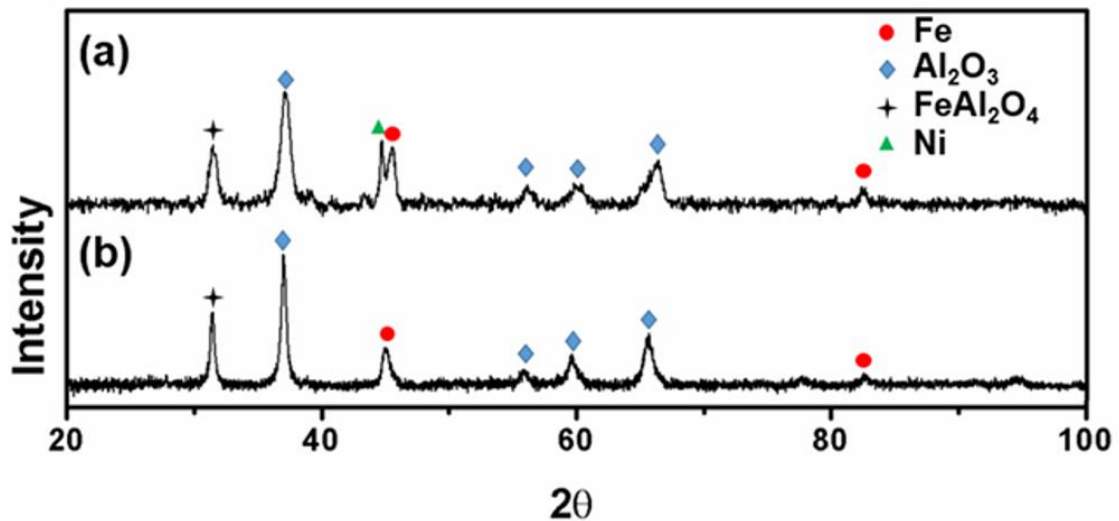


Figure 4.4: XRD results of (a) Ni-Alumina coating and (b) PEA Alumina coating

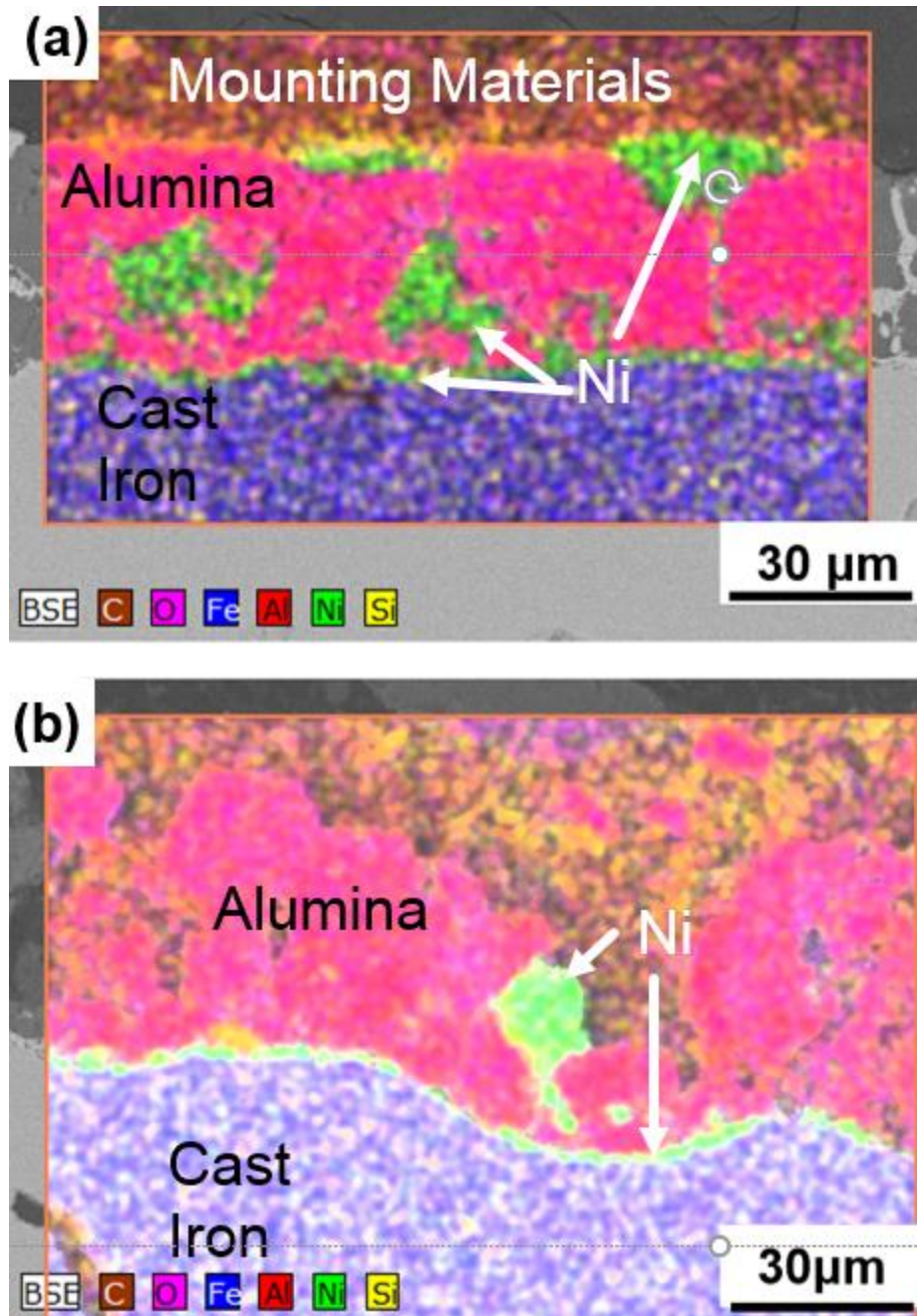


Figure 4.5: (a)(b) EDX mapping analysis of Ni-Alumina coating with 30 min and 10 min electroless nickel plating, respectively

From the EDX mapping analysis results shown in Figure 4.5 (a) and (b), nickel was illustrated in green colour. The blue and red area were representing iron and oxygen

elements, respectively. The crevice between cast iron substrate and PEA Alumina coating was fixed up by nickel. The holes appeared inside the PEA Alumina coating as well, and were also filled up by nickel.

#### 4.2.3 Generating Mechanism

From the observation of cross-section of coatings shown in Figure 4.6 (a), the interface between cast iron substrate and PEA Alumina coating was occupied by nickel. Not too many micropores were filled up by nickel, and there was not any nickel found on the top of coating surface. In Figure 4.6 (b), the electroless nickel plating process was 30 min. The iron-alumina interface, cracks and holes were fully occupied, and some nickel grew on the top of coating surface.

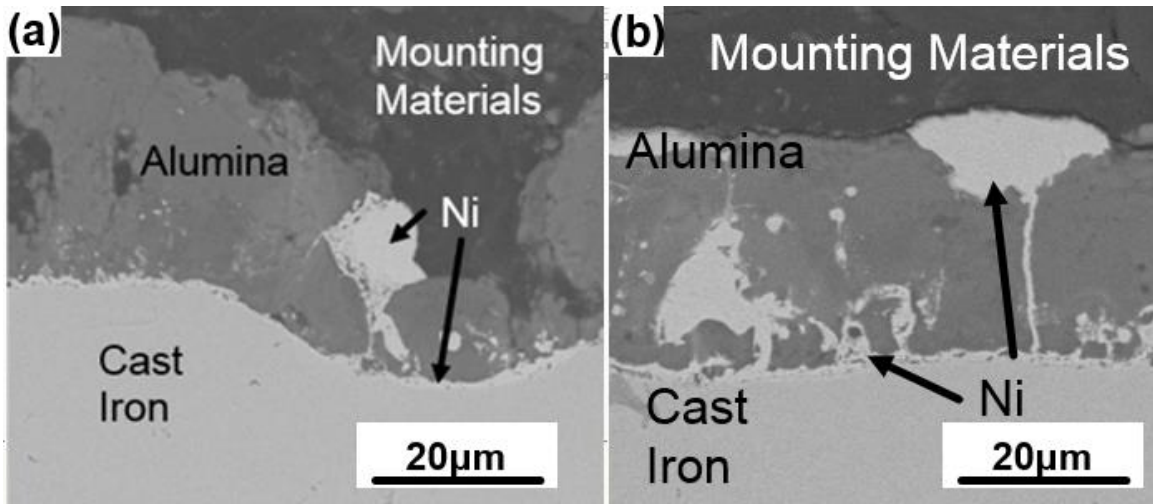


Figure 4.6: SEM images of Ni-Alumina coating with electroless nickel plating duration of (a) 10 min and (b) 30 min

Generally, electroless nickel can only deposit on ferrous alloys including cast iron, steel, and stainless steel. Thus, nickel cannot generate on alumina without any catalyst. The plating solution could permeate on the cast iron- alumina interface through pores and

tunnels, so the nickel started generating from the cast iron substrate. Then, nickel grew out from the tunnels to reach the top surface and clogged the micropores.

In addition, the nickel depositing rate on cast iron was only 25  $\mu\text{m}$  per hour on average. However, the coating thickness shown in Figure 4.6 was about 25  $\mu\text{m}$ , and nickel could still appear on the top surface. The main reason was that the PEA Alumina coating structure influenced the nickel growing direction, but the amount of nickel would be the same in same deposition duration.

However, too much nickel appearing on the surface could cause a negative influence on coating in wear behaviours. Therefore, the ideal condition was that nickel could only occupy the pores but was not spreading on the top surface. In this case, to generate a 25  $\mu\text{m}$  thick Ni-Alumina coating 20 - 30 min electroless nickel plating was needed.

#### ***4.3 500 °C heated PEA Alumina Coatings***

Some PEA Alumina coated cast iron samples were heated up to 500 °C, and the surface morphology and chemical compounds were compared with as-coated one. The differences in morphology in these two coatings were mainly discussed by comparing the porous structure and cracks. The difference in chemical valence of two samples was discussed by comparing the iron-oxygen compounds.

##### ***4.3.1 Surface Morphology***

Figure 4.7 illustrated the surface structure of (a) 500 °C PEA Alumina coating as-coated and (b) PEA Alumina coating. Comparing with as-coated PEA Alumina coating, 500 °C heated sample had the similar surface structure. The coatings contained a plenty of micropores and cracks on the surfaces.

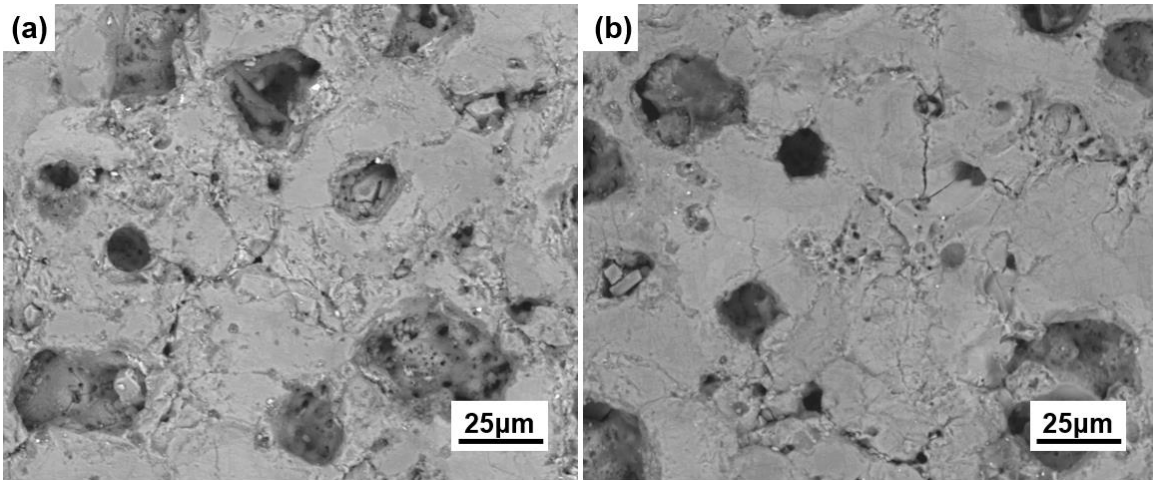


Figure 4.7: SEM images of PEA Alumina coatings (a) 500 °C heated and (b) as-coated

#### 4.3.2 Chemical Compounds

Point A in Figure 4.8 (a) and Point B in Figure 4.8 (b) were alumina coating materials selected from 500 °C heated and as-coated PEA Alumina coatings, respectively.

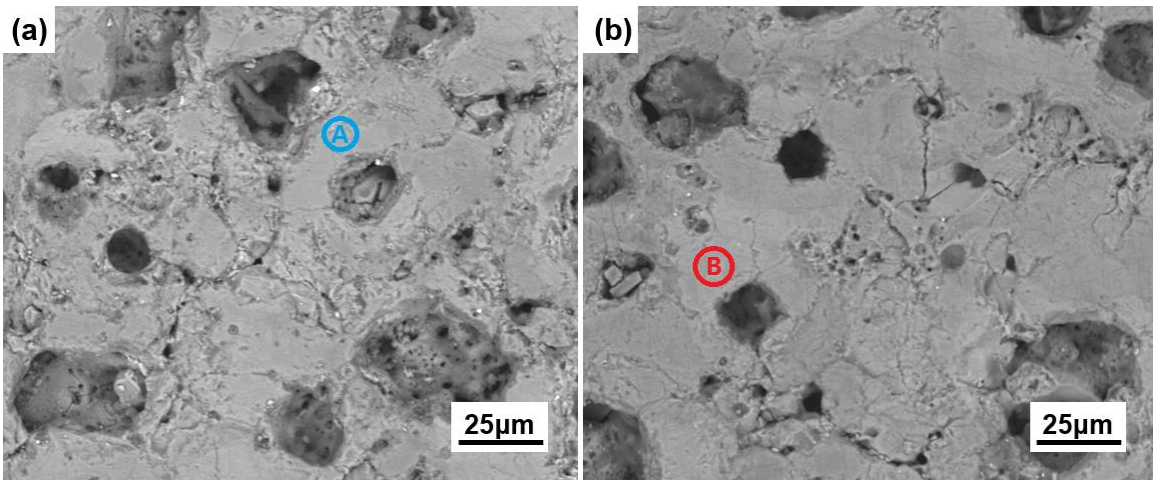


Figure 4.8: Selected points for EDX point analysis on (a) 500 °C heated and (b) as-coated

PEA Alumina coatings



Table 4.2: EDX elements analysis of as-coated and 500 °C heated PEA Alumina coatings

<b>Element</b>	<b>Atomic % @ A</b>	<b>Atomic % @ B</b>
O	60.06	58.72
Al	29.56	27.59
Fe	10.38	13.69

From the EDX analysis results shown in Table 4.2, there were oxygen, aluminum and iron compounds were figured out. Every two aluminum ions could carry three oxygen ions to form  $\text{Al}_2\text{O}_3$ . The rest of oxygen could build iron-oxygen compounds with iron ions. However, the residual oxygen ions carried different amounts of iron ions in two coatings. The O/Fe ratio is to examine the iron-oxygen compounds structure. The O/Fe ratio of ferrous oxide ( $\text{FeO}$ ) is 1 and the ratio of ferric oxide ( $\text{Fe}_2\text{O}_3$ ) is 1.5. Ferrous oxide could transfer to ferric oxide by oxidizing. After some calculations, the O/Fe ratios of as-coated and 500 °C heated PEA Alumina coatings were about 1.25 and 1.5, respectively. Therefore, the iron-oxygen compounds in as-coated sample was in a midrange between ferrous oxide and ferric oxide, and some  $\text{FeO}$  compounds were not oxidized into ferric oxide. The 500 °C heated PEA Alumina coatings were fully oxidized in heat treatment, and the iron-oxygen compounds were presented as ferric oxide.

#### 4.4 Microhardness of Coatings

The microhardness of coatings was measured by 20 times Vickers Hardness Test in 25 grams of load, and the data was summarized in Figure 4.

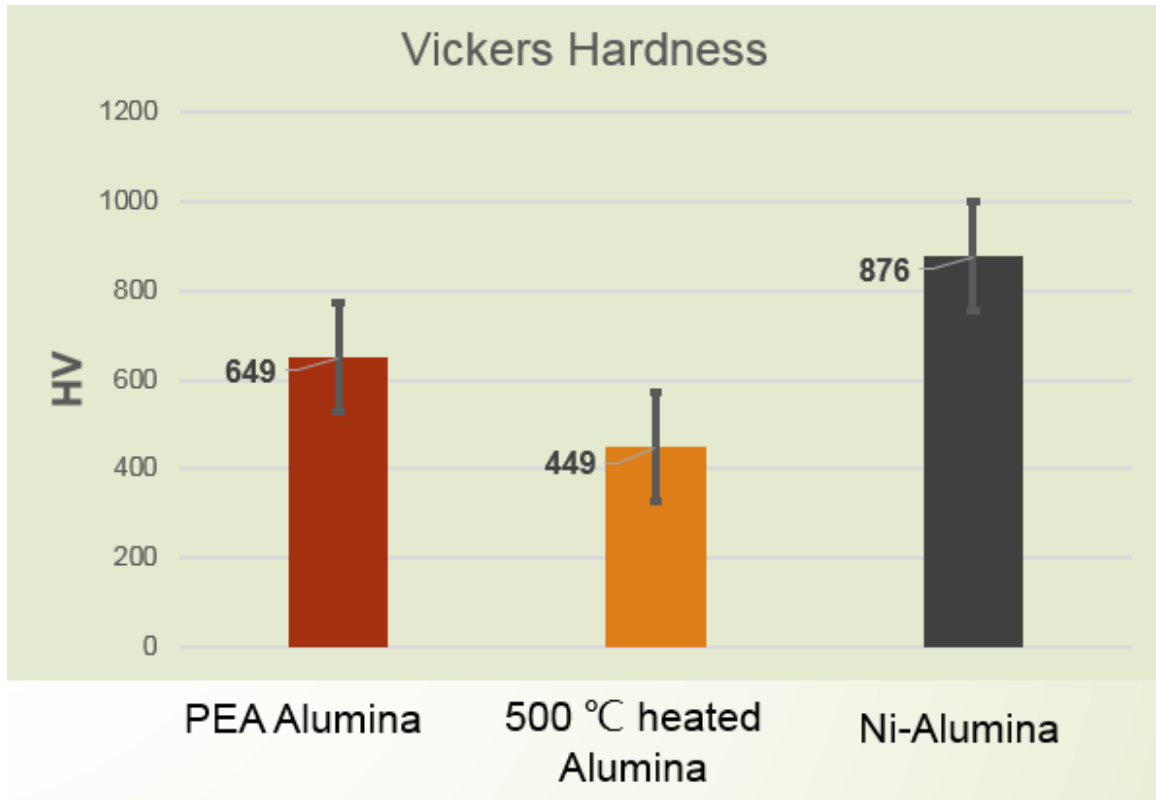


Figure4.9: Vickers Microhardness results of as-coated PEA Alumina coating, 500 °C heated PEA Alumina coating and Ni-Alumina coating

As-coated PEA Alumina coating had hardness of 520 - 780 HV with an average of 649 HV. The average microhardness of 500 °C heated PEA Alumina coating was 449 HV and the hardness varied from 330 - 580 HV. The Ni-Alumina coating had the highest microhardness of 876 HV, and the hardness varied from 740 - 1000 HV.

According to the online data, the microhardness of compact-structure Alumina is 2000 HV, and the hardness of electroless nickel plating is 500 - 600 HV. [31] [33] The reason

why the PEA Alumina coating had much lower hardness than compact-structure alumina is that the PEA Alumina coating has a porous structure. When the indenter applied force on the coating surface, there was not only the compressive stress on the top of the surface but also some shear stress.

From the data shown in Figure 4.9, 500 °C heated PEA Alumina coating had lower microhardness than as-coated PEA Alumina coating. Some cracks appearing inside the coating because of heating expansion was one of the reasons. In addition, the oxidization on coating-substrate interface could decrease the binding force between coating and cast iron substrate.

Ni-Alumina coating had the hardness of 876 HV on average, which was the highest in three coatings. The Ni-Alumina coating consisted of PEA Alumina coating and electroless nickel plating, but the microhardness of it was higher than each of PEA Alumina coating and electroless nickel plating. The micropores were occupied by nickel in the Ni-Alumina coating, which created a flatter surface than PEA Alumina coating. The stress applied by indenter was mostly the compressive stress on the top of the coating surface. Therefore, filling up micropores could enhance the hardness.

#### ***4.5 Summary***

Plasma electrolytic aluminating (PEA) and Ni-Alumina coatings were successfully generated on gray cast iron. The PEA Alumina coating had a porous structure with high roughness. Alumina and hercynite ( $\text{FeAlO}_2$ ) were found in the PEA Alumina coatings, where hercynite could be treated as a combination of aluminum oxide and ferrous oxide. The hercynite compounds were formed because of the plasma with high current. The high current plasma impacted on the cast iron substrate and some melted iron were oxidized. The ferrous oxide and alumina were combined and formed new compounds of hercynite.

Electroless nickel could not plate on the alumina coating surface directly. The electroless nickel plating solution could permeate on the cast iron substrate-alumina interface through micropores and tunnels. Therefore, the nickel started generating from the cast iron substrate, and then grew out from the tunnels to reach the top surface and clogged the micropores. 30 min electroless nickel plated Ni-Alumina coating could fill up the micropores and cracks. The porous structure of coating could cause a pitting corrosion, and nickel had overcome this problem. To decrease the influence in wear behaviours, generating a 25  $\mu\text{m}$  thick Ni-Alumina coating 20 - 30 min would be an ideal electroless nickel plating duration.

500 °C heat treatment did not change the morphology of PEA Alumina coating obviously, but the chemical compounds were different. The O/Fe ratios of as-coated PEA Alumina coatings were about 1.25, which was in a midrange between ferrous oxide and ferric oxide, and some FeO compounds were not oxidized into ferric oxide. The O/Fe ratios of 500 °C heated PEA Alumina coatings were about 1.5. Coatings were fully oxidized in heat treatment, and the iron-oxygen compounds were presented as ferric oxide.

The microhardness was tested by Vickers hardness tester in three coatings. As-coated PEA Alumina coating had an average hardness of 649 HV, and 500 °C heated sample had an average of 449 HV. The oxidization on coating-substrate interface could decrease the binding force between PEA Alumina coating and cast iron substrate. In addition, heating expansion could make the coating have more cracks. Ni-Alumina coating had the highest performance in hardness which was 876 HV. The micropores were occupied by nickel in the Ni-Alumina coating, which created a flatter surface than PEA Alumina coating. The stress applied by indenter was the compressive stress but not shear stress on the top of the coating surface. Therefore, filling up micropores could enhance the hardness.

## CHAPTER 5

### Wear Behaviours of Coatings against Steel and WC Balls

In this chapter, the wear behaviours including coefficient of friction (COF), wear track morphology and element analysis were introduced. The COF data was obtained from 150 m distance, 5 N load dry sliding against SAE 52100 steel ball and tungsten carbide (WC) ball. The wear behaviours of PEA Alumina coating were introduced first, and they were compared with wear behaviours of Ni-Alumina coating and 500 °C heated PEA Alumina coating, respectively. The wear mechanisms were also discussed by analyze the wear track morphology and chemical compositions.

#### 5.1 Wear Behaviours of PEA Alumina Coatings on Gray Cast Iron

Figure 5.1 was illustrating the Coefficient of Friction (COF) of PEA Alumina coating against steel ball and tungsten carbide ball.

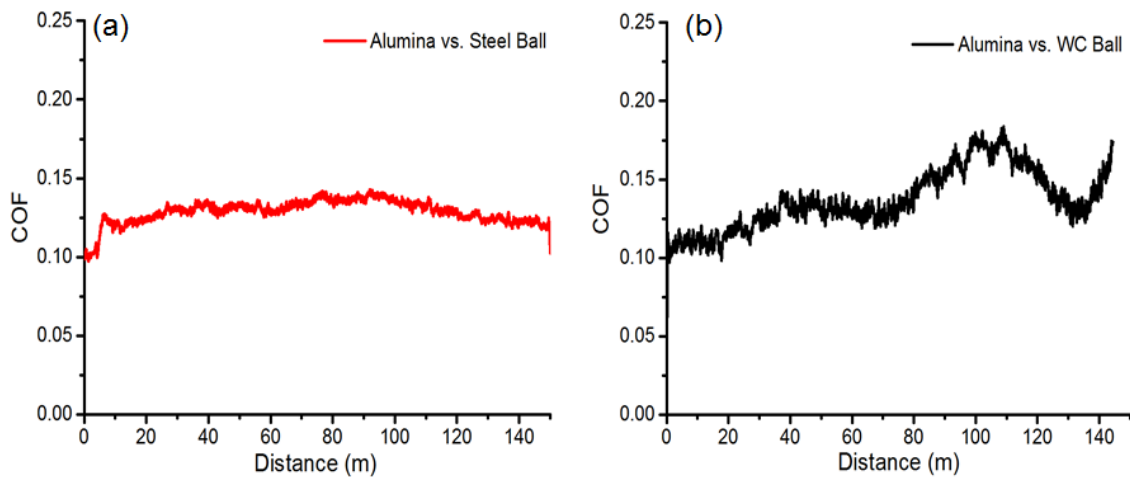


Figure 5.1: COF data of PEA Alumina coatings against (a) steel ball and (b) WC ball

As shown in Figure 5.1 (a), PEA Alumina coating had an average COF about 0.13 against SAE 52100 steel ball in 150 m 5 N Pin-on-Disk dry sliding tests. There was no

galling behaviour started. In Figure 5.1 (b), the COF of coating was about 0.15 against tungsten carbide ball, and the galling behaviour was not found obviously. The steel ball was slightly softer, and the WC ball was much harder than PEA Alumina coating. Therefore, there should be some materials from steel ball transferred on the coating top surface. The hardness of steel ball could not harm to the PEA Alumina coating, so the COF data obtained had not a huge fluctuate. There should not be materials transferred from WC ball on PEA Alumina coating, but the WC ball could change the morphology by compressing coating surface.

### *5.1.1 Wear Track Morphology*

Figure 5.2 was illustrating the Scanning Electron Microscopy (SEM) images of the wear tracks of PEA Alumina coating against steel ball and tungsten carbide ball.

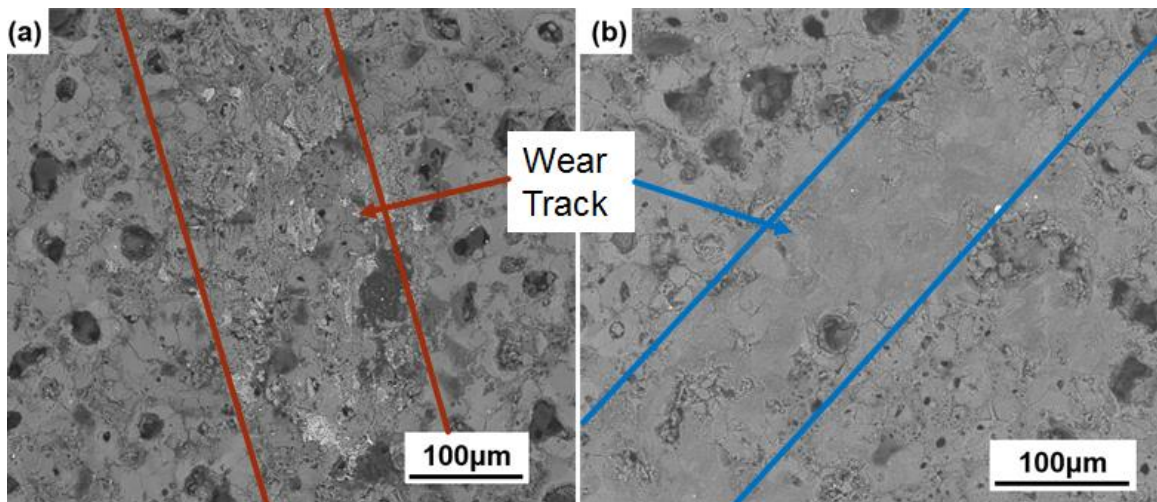


Figure 5.2: SEM images of wear tracks of PEA Alumina coating against (a) steel ball and (b) WC ball

The bright spots in Figure 5.2 should be the material transfer particles, and the dark spots should be the PEA Alumina coating itself. It could be observed in Figure 5.2 (a) that

materials from steel ball transferred on the coating surface. There was not any material transfer behaviour found on the coating surface shown in Figure 5.2 (b). The SAE 52100 steel ball has lower hardness than PEA Alumina coating and the tungsten carbide ball has higher hardness than the PEA Alumina coating. Softer ball materials could stick on the coating surface in the wear tests, and harder ball materials could smash the coating top surface. Some loose coating materials were crushed and formed a flat wear track.

### 5.1.2 Chemical Composition

Figure 5.3 was illustrating the selected points in wear tracks for Energy-Dispersive X-Ray Spectroscopy (EDX) element analysis corresponding to Figure 5.2.

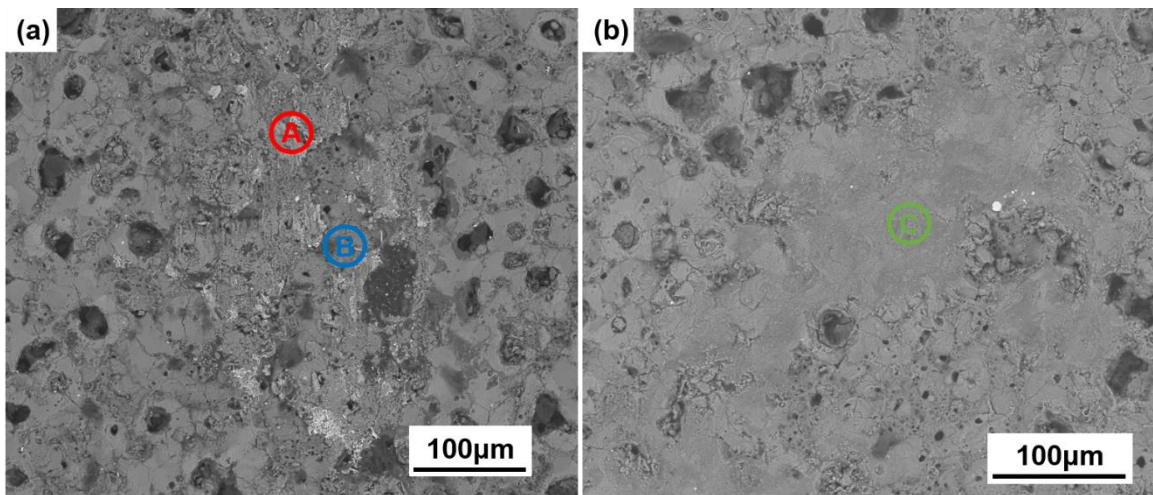


Figure 5.3: Selected points for EDX point analysis of PEA Alumina coatings wear tracks against (a) steel ball and (b) WC ball

To prove the discussion about the wear track material transfer behaviours, Point A, B and C were selected spots to analyze the proportion of elements by Energy-Dispersive X-Ray Spectroscopy (EDX). Due to the high surface roughness of PEA Alumina coating, different spots had different wear behaviours against the balls. Spots at thicker coating



might have more contact area and more load than spots at thinner coating. As is shown in Figure 5.3 (a), Point A from the wear track of PEA Alumina coating against steel ball was selected because there were some steel ball materials adhering on the coating surface. There were not much steel ball materials observed at Point B which was shown in Figure 5.3 (a). The wear track of PEA Alumina coating was found in high flatness without any materials transferred from the WC ball, so the chemical elements were similar on every spot in the wear track.

Table 5.1: EDX elements analysis of PEA Alumina coatings wear tracks

<b>Element</b>	<b>At% @A</b>	<b>At% @B</b>	<b>At% @C</b>
O	45.98	57.76	57.57
Al	6.76	29.06	31.07
Fe	47.26	13.18	11.36

From the proportion of chemical elements in Table 5.1, Oxygen (O), Aluminum (Al) and Iron (Fe) were found at Point A, B and C. Oxygen could come from alumina ( $Al_2O_3$ ) and FeO (or  $FeAlO_2$ ), and Al should be from the alumina. Fe could be from FeO and the iron metal. The chemical contents at Point B were extremely similar with the contents of as-coated PEA Alumina coating in Table 4.1. Therefore, it could be claimed that there were no materials transferred on Point B and other places in dark area in wear track. There were much higher Fe and at Point A than at Point B, so it was the proof that a plenty of iron on wear track was coming from the steel ball. The chemical compositions at Point C were

similar with the PEA Alumina coating itself, so the materials found in wear track did not contain ball materials.

## 5.2 Wear Behaviours of Ni-Alumina Coatings on Gray Cast Iron

Figure 5.4 was illustrating the comparisons of Coefficient of Friction of PEA Alumina and Ni-Alumina coatings against steel ball and tungsten carbide ball.

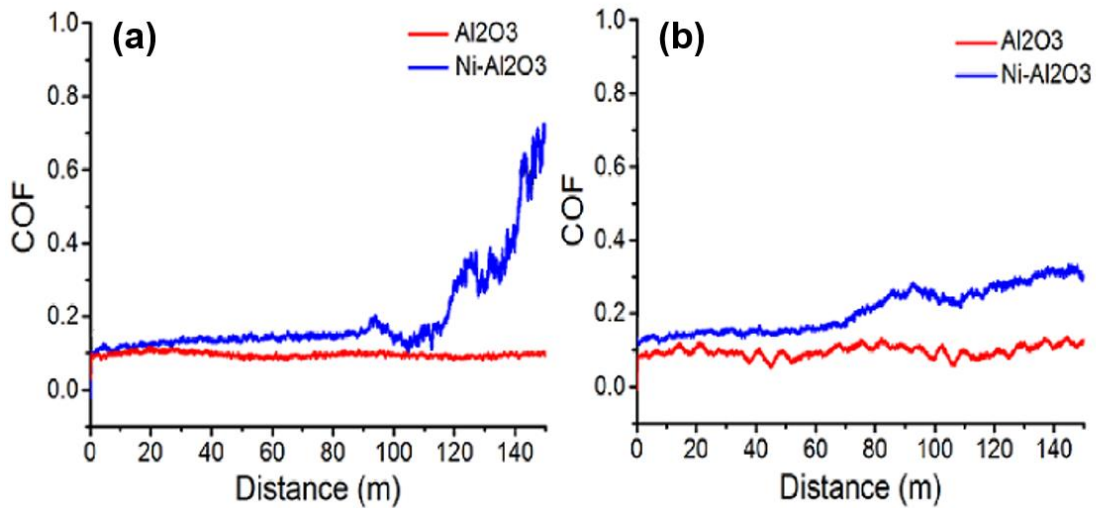


Figure 5.4: Comparison in COF data of PEA Alumina coatings and Ni-Alumina coating against (a) steel ball and (b) WC ball

In Figure 5.4 (a), Ni-Alumina coating had about 0.15 COF in the first 100 m sliding test. However, it started galling after 100 m, and the COF rapidly went up to 0.6. In Figure 5.4 (b), Ni-Alumina had higher COF than PEA Alumina coating in dry sliding tests. The COF value tended to increase after 100 m sliding, but the performance was not the same as COF data against steel ball. In the beginning of slide test, there was not too much nickel revealed on the top surface, so the COF of Ni-Alumina coating was not much higher than PEA Alumina coating. Along with the sliding distance, nickel as an adhesive metal could

stick with ball materials to form a material transfer layer. The material transfer layer was the reason of COF increasing.

### 5.2.1 Wear Track Morphology

Figure 5.5 was illustrating the Scanning Electron Microscopy (SEM) images of the wear tracks of Ni-Alumina coating against steel ball and tungsten carbide ball.

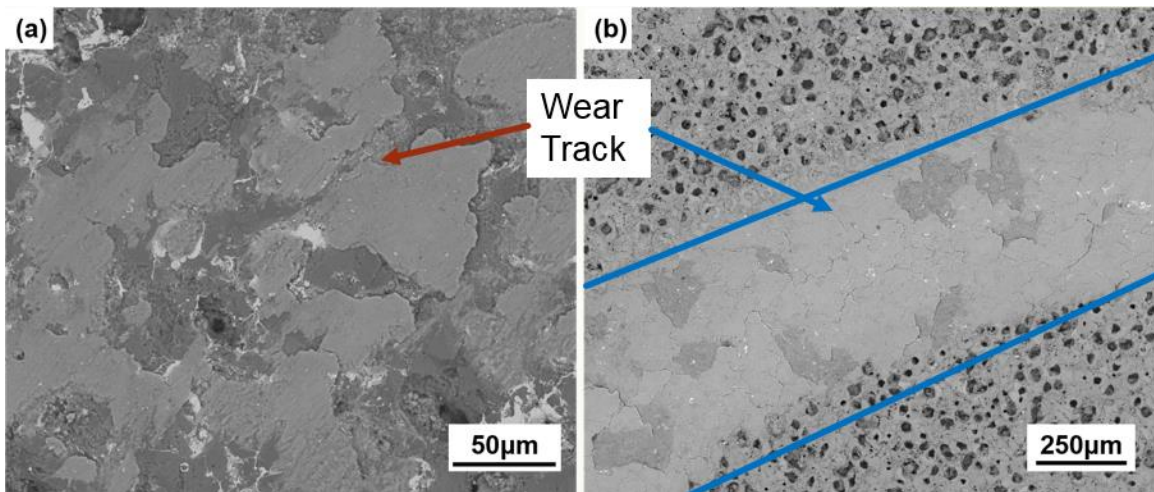


Figure 5.5: SEM Images of Ni-Alumina wear tracks against (a) steel ball and (b) WC ball

Figure 5.5 (a) was illustrating the wear track of Ni-Alumina coating against steel ball. The wear behaviour was adhesive wear. Ni-Alumina coating could form a material mixture layer with ball materials. The material transfer layer was much thicker than PEA Alumina coating against steel ball. Figure 5.5 (b) was presenting the wear track of Ni-Alumina coating against WC ball. The coating top surface was crushed by WC ball and formed a flat layer on the wear track, but some of layer materials were peeled off. WC ball as a hard material could crush the top surface of coating. The coating itself was not affected, so this layer could protect the Ni-Alumina coating.

### 5.2.2 Chemical Composition

Figure 5.6 was illustrating the selected points in wear tracks for Energy-Dispersive X-Ray Spectroscopy (EDX) element analysis corresponding to Figure 5.5.

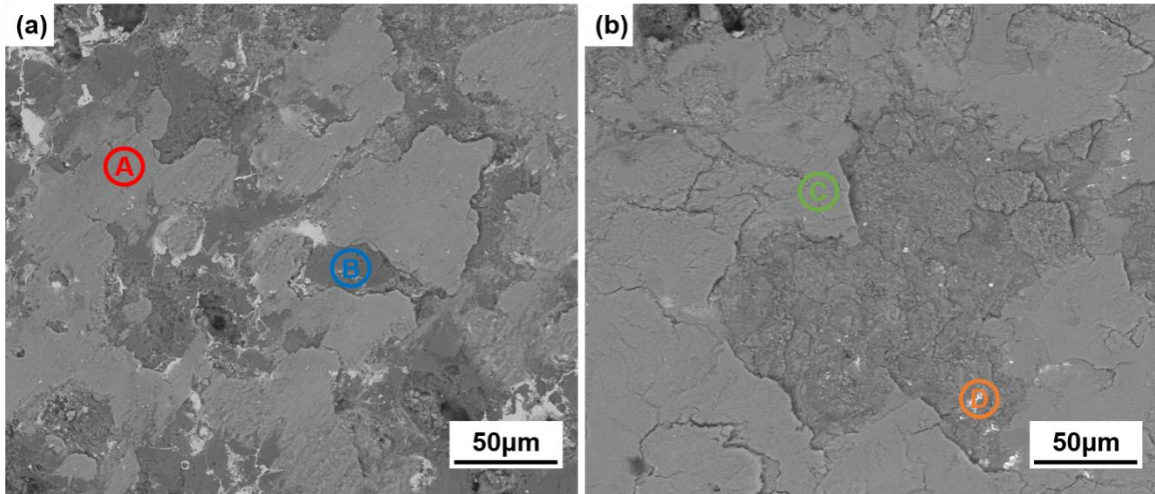


Figure 5.6: Selected points for EDX point analysis of Ni-Alumina coatings wear tracks against (a) steel ball and (b) WC ball

Point A in Figure 5.6 (a) was the wear track of Ni-Alumina coating against steel ball with a material mixture layer, and Point B was the wear track without the layer. Point C in Figure 5.6 (b) was the wear track of Ni-Alumina coating against WC ball with the flat materials layer, and Point D was the wear track with the layer peeled off.

Table 5.2: EDX elements analysis of Ni-Alumina coatings wear tracks

<b>Element</b>	<b>At% @A</b>	<b>At% @B</b>	<b>At% @C</b>	<b>At% @D</b>
O	60.67	56.15	61.31	57.07
Al	9.54	31.12	25.79	26.33
Fe	28.20	8.32	9.47	8.09
Ni	1.59	4.42	1.91	7.98
W	N/A	N/A	1.53	0.53

From Table 5.2, oxygen, aluminum, iron, and nickel were observed in the wear track of Ni-Alumina coating against steel ball, and some tungsten particles were also found in the wear track of Ni-Alumina coating against WC ball. There was many iron and few aluminum and nickel found at Point A. This result represented steel ball materials transferred on the coating and alumina and nickel on the coating surface was covered. There was few iron and many aluminum found at Point B, which meant that Point B was still the Ni-Alumina coating itself.

From the EDX results of Ni-Alumina coating against WC ball, there was tungsten found in the wear track. WC as a material with high hardness would not easily transfer on sample in sliding tests. However, nickel from Ni-Alumina coating could adhere some WC ball materials on the coating surface. There were 1.53 and 0.53 atomic percent of tungsten particles were found at Point C and Point D, respectively. Therefore, the wear track was covered by Ni-Alumina-W mixture layer. The material mixture layer was damage, but there were still some tungsten compounds appearing at Point D. Therefore, material on Point D was the material mixture layer, and the Ni-Alumina coating was not exposed. This material mixture layer could be considered as a protection shell on the coating.

### 5.3 Wear Behaviours of 500°C heated PEA Alumina Coatings

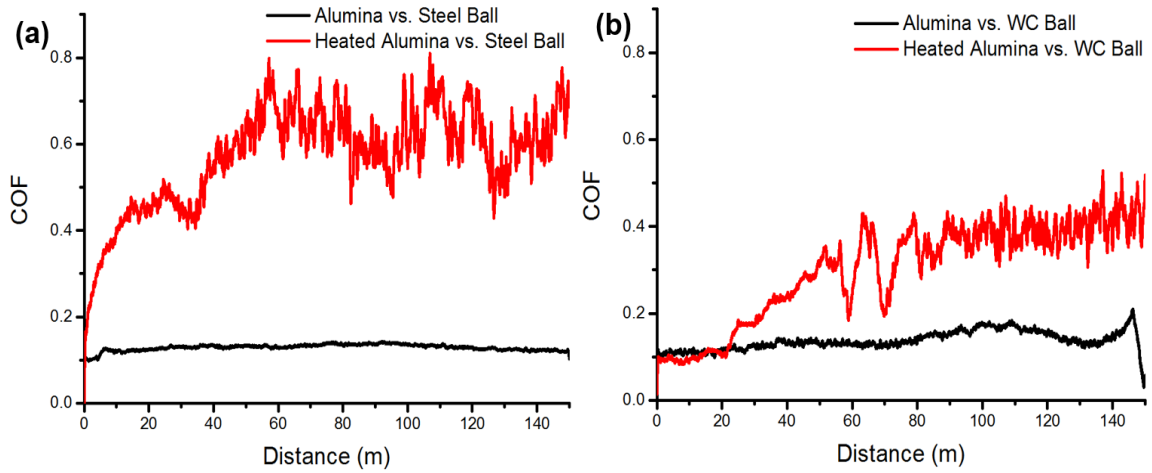


Figure 5.7: Comparison in COF data of as-coated and 500 °C heated PEA Alumina coatings against (a) steel ball and (b) WC ball

From Figure 5.7 (a), COF of 500 °C heated PEA Alumina coatings against steel ball increased rapidly and remained on 0.65. The coating suffered from severe galling behaviour which came from the material transfer problem. In Figure 5.7 (b), the coating had a similar galling tendency with graph shown in Figure 5.7 (a). The final COF of heated PEA Alumina coating against WC ball was around 0.4. Comparing with as-coated PEA Alumina coatings, 500 °C heat treatment resulted in high coefficient of friction and poor durability.

### 5.3.1 Wear Track Morphology

Figure 5.8 was illustrating the SEM images of the wear tracks of unheated and 500 °C heated PEA Alumina coating against steel ball.

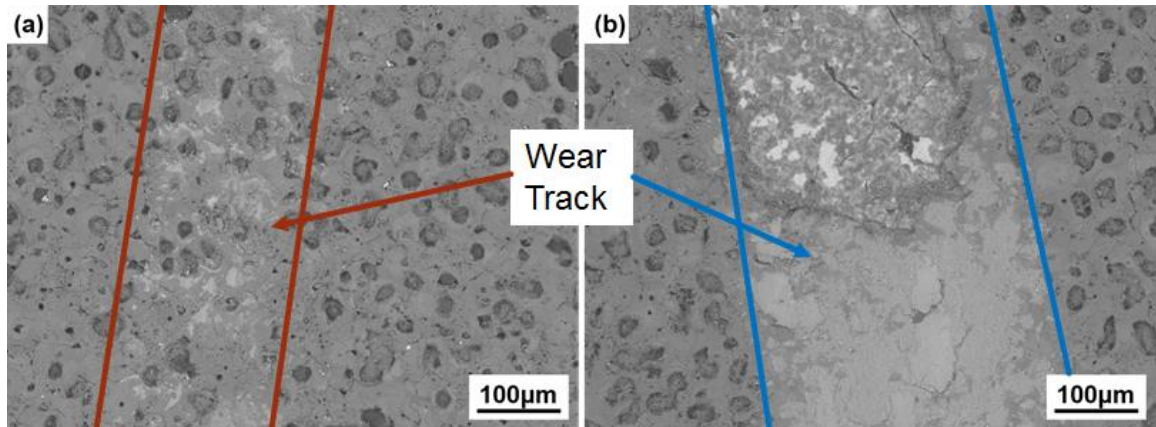


Figure 5.8: SEM Images of PEA Alumina coatings wear tracks (a) as-coated and (b) 500 °C heated against steel ball

Figure 5.8 illustrated the comparisons in PEA Alumina coatings wear track morphology between (a) as-coated and (b) 500 °C heated against steel ball. The wear track widths of as-coated and heated coatings were about 150 and 300 µm, respectively. Because the heated coating had less microhardness than unheated one, so it would have more abrasion. The as-coated sample was partially covered by steel ball materials, and the micropores on the coating surface could easily figured out. In Figure 5.8 (b), the wear track was presenting a thick and wide coating-ball material transfer layer. In addition, it could be easily figured out that a part of coating was lost in the dry sliding wear test.

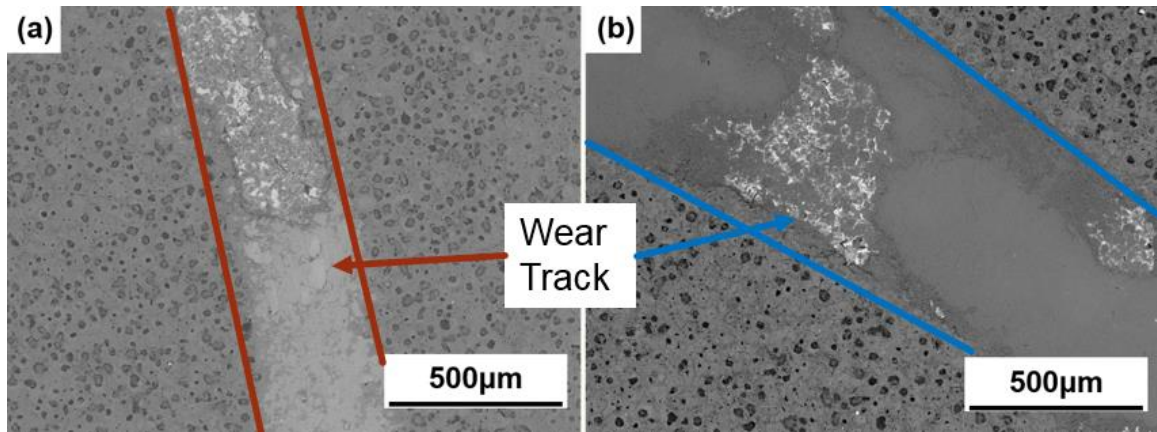


Figure 5.9: SEM Images of 500 °C heated PEA Alumina coatings wear tracks against (a) steel ball and (b) WC ball

From the SEM observation of 500 °C heated PEA Alumina coatings wear tracks against Figure 5.9 (a) steel ball and Figure 5.9 (b) WC ball, both coatings were partially damaged. The wear track width in Figure 5.9 (a) was 300 µm, and it was even wider in Figure 5.9 (b). The remaining coating in Figure 5.9 (a) was a thick coating-ball material transfer layer. There should not be WC particles transferring on the coating surface because of the large difference in microhardness. The residual coating in Figure 5.9 (b) was illustrating that some loose coating materials were crushed and formed a flat wear track.

### ***5.3.2 Chemical Compounds***

Figure 5.10 was illustrating the selected points in wear tracks for Energy-Dispersive X-Ray Spectroscopy (EDX) element analysis corresponding to Figure 5.8.



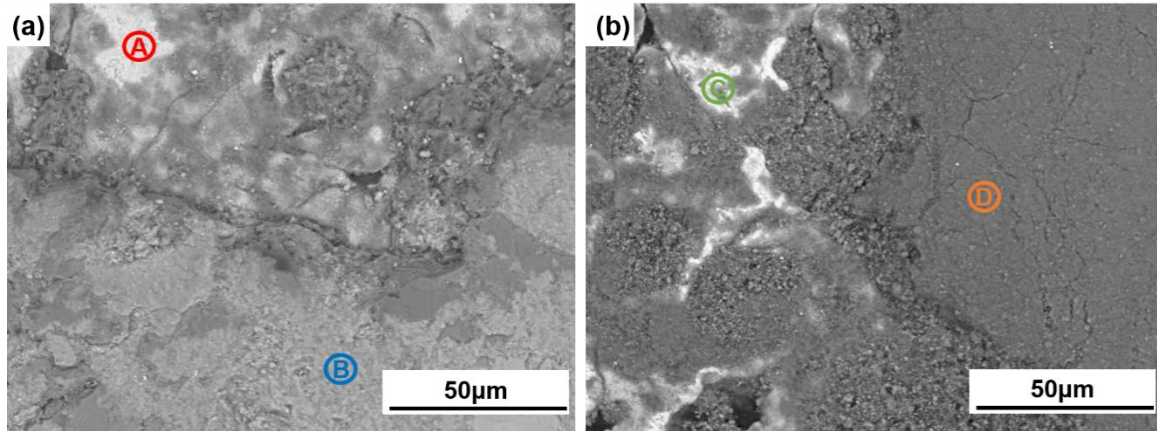


Figure 5.10: Selected points for EDX point analysis of 500 °C heated PEA Alumina coatings wear tracks against (a) steel ball and (b) WC ball

Point A in Figure 5.10 (a) was the broken 500 °C heated PEA Alumina coating, and Point B was representing the material transfer layer in wear track against steel ball. Point C in Figure 5.10 (b) was the coating broken by WC ball, and Point D was the remaining coating layer in the wear track.

Table 5.3: EDX elements analysis of 500 °C heated PEA Alumina coatings wear tracks

<b>Element</b>	<b>At% @A</b>	<b>At% @B</b>	<b>At% @C</b>	<b>At% @D</b>
O	25.05	58.60	40.78	63.33
Al	8.56	7.76	20.71	25.79
Fe	66.38	33.64	38.51	10.88

From the EDX results shown in Table 5.3, there were 66.38 atomic percentage of iron particles pointed out at Point A, and this spot only contained 8.56 atomic percentage of aluminum. The oxygen content was only 25.05 at%, which could not cause entire iron

particles to form iron-oxygen compounds. Therefore, the elements at Point A were mostly the exposed cast iron substrate. The iron at Point B was 33.64 at%, and that was coming from PEA Alumina coating and steel ball. The EDX point analysis results at Point D presented the same chemical composition as an intact coating surface. Point C had a much higher composition of iron and lower composition of oxygen than Point D. Thus, some coating besides point C were cast iron substrate.

#### ***5.4 Wear Mechanisms Analysis***

From the results shown above, as-coated PEA Alumina coating had lower and more stable coefficient of friction than Ni-Alumina coating and 500 °C heated PEA Alumina coating. The as-coated PEA Alumina coating and Ni-Alumina coating survived from the 5 N 150 m dry sliding tests. Unfortunately, the 500 °C heated PEA Alumina coating did not overcome the test conditions, and some spots of coating were damaged.

The PEA Alumina coating had a reduce surface area because of micropores, and that was a factor of low COF. Steel ball materials could transfer on the coating surface because it was softer than the coating. After the material transfer particles deposited on the coating surface, steel ball would slide with the material transfer layer. The steel ball could neither crash the coating surface nor fill the micropores. Therefore, the COF data would stay constant as if the material transfer particles covered more area. The tungsten carbide (WC) ball was much harder than the coating, so it could smash the coating top surface. These smashed coating particles formed a flat and smooth layer without any micropores covering the coating surface. The contacting surface area was increased in this process, so that could explain why the COF of coating vs. WC was higher than coating vs. steel ball.

Applying electroless nickel plating occupied the crevices and micropores in PEA Alumina coating, so the Ni-Alumina coating had a larger surface contacting area. Ni-Alumina coating performed a higher in microhardness and higher stickiness than PEA Alumina coating. Nickel could adhere off the steel and WC balls materials and formed a material mixture transfer layer, although WC was harder than the coating. The balls started sliding with the material mixture layer after 100 m pin-on-disk wear tests, and the COF suddenly went up. Because of the high hardness of WC ball, it had peeled off some of material mixture layer, but the Ni-Alumina coating was keeping intact. Therefore, the material mixture transfer layer on Ni-Alumina coating could protect the coating. Moreover, from the SEM images, the forming processes of material mixture layers with steel and WC were slightly different. In the steel ball case, the ball was adhered by nickel first, and then some nickel was taken away by the ball. Nickel detached some surrounding alumina coating materials and it mixed with the coating and steel ball. Along with the slide distanced increased, the mixed materials were more and more uniform and spread on the coating surface. In the WC ball case, the ball initially smashed the top layer of the coating. Nickel in the coating peeled off some tungsten from the ball and mixed with the smashed alumina. In summary, the steel ball-coating mixture layer was adhering on the coating surface, and the WC ball-coating mixture layer was compressed in the wear track.

As-coated PEA Alumina coating contained more ferrous oxide (FeO) compounds than 500 °C heated PEA Alumina coating, and that was a reason why the it had a better anti-wear performance. In addition, 500 °C heat treatment caused a decreasing in microhardness. The coating-substrate binding force declined because of the oxidation. There were more cracks appearing as well, so which would cause the coating to be more fragile.

## ***5.5 Summary***

The Coefficient of Friction (COF) data was recorded by 5 N-150 m low speed Pin-on-Disk (POD) dry sliding tests. The tested specimens were as-coated PEA Alumina coating, Ni-Alumina coating and 500 °C heat treated coating. The testing ball materials were SAE 52100 steel and tungsten carbide (WC). After the sliding tests, wear tracks of samples were observed by Scanning Electron Microscopy (SEM). The element compositions in wear tracks were analyzed by Energy-Dispersive X-Ray Spectroscopy (EDX).

PEA Alumina coatings were survived from the wear tests. The COF results of the coating against steel ball and WC ball were remaining on low positions. There were few steel ball particles transferred on the coating surface. The coating surface was not destroyed by steel ball, and the micropores were still visible in the wear track. The WC ball smashed the top layer of the coating and created a new flat layer. The chemical composition on the new layer was the same with as-coated PEA Alumina coating, so there was no material transferred from WC ball.

Ni-Alumina coatings remained intact after the dry sliding tests. The COF results of Ni-Alumina coating against steel ball and WC ball were staying low first, but they increased rapidly after 100 m sliding distance. A mixture of steel ball and coating materials was spread on the wear track. This material mixture transfer layer was adhering on the coating surface, but it did not cover all over the wear track. Nickel had adhered some tungsten from WC ball which was hard to transfer on coating. The Ni-Alumina coating had also formed a material mixture transfer layer with ball material. The layer was compressed

in the wear track and covered all area in wear track. Some spots of layer were peeled off, but the Ni-Alumina coating was remaining safe.

500 °C heat treated coating had the worst performances in wear tests. The coatings were peeled off by the steel ball and the WC ball. The COF results of the heated coatings were much higher than the results of unheated coatings. The coating was facing a severe material transfer problem as well. The wear tracks were also wider than unheated coatings. Therefore, the 500 °C heat treatment negatively affected the wear behaviours of PEA Alumina coatings.

The wear mechanisms could be summarized as follows. The contacting area was a factor of COF results. Smaller surface contacting area with balls had lower COF. PEA Alumina coatings had a plenty of micropores on the surface, so the surface area was reduced. Sliding with steel ball did not enlarged the contact area too much, so the COF could remain in constant. WC ball smashed the top layer of PEA Alumina coating and formed a new layer in the wear track without micropores. Then the contacting area would be increased, so the COF of PEA Alumina coating against WC ball was higher than it against steel ball. Micropores on the top surface were occupied by nickel in Ni-Alumina coating, so the surface area was enlarged. Therefore, the COF results of Ni-Alumina coatings were higher than PEA Alumina coatings. In addition, nickel as a sticky material could adhere some ball materials and form coating-ball material mixture transfer layers. The layers could be considered as protection for coatings. As-coated PEA Alumina coatings contained more ferrous oxide (FeO) than 500 °C heated samples. The ferrous oxide was fully oxidized into ferric oxide (Fe<sub>2</sub>O<sub>3</sub>) in heat treating process. Therefore, ferrous oxide had better anti-wear performances than ferric oxide.

## CHAPTER 6

### Electrochemical Corrosion Behaviours

In Chapter 6, the anti-corrosion behaviours PEA Alumina and Ni-Alumina coated gray cast iron were investigated by electrochemical tests. The coatings were immersed into 3.5 wt% sodium chloride (NaCl) solution to figure out the Open Circuit Potential (EOC), Polarization Resistance ( $R_p$ ) and Electrochemical Impedance Spectroscopy (EIS) results. The immersing durations of EOC,  $R_p$  and EIS tests were 120 hours, 1 hour and 1 hour, respectively.

#### 6.1 Open Circuit Potential Tests

Figure 6.1 was illustrating the tendency of 120-hour open circuit potentials of PEA Alumina coating and Ni-Alumina coating.

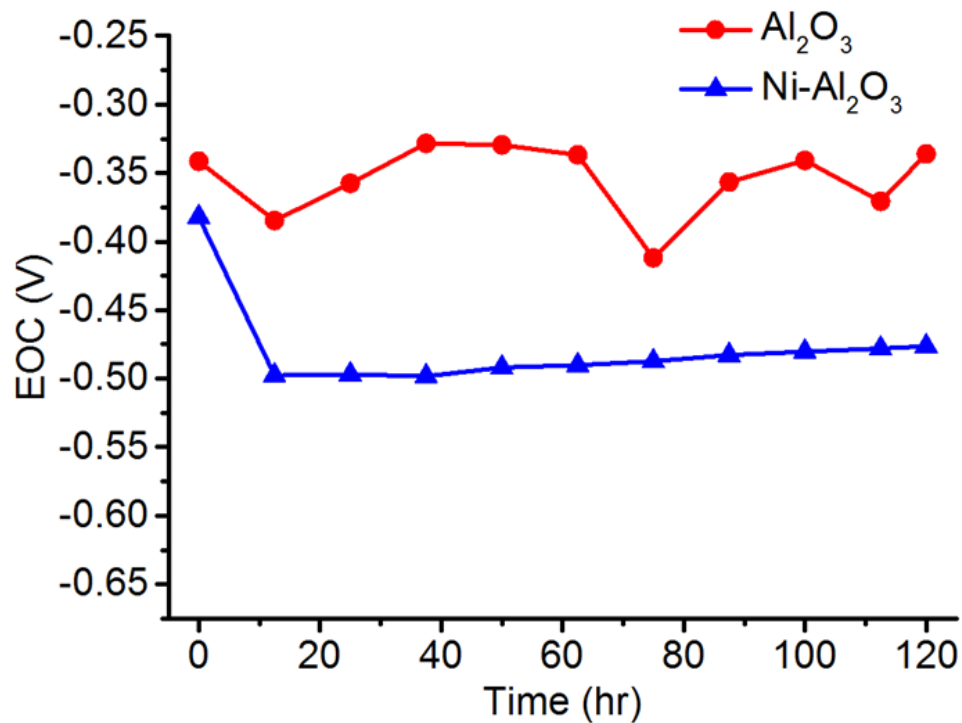


Figure 6.1: EOC results of PEA Alumina coating and Ni-Alumina coating

The EOC of PEA Alumina coating graph was presenting a vibrating line, which could come from the pitting corrosion. Because of the porous structure of PEA Alumina coating, corrosive solution could permeate onto the cast iron substrate through some cracks and micropores. Pitting corrosion behaviour damaged the anodic passive layer on the interface between cast iron substrate and PEA Alumina coating. The average of EOC of PEA Alumina coating was about -0.35 V which was higher than the EOC of Ni-Alumina coating. The reason why Ni-Alumina coating had higher open circuit potential was that nickel in the micropores could increase the electrical conductivity. The EOC of Ni-Alumina coating was keeping constant on negative 0.48 V, so the coating formed a stable passive layer. Therefore, Ni-Alumina coating had a better stability than PEA Alumina coating.

### ***6.2 Polarization Resistance Tests***

The Tafel plots of PEA Alumina coating and Ni-Alumina coating after 1-hour Polarization Resistance ( $R_p$ ) tests were illustrated in Figure 6.2. The results of corrosion potential ( $E_{\text{corr}}$ ), corrosion current ( $I_{\text{corr}}$ ), cathodic Tafel constant ( $\beta_c$ ) and anodic Tafel constant ( $\beta_a$ ) were figured out in Figure 6.2 and summarized in Table 6.1.

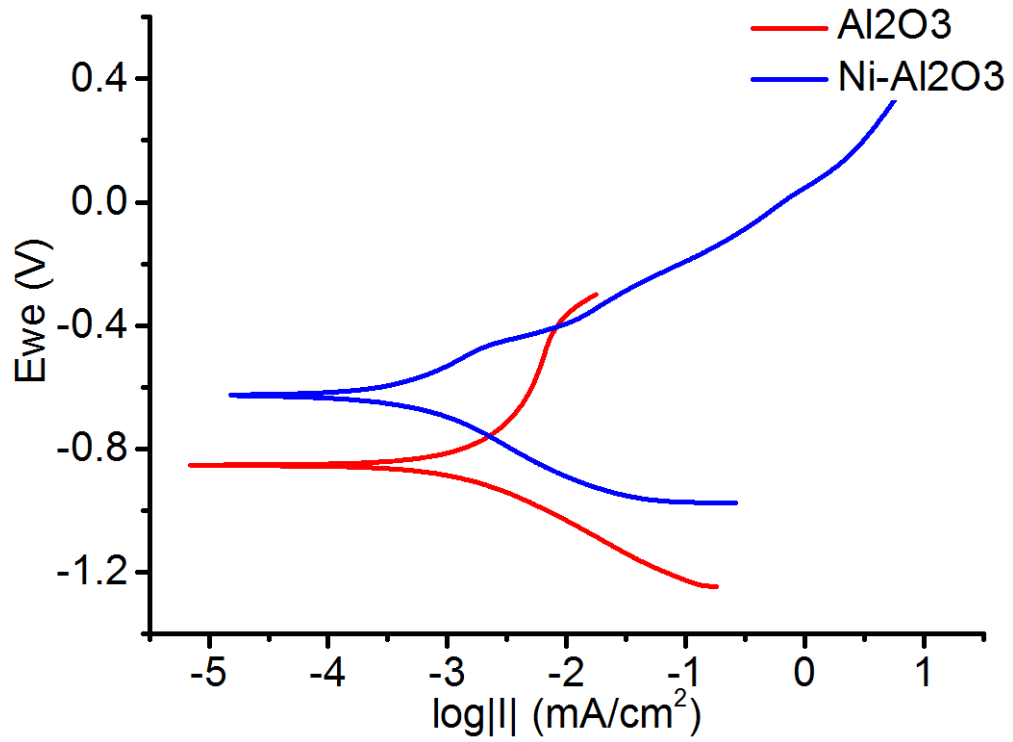


Figure 6.2: Rp results of PEA Alumina coating and Ni-Alumina coating

Table 6.1: Kinetic parameters from the polarization resistance tests

	PEA Alumina Coating	Ni-Alumina Coating
$E_{corr}$ (mV)	-853.248	-626.817
$I_{corr}$ ( $\mu$ A)	1.960	0.492
$\beta_c$	243.3	193.3
$\beta_a$	514.4	238.3
$R_p$ (k $\Omega$ )	36.59	94.192



The current potentials of PEA Alumina coating and Ni-Alumina coating were -853 mV and -626 mV, respectively. The corrosion currents were 1.960  $\mu\text{A}$  and 0.492  $\mu\text{A}$  for PEA Alumina coating and Ni-Alumina coating, respectively. Less corrosion potential resulted in high thermodynamic tendency of corrosion occurring. Ni-Alumina coating had much lower corrosion current than PEA Alumina coating, which meant the Ni-Alumina coating could provide a more reliable protection in corrosion for cast iron.

The Polarization Resistance ( $R_p$ ) results were calculated by Stern-Geary equation [87]:

$$R_p = \frac{\beta_c \times \beta_a}{2.303 \times (\beta_c + \beta_a) \times I_{corr}} \quad (\text{Eq. 2})$$

The polarization resistances of PEA Alumina coating and Ni-Alumina coating were 36.59 k $\Omega$  and 94.19 k $\Omega$ , respectively. Higher  $R_p$  value had better anti-corrosion performance. Therefore, Ni-Alumina coating had better behaviours than PEA Alumina coating in Polarization Resistance ( $R_p$ ) tests.

### **6.3 Electrochemical Impedance Spectroscopy Tests**

After immersing the PEA Alumina coating and Ni-Alumina coating in 3.5 wt% NaCl solution for 1 hour, the Electrochemical Impedance Spectroscopy (EIS) results were shown in Figure 6.3. Figure 6.3 (a) and Figure 6.3 (b) were illustrating the Nyquist plots, respectively. Where  $\text{Re}(Z)$  was the real part resistance in Ohm ( $\Omega$ ) and  $\text{Im}(Z)$  was the imaginary part resistance. Figure 6.3 (c) and (d) were presenting the Bode plots of PEA Alumina coating and Ni-Alumina coating, respectively. Where  $\log(f)$  was the logarithm of signal frequency and  $\log(|Z|)$  was the logarithm of resistance.

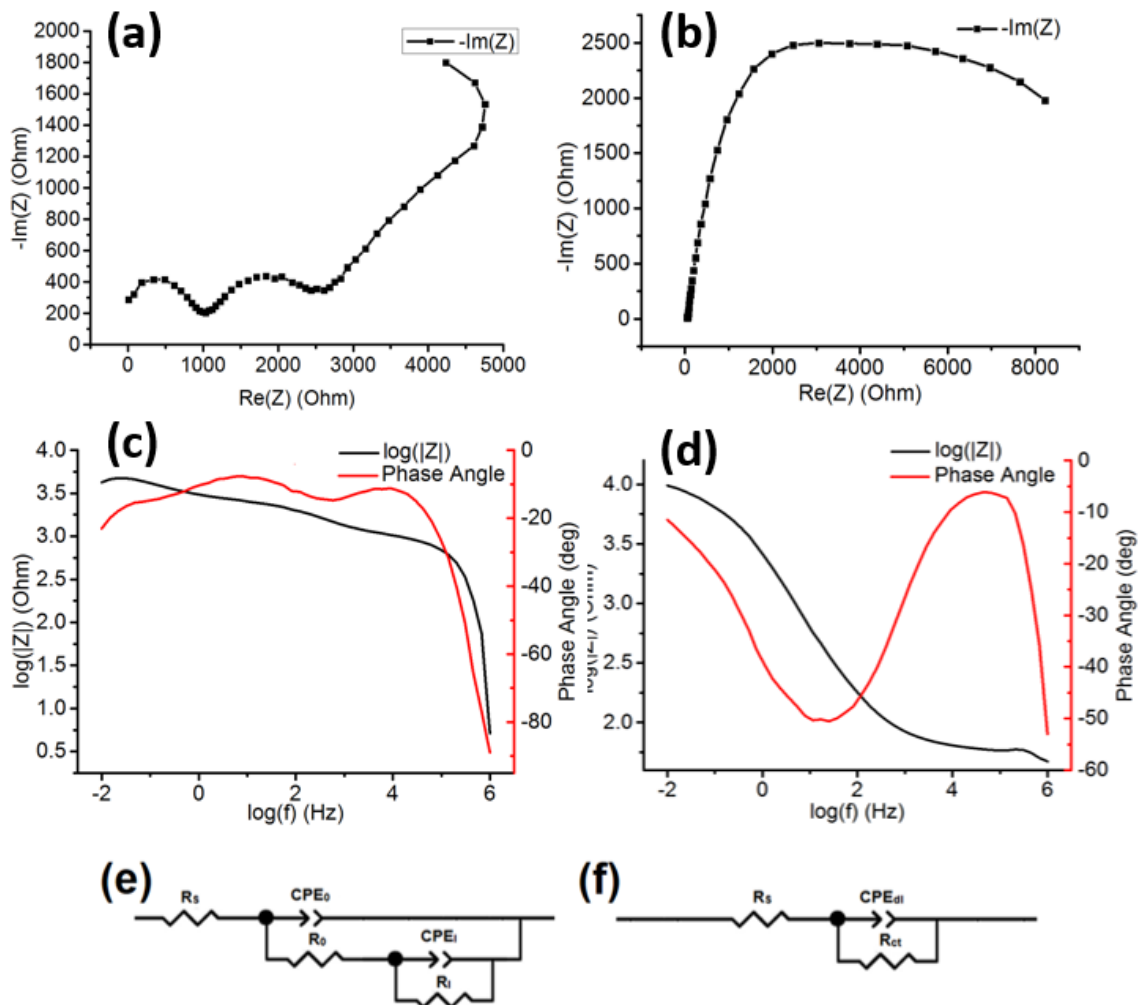


Figure 6.3: (a), (b) Nyquist plots of PEA Alumina and Ni-Alumina coated cast iron; (c), (d) Bode plots corresponding to EIS spectra in (a) and (b), respectively; (e), (f) equivalent circuits of PEA Alumina and Ni-Alumina coated cast iron, respectively.

The equivalent circuits of PEA Alumina and Ni-Alumina coated cast iron were shown in Figure 6.3 (e) (f). Because the inner part of PEA Alumina coating had lower porosity than the outer part, the coating was divided in two parts to test the resistance separately. The nickel sealed the micropores and the crevices, so there would not be any difference in

porosity inside the coating. The Ni-Alumina coating was considered as a whole resistor or capacitor. Where  $R_S$  was the resistance of NaCl solution;  $R_O$  was the outer layer resistance; and  $R_I$  was the inner layer resistance.  $R_{ct}$  was the critical resistance of Ni-Alumina coating. Due to the surface is not homogenous, the impedance of Constant Phase Element (CPE) would be calculated by **Eq. 3**:

$$Z_{CPE} = \frac{1}{T(j\omega)^P} \text{ (Eq. 3)}$$

Where  $T$  is the CPE constant;  $j$  is the imaginary unit;  $\omega$  is the angular frequency; and  $P$  is resistor-capacitor constant. The angular frequency is defined as  $\omega = 2\pi f$ , and  $f$  is frequency which was shown in the Bode plots in Figure 6.3 (c)(d). The constant  $P$  is to determine that the CPE in the circuit is a resistor or a capacitor. The value of  $P$  varies from 0 to 1, in which 0 is pure resistor, and 1 is pure capacitor.

Table 6.2 summarized the fitted parameters of EIS curves. The inner resistance of PEA Alumina coating was much higher than the outer resistance, so the net resistance was more depended on the resistance of inner layer.

Table 6.2: Parameters of EIS curves

	$R_S$ ( $\Omega$ )	$CPE_O$ (mF)	$P_O$	$R_O$ ( $\Omega$ )	$CPE_I$ (mF)	$P_I$	$R_I$ ( $\Omega$ )
PEA Alumina Coating	53.4	2.68 E-8	0.69	1824	1.87 E-4	0.255	3324

	$R_s$ ( $\Omega$ )	$CPE_{dl}$ (mF)	P	$R_{ct}$ ( $\Omega$ )
Ni-Alumina Coating	54.88	7.14 E-5	0.636	8756

The maximum resistance of PEA Alumina coating could reach 5 k $\Omega$  with a frequency of 0.022 Hz, but the resistance dropped back to 4.24 k $\Omega$  at 0.01 Hz. The maximum resistance of the Ni-Alumina coating was about 9 k $\Omega$  at frequency of 0.01 Hz. Higher resistance was referring better performance in EIS tests. Therefore, Ni-Alumina could give a better protection to the cast iron substrate than PEA Alumina coating.

#### **6.4 Summary**

PEA Alumina coating and Ni-Alumina coating were tested the anti-corrosion behaviours by Open Circuit Potential (EOC), Polarization Resistance ( $R_p$ ) and Electrochemical Impedance Spectroscopy (EIS) corrosion tests.

PEA Alumina coating had some opened micropores and crevices, so the corrosive elements in immersing tests could contact the cast iron substrate. Pitting corrosion would happen on the spots permeated by NaCl solution, and that would destroy the barrier layer on the interface between cast iron substrate and PEA Alumina coating. Applying electroless nickel plating could fill up these pores and cracks, which could prevent from a pitting corrosion.

Ni-Alumina coating had a lower open circuit potential than PEA Alumina coating because nickel in micropores and cracks increased the electrical conductivity. However, it had a more uniform EOC plot than PEA Alumina coating, which meant it had a stable passive layer and not suffering from pitting corrosion. In addition, Ni-Alumina coating had lower corrosion potential ( $E_{\text{corr}}$ ) and corrosion current ( $I_{\text{corr}}$ ) but higher Polarization Resistance ( $R_p$ ) than PEA Alumina coating. Therefore, Ni-Alumina coating had a lower thermodynamic tendency in corrosion and giving a better protection to cast iron substrate. Moreover, as result of the Electrochemical Impedance Spectroscopy (EIS) data, it could also be concluded that Ni-Alumina coating was more reliable than PEA Alumina coating in anti-corrosion behaviours.

## CHAPTER 7

### Conclusions and Future Works

In this study, PEA Alumina and Ni-Alumina coatings were deposited on gray cast iron. In addition, 500 °C heated PEA Alumina coatings were made to compare with as-coated PEA Alumina coatings. Surface morphology and chemical compositions of coatings were detected by Scanning Electron Microscopy (SEM) and Energy-Dispersive X-Ray Spectroscopy (EDX). The wear behaviours and mechanisms of coatings were investigated by observing Coefficient of Friction (COF), wear track morphology and chemical compositions. The anti-corrosion behaviours of coatings were tested by electrochemical workstation in three methods: Open Circuit Potential (EOC), Polarization Resistance (Rp) and Electrochemical Impedance Spectroscopy (EIS).

#### *7.1 Conclusions*

ASTM A247 Gray cast iron specimens were used as substrate materials to generate PEA Alumina and Ni-Alumina coatings. The original PEA Alumina coating was 30-35 µm in thickness, and they were polished to 25-30 µm. The polished samples were used to create Ni-Alumina coatings and they were applied on Pin-on-Disk (POD) tribology tests. A high current density was mandatory to form a passive layer in PEA coating process because cast iron is a non-valve metal. The high current plasma discharging melted some cast iron and formed coatings with high porosity. Crevice on the interface between cast iron substrate and PEA Alumina coating were found. Applying electroless nickel plating sealed the crevice, cracks and micropores. To make 25-30 µm Ni-Alumina coatings, 30 min nickel plating process was needed. The PEA Alumina coating was made from aluminum oxide ( $\text{Al}_2\text{O}_3$ ) and hercynite ( $\text{FeAlO}_2$ ), and the hercynite could be considered as a combination

of alumina and ferrous oxide (FeO). The 500 °C heat treated PEA Alumina coated samples had different chemical compounds with as-coated PEA Alumina coating. The O/Fe ratio of heated and unheated coatings was calculated. The O/Fe ratios of FeO and ferric oxide ( $\text{Fe}_2\text{O}_3$ ) are 1 and 1.5, respectively. The as-coated coating had an O/Fe ratio of 1.25, which was a midrange of ferrous oxide and ferric oxide. The O/Fe ratio of 500 °C heat treated PEA Alumina coating was about 1.5, thus the iron-oxygen compounds were ferric oxide. The FeO particles were fully oxidized into  $\text{Fe}_2\text{O}_3$  in the 500 °C heat treating process.

PEA Alumina coating had lower COF than Ni-Alumina coating, and it did not occur the galling issue in 150 m dry sliding tests against steel ball and WC ball. The COF of PEA Alumina coating against SAE 52100 steel ball and tungsten carbide (WC) balls were 0.13 and 0.15, respectively. There were some steel ball materials were transferred on the coating surface, but there were no WC particles found on coating. In addition, because of high hardness of WC ball, the PEA Alumina coating wear track was smashed and formed a flat alumina layer. In Ni-Alumina coating vs. steel ball wear tests, an O-Al-Fe-Ni material mixture layer were spread on the coating. However, the material mixture layer did not cover all of wear track area, and there was still some Ni-Alumina coating observed. In Ni-Alumina coating vs. WC ball wear tests, a flat O-Al-Fe-Ni-W material mixture layer was explored. The smooth material mixture layer covered all over the wear track, and part of it was peeled off. The Ni-Alumina coating underneath peeled-off area was still intact, so the material mixture layer could protect the coating itself.

500 °C heated PEA Alumina coating had lower microhardness and higher COF than as-coated one. In addition, the galling behaviour of 500 °C heated PEA Alumina coating started much earlier and easier to be broken. 500 °C heated PEA Alumina coating suffered

from severe wear behaviours. Galling behaviours started in the beginning of wear tests. The main difference between heated and unheated samples was that unheated coating contained  $\text{FeAlO}_2$  or  $\text{FeO}$ . The  $\text{FeO}$  compounds in as-coated PEA Alumina coating were fully oxidized into  $\text{Fe}_2\text{O}_3$  in heat treatment. Therefore, it could be concluded that  $\text{FeO}$  is an element with lower COF and longer durability than  $\text{Fe}_2\text{O}_3$ .

PEA Alumina and Ni-Alumina coatings were compared in corrosion resistance by electrochemical tests. The samples were immersed into 3.5 wt.% sodium chloride ( $\text{NaCl}$ ) solution. PEA Alumina coating had a higher Open Circuit Potential (EOC) than Ni-Alumina coating, because nickel in micropores and crevices increased the electrical conductivity. However, the EOC plot of PEA Alumina coating was unstable with some fluctuations, hence the pitting corrosion behaviour might occur. Ni-Alumina coating had a stable EOC plot, thus it was performing a uniform passive layer. By analyzing the Tafel plots of two coatings, Ni-Alumina coating had lower corrosion potential ( $E_{\text{corr}}$ ) and corrosion current density ( $I_{\text{corr}}$ ) than PEA Alumina coating. In addition, in Nyquist plots and Bode plots, Ni-Alumina coating had also a better anti-corrosion performance than PEA Alumina coating. Therefore, in anti-corrosion point of view, Ni-Alumina coating is better than PEA Alumina coating.

To sum up, PEA Alumina and Ni-Alumina coatings could provide a valuable wear and corrosion resistance. In addition, PEA Alumina coating had lower COF than Ni-Alumina coating. In the 150 m dry sliding tests, the galling phenomenon did not occur on PEA Alumina coating, and it happened on Ni-Alumina coating after 90 m. In the anti-corrosion point of view, Ni-Alumina coating performed better than the PEA Alumina coating in electrochemical tests.



## ***7.2 Future Works***

The PEA Alumina and Ni-Alumina coating process could be optimized in the future. Optimizing the coating process could not only eliminate the error in different samples but also have higher efficiency. 500 °C used in this study is the maximum engineering temperature, and elevated temperatures of 100 °C, 200 °C and 300 °C would be applied on PEA Alumina coating in further investigation. The aim of doing this is to figure out the maximum heat treatment temperature which will not affect the COF and durability of PEA Alumina coatings. In addition, lubricated sliding tribology tests are also valuable to explore the wear behaviours of PEA Alumina and Ni-Alumina coatings.

## REFERENCES/BIBLIOGRAPHY

- [1] W.R. Whitney, THE CORROSION OF IRON, *J. Am. Chem. Soc.* 25 (1903) 394–406.
- [2] L.N.B. Walker, William H., Anna M. Cederholm, THE CORROSION OF IRON AND STEEL, *J. Am. Chem. Soc.* 29.9 (1907) 1251–1264.
- [3] T.T. Nakamura, Shun-ichi, Keita Suzumura, Mechanical Properties and Remaining Strength of Corroded Bridge Wires, *Struct. Eng. Int.* 14.1 (2004) 50–54.
- [4] Cairns, J., Plizzari, G. A., Du, Y., Law, D. W., & Franzoni, C. (2005). Mechanical properties of corrosion-damaged reinforcement. *ACI Materials Journal*, 102(4), 256.
- [5] Grahame, C. A. A. (1952). *U.S. Patent No. 2,615,840*. Washington, DC: U.S. Patent and Trademark Office.
- [6] Isidore, G., Miller, W. L., & Sidney, T. (1961). *U.S. Patent No. 2,992,945*. Washington, DC: U.S. Patent and Trademark Office.
- [7] Beghin, A. J., Hamberg, J. P. F., & Smith, H. E. (1951). *U.S. Patent No. 2,558,167*. Washington, DC: U.S. Patent and Trademark Office.
- [8] Nie, X., Meletis, E. I., Jiang, J. C., Leyland, A., Yerokhin, A. L., & Matthews, A. (2002). Abrasive wear/corrosion properties and TEM analysis of Al<sub>2</sub>O<sub>3</sub> coatings fabricated using plasma electrolysis. *Surface and Coatings Technology*, 149(2-3), 245-251.

- [9] Schacht, M., Boukis, N., & Dinjus, E. (2000). Corrosion of alumina ceramics in acidic aqueous solutions at high temperatures and pressures. *Journal of materials science*, 35(24), 6251-6258.
- [10] Lv, G., Chen, H., Gu, W., Feng, W., Li, L., & Niu, E. (2009). Effects of graphite additives in electrolytes on the microstructure and corrosion resistance of Alumina PEO coatings. *Current Applied Physics*, 9(2), 324–328.
- [11] Zhao, C., Zha, W., Cai, R., Nie, X., & Tjong, J. (2019). A New Eco-friendly Anticorrosion Strategy for Ferrous Metals: Plasma Electrolytic Aluminating. *ACS Sustainable Chemistry & Engineering*, 7(5), 5524-5531.
- [12] Lu, G., & Zangari, G. (2002). Corrosion resistance of ternary Ni–P based alloys in sulfuric acid solutions. *Electrochimica Acta*, 47(18), 2969-2979.
- [13] Mallory, G. O., & Hajdu, J. B. (1990). Electroless plating: fundamentals and applications. William Andrew.
- [14] Małeckı, A., & Mıcek-Ilnicka, A. (2000). Electroless nickel plating from acid bath. *Surface and Coatings Technology*, 123(1), 72-77.
- [15] Yamada, T., Yamamoto, A., Fujiwara, M., & Kunugi, Y. (1993). Strength evaluation and effect of graphite on strength of electroless nickel plating on cast iron. *Journal of materials science*, 28(13), 3513-3518.
- [16] Alirezaei, S., Monirvaghefi, S. M., Salehi, M., & Saatchi, A. (2007). Wear behavior of Ni–P and Ni–P–Al<sub>2</sub>O<sub>3</sub> electroless coatings. *Wear*, 262(7-8), 978-985.

- [17] Uchida, H., Kiso, M., Nakamura, T., Kamitamari, T., Susuki, R., & Shimizu, K. (1999). *U.S. Patent No. 5,910,340*. Washington, DC: U.S. Patent and Trademark Office.
- [18] Feng, Q., Li, T., Teng, H., Zhang, X., Zhang, Y., Liu, C., & Jin, J. (2008). Investigation on the corrosion and oxidation resistance of Ni–Al<sub>2</sub>O<sub>3</sub> nano-composite coatings prepared by sediment co-deposition. *Surface and Coatings Technology*, 202(17), 4137-4144.
- [19] Szczygieł, B., & Kołodziej, M. (2005). Composite Ni/Al<sub>2</sub>O<sub>3</sub> coatings and their corrosion resistance. *Electrochimica Acta*, 50(20), 4188-4195.
- [20] Banerji, A., Lukitsch, M. J., McClory, B., White, D. R., & Alpas, A. T. (2017). Effect of iron oxides on sliding friction of thermally sprayed 1010 steel coated cylinder bores. *Wear*, 376, 858-868.
- [21] Hosking, N. C., Ström, M. A., Shipway, P. H., & Rudd, C. D. (2007). Corrosion resistance of zinc–magnesium coated steel. *Corrosion science*, 49(9), 3669-3695.
- [22] Friend, W. Z. (1980). *Corrosion of nickel and nickel-base alloys* (Vol. 248). New York: Wiley.
- [23] Nam, K. S., Lee, K. H., Kwon, S. C., Lee, D. Y., & Song, Y. S. (2004). Improved wear and corrosion resistance of chromium (III) plating by oxynitrocarburising and steam oxidation. *Materials Letters*, 58(27-28), 3540-3544.
- [24] Masaki, S., Inoue, H., & Honma, H. (1998). Mirror-bright silver plating from a cyanide-free bath. *Metal Finishing*, 96(1), 16-22.
- [25] Yablonsky, A., Bolo, E. R., & Reggi, J. D. (1997). *U.S. Patent No. 5,647,996*. Washington, DC: U.S. Patent and Trademark Office.

- [26] Namasivayam, C., & Ranganathan, K. (1993). Waste Fe (III)/Cr (III) hydroxide as adsorbent for the removal of Cr (VI) from aqueous solution and chromium plating industry wastewater. *Environmental Pollution*, 82(3), 255-261.
- [27] Raj, L. M. I., Sathishkumar, J., Kumaragurubaran, B., & Gopal, P. (2013). Analysis of hard chromium coating defects and its prevention methods. *International Journal of Engineering and Advanced Technologi (IJEAT)*, 2, 427-432.
- [28] Yang, Z. (2011). Alternatives to hard chromium plating on piston rods.
- [29] Rashidi, A. M., & Amadeh, A. (2010). Effect of electroplating parameters on microstructure of nanocrystalline nickel coatings. *Journal of Materials Science & Technology*, 26(1), 82-86.
- [30] Younes, O., Zhu, L., Rosenberg, Y., Shacham-Diamand, Y., & Gileadi, E. (2001). Electroplating of amorphous thin films of tungsten/nickel alloys. *Langmuir*, 17(26), 8270-8275.
- [31] Loto, C. A. (2016). Electroless nickel plating—a review. *Silicon*, 8(2), 177-186.
- [32] Osifuye, O. C. (2014). Electrochemical corrosion resistance of electroless plated mild steel.
- [33] Van Den Meerakker, J. E. A. M. (1981). On the mechanism of electroless plating. II. One mechanism for different reductants. *Journal of Applied Electrochemistry*, 11(3), 395-400.
- [34] Mallory, G. O., & Hajdu, J. B. (1990). *Electroless plating: fundamentals and applications*. William Andrew.

- [35] Li, Q., Fan, S., Han, W., Sun, C., & Liang, W. (1997). Coating of carbon nanotube with nickel by electroless plating method. *Japanese Journal of Applied Physics-Part 2 Letters*, 36(4), 501-503.
- [36] Crehan, W. J. (1954). *U.S. Patent No. 2,690,402*. Washington, DC: U.S. Patent and Trademark Office.
- [37] Ehram, R., & Raymond, J. L. (1998). *U.S. Patent No. 5,843,538*. Washington, DC: U.S. Patent and Trademark Office.
- [38] Liu, Z., & Gao, W. (2006). Electroless nickel plating on AZ91 Mg alloy substrate. *Surface and Coatings Technology*, 200(16-17), 5087-5093.
- [39] Sharma, A. K., Suresh, M. R., Bhojraj, H., Narayanamurthy, H., & Sahu, R. P. (1998). Electroless nickel plating on magnesium alloy. *Metal finishing*, 96(3), 10-19.
- [40] Amin, S., & Panchal, H. (2016). A review on thermal spray coating processes. *transfer*, 2(4).
- [41] Rigney, D. V., Viguie, R. U. D. O. L. F. O., Wortman, D. J., & Skelly, D. W. (1997). PVD thermal barrier coating applications and process development for aircraft engines. *Journal of thermal spray technology*, 6(2), 167-175.
- [42] Abd Malek, M. H., Saad, N. H., Abas, S. K., & Shah, N. M. (2013, June). Thermal arc spray overview. In *IOP Conference Series: Materials Science and Engineering* (Vol. 46, No. 1, p. 012028). IOP Publishing.

- [43] Paredes, R. S., Amico, S. C., & d'Oliveira, A. S. C. M. (2006). The effect of roughness and pre-heating of the substrate on the morphology of aluminium coatings deposited by thermal spraying. *Surface and Coatings Technology*, 200(9), 3049-3055.
- [44] Dhiman, R., McDonald, A. G., & Chandra, S. (2007). Predicting splat morphology in a thermal spray process. *Surface and Coatings Technology*, 201(18), 7789-7801.
- [45] Deshpande, S., Kulkarni, A., Sampath, S., & Herman, H. (2004). Application of image analysis for characterization of porosity in thermal spray coatings and correlation with small angle neutron scattering. *Surface and coatings technology*, 187(1), 6-16.
- [46] Baptista, A., Silva, F., Porteiro, J., Míguez, J., & Pinto, G. (2018). Sputtering physical vapour deposition (PVD) coatings: A critical review on process improvement and market trend demands. *Coatings*, 8(11), 402.
- [47] Schneider, J. M., Rohde, S., Sproul, W. D., & Matthews, A. (2000). Recent developments in plasma assisted physical vapour deposition. *Journal of Physics D: Applied Physics*, 33(18), R173.
- [48] Choy, K. L. (2003). Chemical vapour deposition of coatings. *Progress in materials science*, 48(2), 57-170.
- [49] Jones, A. C., & Hitchman, M. L. (Eds.). (2009). *Chemical vapour deposition: precursors, processes and applications*. Royal society of chemistry.
- [50] Bryant, W. A. (1977). The fundamentals of chemical vapour deposition. *Journal of Materials science*, 12(7), 1285-1306.

- [51] Weyher, J. L., Brown, P. D., Zauner, A. R. A., Müller, S., Boothroyd, C. B., Foord, D. T., ... & Porowski, S. (1999). Morphological and structural characteristics of homoepitaxial GaN grown by metalorganic chemical vapour deposition (MOCVD). *Journal of Crystal Growth*, 204(4), 419-428.
- [52] Natali, M., Carta, G., Rigato, V., Rossetto, G., Salmaso, G., & Zanella, P. (2005). Chemical, morphological and nano-mechanical characterizations of Al<sub>2</sub>O<sub>3</sub> thin films deposited by metal organic chemical vapour deposition on AISI 304 stainless steel. *Electrochimica Acta*, 50(23), 4615-4620.
- [53] Baptista, A., Silva, F. J. G., Porteiro, J., Míguez, J. L., Pinto, G., & Fernandes, L. (2018). On the physical vapour deposition (PVD): evolution of magnetron sputtering processes for industrial applications. *Procedia Manufacturing*, 17, 746-757.
- [54] Humphreys, R. G., Satchell, J. S., Chew, N. G., Edwards, J. A., Goodyear, S. W., Blenkinsop, S. E., ... & Cullis, A. G. (1990). Physical vapour deposition techniques for the growth of YBa<sub>2</sub>Cu<sub>3</sub>O<sub>7</sub> thin films. *Superconductor Science and Technology*, 3(1), 38.
- [55] Ali, N., Teixeira, J. A., Addali, A., Saeed, M., Al-Zubi, F., Sedaghat, A., & Bahzad, H. (2019). Deposition of Stainless Steel Thin Films: An Electron Beam Physical Vapour Deposition Approach. *Materials*, 12(4), 571.
- [56] Aykut, Ş., Bağcı, E., Kentli, A., & Yazıcıoğlu, O. (2007). Experimental observation of tool wear, cutting forces and chip morphology in face milling of cobalt based super-alloy with physical vapour deposition coated and uncoated tool. *Materials & design*, 28(6), 1880-1888.



- [57] Yerokhin, A. L., Nie, X., Leyland, A., Matthews, A., & Dowey, S. J. (1999). Plasma electrolysis for surface engineering. *Surface and coatings technology*, 122(2-3), 73-93.
- [58] Arrabal, R., Mohedano, M., Matykina, E., Pardo, A., Mingo, B., & Merino, M. C. (2015). Characterization and wear behaviour of PEO coatings on 6082-T6 aluminium alloy with incorporated  $\alpha$ -Al<sub>2</sub>O<sub>3</sub> particles. *Surface and Coatings Technology*, 269, 64-73.
- [59] Hakimizad, A., Raeissi, K., Golozar, M. A., Lu, X., Blawert, C., & Zheludkevich, M. L. (2017). The effect of pulse waveforms on surface morphology, composition and corrosion behavior of Al<sub>2</sub>O<sub>3</sub> and Al<sub>2</sub>O<sub>3</sub>/TiO<sub>2</sub> nano-composite PEO coatings on 7075 aluminum alloy. *Surface and Coatings Technology*, 324, 208-221.
- [60] Erfanifar, E., Aliofkhazraei, M., Nabavi, H. F., Sharifi, H., & Rouhaghdam, A. S. (2017). Growth kinetics and morphology of plasma electrolytic oxidation coating on aluminum. *Materials Chemistry and Physics*, 185, 162-175.
- [61] Guan, Y., Xia, Y., & Li, G. (2008). Growth mechanism and corrosion behavior of ceramic coatings on aluminum produced by autocontrol AC pulse PEO. *Surface and Coatings Technology*, 202(19), 4602-4612.
- [62] Gnedenkov, A. S., Sinebryukhov, S. L., Mashtalyar, D. V., & Gnedenkov, S. V. (2012). Microscale morphology and properties of the PEO-coating surface. *Physics Procedia*, 23, 98-101.
- [63] Kasalica, B., Radić-Perić, J., Perić, M., Petković-Benazzouz, M., Belča, I., & Sarvan, M. (2016). The mechanism of evolution of microdischarges at the beginning of the PEO process on aluminum. *Surface and Coatings Technology*, 298, 24-32.

- [64] Karlsson, P., Gård, A., Krakhmalev, P., & Bergström, J. (2012). Galling resistance and wear mechanisms for cold-work tool steels in lubricated sliding against high strength stainless steel sheets. *Wear*, 286, 92-97.
- [65] Das, D., Ray, K. K., & Dutta, A. K. (2009). Influence of temperature of sub-zero treatments on the wear behaviour of die steel. *Wear*, 267(9-10), 1361-1370.
- [66] Das, D., Dutta, A. K., & Ray, K. K. (2009). Correlation of microstructure with wear behaviour of deep cryogenically treated AISI D2 steel. *Wear*, 267(9-10), 1371-1380.
- [67] Sapate, S. G., & RamaRao, A. V. (2006). Erosive wear behaviour of weld hardfacing high chromium cast irons: effect of erodent particles. *Tribology International*, 39(3), 206-212.
- [68] Chatterjee, S., & Pal, T. K. (2003). Wear behaviour of hardfacing deposits on cast iron. *Wear*, 255(1-6), 417-425.
- [69] Modi, O. P., Mondal, D. P., Prasad, B. K., Singh, M., & Khaira, H. K. (2003). Abrasive wear behaviour of a high carbon steel: effects of microstructure and experimental parameters and correlation with mechanical properties. *Materials Science and Engineering: A*, 343(1-2), 235-242.
- [70] Luo, Q., Xie, J., & Song, Y. (1995). Effects of microstructures on the abrasive wear behaviour of spheroidal cast iron. *Wear*, 184(1), 1-10.
- [71] Ramesh, C. S., & Ahamed, A. (2011). Friction and wear behaviour of cast Al 6063 based in situ metal matrix composites. *Wear*, 271(9-10), 1928-1939.

- [72] Dwivedi, D. K. (2010). Adhesive wear behaviour of cast aluminium–silicon alloys: Overview. *Materials & Design (1980-2015)*, 31(5), 2517-2531.
- [73] Terleeva, O. P., Slonova, A. I., Rogov, A. B., Matthews, A., & Yerokhin, A. (2019). Wear resistant coatings with a high friction coefficient produced by plasma electrolytic oxidation of Al alloys in electrolytes with basalt mineral powder additions. *Materials*, 12(17), 2738.
- [74] Matykina, E., Garcia, I., Arrabal, R., Mohedano, M., Mingo, B., Sancho, J., ... & Pardo, A. (2016). Role of PEO coatings in long-term biodegradation of a Mg alloy. *Applied Surface Science*, 389, 810-823.
- [75] Buling, A., & Zerrer, J. (2019). Increasing the application fields of magnesium by ultracera<sup>®</sup>: Corrosion and wear protection by plasma electrolytical oxidation (PEO) of Mg alloys. *Surface and Coatings Technology*, 369, 142-155.
- [76] Li, X., Dong, C., Zhao, Q., Pang, Y., Cheng, F., & Wang, S. (2018). Characterization of microstructure and wear resistance of PEO coatings containing various microparticles on Ti6Al4V alloy. *Journal of Materials Engineering and Performance*, 27(4), 1642-1653.
- [77] Egorkin, V. S., Vyaliy, I. E., Sinebryukhov, S. L., & Gnedenkov, S. V. (2017). Composition, morphology and tribological properties of PEO-coatings formed on an aluminum alloy D16 at different duty cycles of the polarizing signal. *Non-Ferrous Metals*, 42(1), 12-16.
- [78] Fontana, M. G. (2005). *Corrosion engineering*. Tata McGraw-Hill Education.

- [79] Ezuber, H. M. (2009). Influence of temperature and thiosulfate on the corrosion behavior of steel in chloride solutions saturated in CO<sub>2</sub>. *Materials & Design*, 30(9), 3420-3427.
- [80] Akinribide, O. J., Akinwamide, S. O., Ajibola, O. O., Obadele, B. A., Oluwagbenga Olusunle, S. O., & Olubambi, P. A. (2019). Corrosion behavior of ductile and austempered ductile cast iron in 0.01 M and 0.05 M NaCl Environments. *Procedia Manufacturing*, 30, 167-172.
- [81] Ezuber, H., El-Houd, A., & El-Shawesh, F. (2008). A study on the corrosion behavior of aluminum alloys in seawater. *Materials & Design*, 29(4), 801-805.
- [82] Xu, W., Han, E. H., & Wang, Z. (2019). Effect of tannic acid on corrosion behavior of carbon steel in NaCl solution. *Journal of Materials Science & Technology*, 35(1), 64-75.
- [83] Seri, O. (1994). The effect of NaCl concentration on the corrosion behavior of aluminum containing iron. *Corrosion science*, 36(10), 1789-1803.
- [84] You, Z., Lai, Y., Zeng, H., & Yang, Y. (2020). Influence of water and sodium chloride content on corrosion behavior of cast iron in silty clay. *Construction and Building Materials*, 238, 117762.
- [85] Hsu, C. H., & Chen, M. L. (2010). Corrosion behavior of nickel alloyed and austempered ductile irons in 3.5% sodium chloride. *Corrosion Science*, 52(9), 2945-2949.

- [86] Zhang, S., Pang, X., Wang, Y., & Gao, K. (2013). Corrosion behavior of steel with different microstructures under various elastic loading conditions. *Corrosion science*, 75, 293-299.
- [87] Li, S. M., Zhang, H. R., & Liu, J. H. (2007). Corrosion behavior of aluminum alloy 2024-T3 by 8-hydroxy-quinoline and its derivative in 3.5% chloride solution. *Transactions of Nonferrous Metals Society of China*, 17(2), 318-325.
- [88] Wang, Z. Y., Teng, M. A., Wei, H., & Yu, G. C. (2007). Corrosion behavior on aluminum alloy LY12 in simulated atmospheric corrosion process. *Transactions of Nonferrous Metals Society of China*, 17(2), 326-334.
- [89] Gnedenkov, S. V., Sinebryukhov, S. L., Mashtalyar, D. V., Nadaraia, K. V., Kiryukhin, D. P., Kichigina, G. A., ... & Buznik, V. M. (2018). Composite coatings formed on the PEO-layers with the use of solutions of tetrafluoroethylene telomers. *Surface and Coatings Technology*, 346, 53-62.
- [90] Ghasemi, A., Raja, V. S., Blawert, C., Dietzel, W., & Kainer, K. U. (2008). Study of the structure and corrosion behavior of PEO coatings on AM50 magnesium alloy by electrochemical impedance spectroscopy. *Surface and Coatings Technology*, 202(15), 3513-3518.
- [91] Akbari, E., Di Franco, F., Ceraolo, P., Raeissi, K., Santamaria, M., & Hakimizad, A. (2018). Electrochemically-induced TiO<sub>2</sub> incorporation for enhancing corrosion and tribocorrosion resistance of PEO coating on 7075 Al alloy. *Corrosion Science*, 143, 314-328.

## VITA AUCTORIS

NAME: Jiayi Sun

PLACE OF BIRTH: Shenyang, Liaoning, China

YEAR OF BIRTH: 1996

EDUCATION: University of Windsor, B.A.Sc., Windsor, ON,  
2014-2018

University of Windsor, M.A.Sc., Windsor, ON,  
2019-2021

ProQuest Number: 28496902

INFORMATION TO ALL USERS

The quality and completeness of this reproduction is dependent on the quality and completeness of the copy made available to ProQuest.



Distributed by ProQuest LLC (2021).

Copyright of the Dissertation is held by the Author unless otherwise noted.

This work may be used in accordance with the terms of the Creative Commons license or other rights statement, as indicated in the copyright statement or in the metadata associated with this work. Unless otherwise specified in the copyright statement or the metadata, all rights are reserved by the copyright holder.

This work is protected against unauthorized copying under Title 17, United States Code and other applicable copyright laws.

Microform Edition where available © ProQuest LLC. No reproduction or digitization of the Microform Edition is authorized without permission of ProQuest LLC.

ProQuest LLC  
789 East Eisenhower Parkway  
P.O. Box 1346  
Ann Arbor, MI 48106 - 1346 USA